Università Campus Bio-Medico di Roma
School of Engineering

PhD Course in Biomedical Engineering
(XX – 2004/2007)

Development and early HTA of novel microfluidic systems for bio-analytical and drug delivery applications

Silvia Petroni

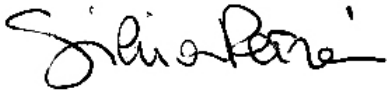

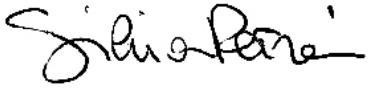

Development and Early HTA of novel microfluidic systems for bio-analytical and drug delivery applications

A thesis presented by
Silvia Petroni
In partial fulfilment of the requirements for the degree of
Doctor of Philosophy
In Biomedical Engineering

Università Campus Bio-Medico di Roma
School of Engineering

Coordinator
Prof. Saverio Cristina

Supervisor
Prof. Eugenio Guglielmelli

Co-Supervisor
Dr. Dino Accoto
Prof. Giuseppe Turchetti
Prof. Paolo Dario

January 2008

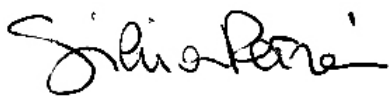

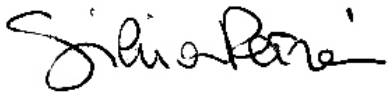

Contents

1 Introduction **1**
1.1 Structure and objectives of the PhD research activity 1

2 Microfluidics and miniaturization: enabling technologies for novel biomechatronic devices **4**
2.1 Mechatronic design of biomedical devices 4
2.2 Basic theory on microfluidics 5
2.3 Examples of application of microfluidics to molecular diagnostics 8
2.4 Novel technologies for bioassays 16
2.4.1 Low-cost dispensing technologies for biomolecules . . . 16
2.4.2 On-chip sample amplification technologies: a feasibility study 20

3 Biomechatronic design and development of a novel system for drug delivery to the brain **28**
3.1 Introduction and state of the art: drug delivery to the CNS . 28
3.2 Modelling of the device architecture 32
3.3 Modelling of the cerebral dynamics 39
3.4 Cerebral system response during infusion: simulation results . 46
3.5 Definition of the testing platform architecture 49
3.6 Simulator fabrication 55
3.7 Assembling of the infusion device 59
3.8 Development of the control systems 65
3.9 Tests on the prototype 70
3.10 Conclusions 77

4 Health Technology Assessment (HTA) procedures for novel biomedical technologies **79**
4.1 A brief overview on HTA 79
4.2 Case study I: Impact of microfluidic systems for molecular and genomic analysis: technological, socio-economic and ethical perspectives 83

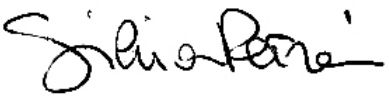

4.2.1 Technological and socio-economic trend 84
4.2.2 Ethical and social open challenges 88
4.3 Case study II: Technological and socio-economical implications in the development of implantable drug infusion systems for brain tumour therapy 90
4.3.1 Epidemiology of brain tumours 90
4.3.2 Overview on cost analysis 91
4.3.3 Future trends in the treatment of brain cancer 92
4.4 Case study III: Early assessment of neuro-rehabilitation technology 96
4.4.1 Rationale for robotic neurorehabilitation 96
4.4.2 The ALLADIN structure and technology 97
4.4.3 System assessment through a SWOT analysis 98
4.5 Conclusions 105

5 Conclusions **106**

References **108**

List of publications **119**

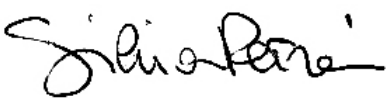

Chapter 1

Introduction

1.1 Structure and objectives of the PhD research activity

The field of bioengineering is a sort of "meeting point" among many different disciplines. The main aim of bioengineering is to apply the latest findings of disciplines like electronics, biology, chemistry, robotics, etc ... (see figure 1.1) to the development of biomedical technologies that can improve diagnostics, therapy and rehabilitation of patients. My PhD research programme is in

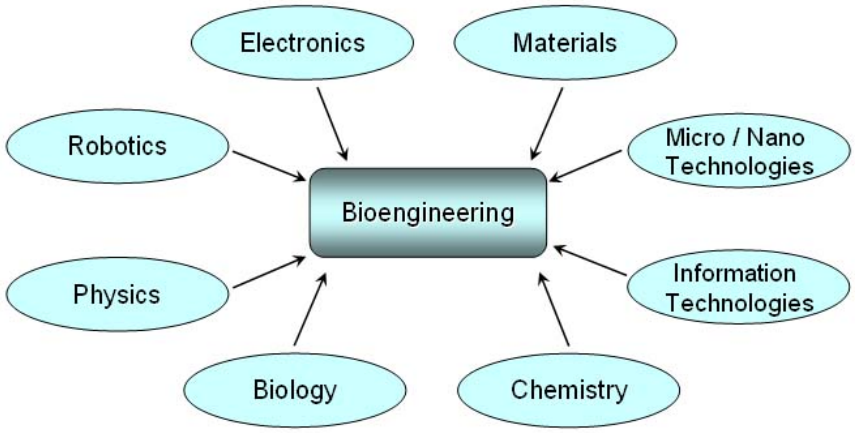

Figure 1.1: The main basic technologies converging into bioengineering.

the frame of Biomedical Robotics, and the main theme concerns the development of mechatronic technologies for biomedical applications; more in detail, the development of novel microfluidic solutions and systems both for molecular diagnostics through on-chip analysis, and for therapy, through targeted drug delivery.

Microfluidics is a multidisciplinary field that investigates the behaviour of fluids at the microscale, with practical applications to the design of systems in which such small volumes of fluids are moved, mixed, or undergo physical transformations, chemical reactions, etc...
Important applications of microfluidics can be found in the field of life-sciences, that, over the last decade, experienced a real breakthrough, due both to the tremendous progress made in the field of miniaturization technologies and to the growing interest in the study of genomics.
The main aims of my research work can be summarized as follows:

- Proposing a novel approach for research activity, combining together a biomechatronic design approach, that is typical of bioengineering, with several "in progress" health technology assessment (HTA) procedures, that are typical of other scientific fields, such as health economics.
- Defining roadmaps of technological innovation for microfluidic systems, especially concerning systems for bioanalytical and drug delivery applications.
- Performing an experimental research activity, from the very early concepts to *in vitro* tests on the prototype, on one of the mentioned technologies (i.e. applications for drug delivery).
- Validating the chosen research approach on other technological applications.

In this dissertation all the mentioned activities are presented, together with the main results. The whole work is divided in two main parts only for convenience reasons.
In the firs part, after a critical investigation on the state-of-the-art in the field of microfluidic applications to biomolecular analysis and drug delivery, two feasibility studies are presented, on possible novel microfluidic solutions for motion, manipulation and dispensing of biological samples for bioassays. In particular, these two case studies relate to two different kinds of technological innovation: the first one is an example of "incremental" innovation, that mainly consisted in improving an existing technology; the second one is an example of thorough innovation, that investigates the feasibility of a bioanalytical system based on a novel approach.
Then, the development of a novel biomechatronic system for direct drug delivery into a tricky anatomic compartment, such as the brain, is presented, starting from a model of interaction of the system with the anatomic location of interest, to the fabrication of an early prototype and of an hardware simulator of the cerebral dynamics for *in vitro* tests.
The second part of the dissertation relates to the application of different early HTA procedures to the aforementioned technologies, in order to test the novel approach adopted for technology development. As a matter of fact,

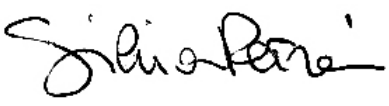

health technology assessment (HTA) is an existing discipline, that usually is used for performing analysis and evaluations on well-established medical technologies. However, sometimes it is too late to perform such evaluations on an already-on-the-market technology, especially in the biomedical field. Several technologies may result ineffective, not user-acceptable, or even harmful, thus leading to a waste of resources and time, that could be avoided by performing such evaluations at every step of development of a certain technology.
Moreover, in the second part of the dissertation, another HTA case study is also presented, not strictly dealt with in the first part of my PhD course, but anyhow performed, with the previously adopted approach, on another emerging biomedical technology currently under development at the Biorobotics & Biomicrosystems Lab at University Campus Bio-Medico.
This is done for showing that there are several ways of performing technology assessment, especially when dealing with technologies that are in their investigational/experimental stage of development. For this reason, for each technology that is assessed, a proper analysis level is kept, in order to provide conclusions and evaluations that are suitable and well-timed with regard to the degree of progress of each technology field.

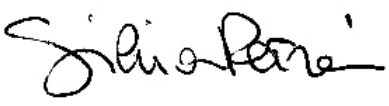

Chapter 2

Microfluidics and miniaturization: enabling technologies for novel biomechatronic devices

2.1 Mechatronic design of biomedical devices

The basic concepts of mechatronic design of systems are particularly suitable for being applied to the biomedical field. A device that has to be applied to human subjects for diagnosis, therapy or rehabilitation purposes must fulfil several specific requirements. Most of these requirements cannot be inserted after the system design (or fabrication) simply as additional components/features, but they have to be carefully taken into account starting from the very early stages of development of the idea.

Strictly speaking, a biomedical device cannot be designed without paying attention to the features of the anatomic location it will come in contact with and to the possible interactions with such a compartment/organ/tissue (see figure 2.1).

The first part of my PhD course has been devoted to the study and development of novel devices to be employed for diagnosis or therapy, especially in the field of microfluidic systems for biomolecular analysis and of systems for drug delivery to tricky anatomic compartments. At present there are several enabling technologies that allow for a proper design of such kind of devices. Progress made in the field of microfluidics as first, and of miniaturization technologies, are the main elements encouraging the spreading of this kind of applications.

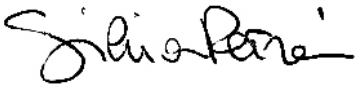

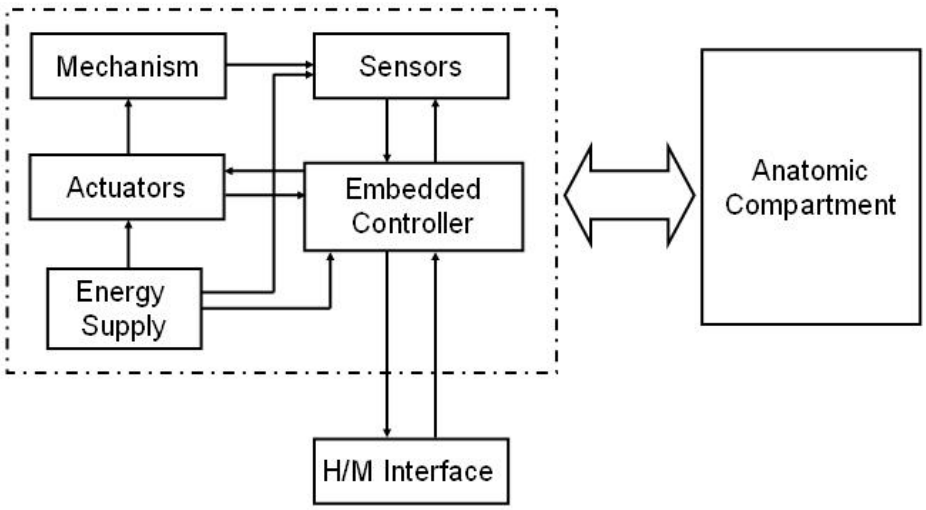

Figure 2.1: Block diagram showing the paradigm of the biomechatronic design: every component constituting a biomechatronic device is continuously in interaction with the anatomic compartment of interest.

2.2 Basic theory on microfluidics

Microfluidics is a multidisciplinary field, transversal to the wide field of microengineering, that investigates the behaviour of fluids at the microscale, with practical applications to the design of systems in which such small volumes of fluids are moved, displaced, mixed, or undergo physical transformations, phase transitions, chemical reactions, etc...
The use of microfluidics, and in particular the motion of fluids subjected to an electric field (i.e. *electrokinetic phenomena*), is a very powerful tool in life-sciences, in that it can be used in a favourable way in most of the processes involved in biological and medical operations, also allowing for parallelization of tasks involved in the procedures [1]. Important applications of microfluidics can be found in the field of life-sciences, that, over the last decade, experienced a real breakthrough. This was due both to the tremendous progress made in the field of miniaturization technologies and to the growing interest in the study of genomics. In particular, since DNA holds the whole genetic information of a subject, being able to manipulate such biomolecules is a fundamental prerequisite for achieving rapid improvements in the field of genetic screening, diagnostics and drug discovery [2, 3, 4, 5]. Electrokinetic phenomena result from the interaction of an electric field with an electric double layer, that is formed on a surface when it comes in contact with a polar medium and gains a net surface charge density [6]. Electrokinetics is a collective term involving several different

phenomena: almost all of them have been exploited to perform microfluidic operations.

Electroosmosis is one of the most popular electrokinetics-based techniques: an applied external electric field forces the ions at the solid-liquid interface to migrate, dragging by viscous forces a thin liquid layer close to the solid; the liquid bulk is then put in motion by momentum diffusion due to viscosity. Electroosmotic velocity in a channel is well represented by the Smoluchowski's equation for the slip velocity, that varies with the applied field [7]:

$$u_s = \frac{\epsilon\zeta}{\eta} E_{||} \tag{2.1}$$

where u_s is the fluid velocity, ϵ_w is the solution permittivity, ζ is the zeta potential η is the fluid viscosity and $E_{||}$ is the component of the electric field that is parallel to the fluid direction.

Electroosmosis has been employed in several applications, such as fluid displacement [8, 9, 10, 11, 12, 13], fluid dispensing [14], fluid mixing [15, 16] and for cells manipulation in general [17], just to name a few. Such technique has several advantages, the main ones being the generation of a flat velocity profile when no external pressure is applied (this is sometimes useful for precisely controlling the amount of liquid displaced) and the possibility to convert electric energy into mechanical energy avoiding any moving parts.

Electrowetting is another electrokinetic principle, that has been successfully investigated for pumping operations [18, 19] and in biological samples dispensing processes [20]. It consists in the motion of liquid droplets inside microchannels covered with electrodes that, when activated, drive the liquid motion. The electrowetting principle can be used in a variety of ways [18]. The main law that regulates electrowetting phenomena is basically a surface tension equilibrium [7]:

$$\gamma_{sg} + \gamma_{sl} + \gamma \cos\theta_{eq} = 0 \tag{2.2}$$

where γ_{sg} and γ_{sl} are the surface tensions at the solid-gas and solid-liquid interface, respectively, and θ_{eq} is the equilibrium contact angle. When a voltage is applied at the electrodes the tension at the liquid-solid interface varies with such voltage:

$$\gamma_{sl} = \gamma_{sl}^{eq} - \frac{cV^2}{2} \tag{2.3}$$

Equation (2.3) shows that the solid-liquid interface behaves as a capacitor with capacitance c: when a voltage V is applied the contact angle changes accounting for the electric energy stored in the interface. Electrowetting on dielectric (*EWOD*) is a particular application of electrowetting, were electrodes are separated from the solution through a thin dielectric layer: this technique has a good adaptability to several different fluids and very low power requirements [21] (Wong et al., 2004). Moreover, the thin insulating

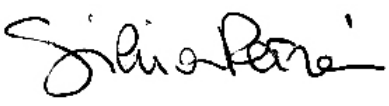

layer used in EWOD, is useful for overcoming the problems related to water electrolysis that occurs at the electrodes [22].
Electrophoresis allows to sort charged particles according to their molecular weight and their charge. To enhance the selectivity particles migrate through a matrix, usually made of gel, under the effect of an externally applied electric field. Migration velocity is given by:

$$v = \mu_e E \tag{2.4}$$

where E is the electric field strength and μ_e is the electrophoretic mobility, that depends both on the molecule and on the fluid properties:

$$\mu_e = \frac{q}{6\pi\eta r} \tag{2.5}$$

where q is the charge of the ion and r its radius and η is the solution viscosity.
Different molecules are identified based on the distance covered within a given time. A schematic of the electrophoretic mechanism is shown in figure 2.2.

Dielectrophoresis works in a similar way as the electrophoresis, with the

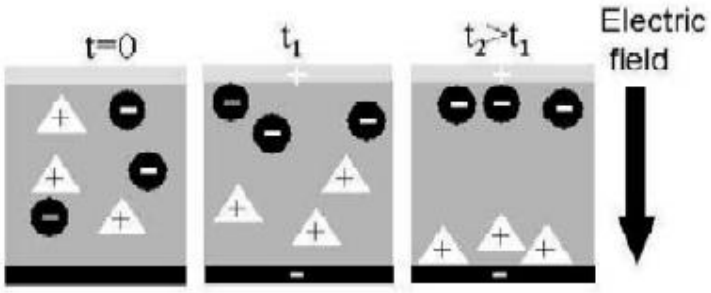

Figure 2.2: Schematic of the electrophoretic separation of particles under the effect of an electric field.

only difference that a polarized uncharged particle suspended in a solution is translated, due to a dipole induced by an external inhomogeneous AC electric field [21]. The time average dielectrophoretic force can be written as [23]:

$$F_{DEP} = 2\pi r^3 \epsilon_s Rek(\omega) \nabla E^2 \tag{2.6}$$

where r is the particle radius, ϵ_s is the solution conductivity, ∇E^2 indicates the electric field gradient and strength and $ReK(\omega)$ is the real part of the Clausius-Mossotti factor, that gives an indication about particle polarizability, and is as follows:

$$k = 4\pi\epsilon_s \left(\frac{\sigma_p^* - \sigma_s^*}{\sigma_p^* + \sigma_s^*} \right) r^3 E \tag{2.7}$$

where σ_p^* and σ_s^* are, respectively, the complex permittivities of the particle and of the solution. Depending on the dielectric properties of the molecules and of the solution, and on the electric field features, particles can move towards region of high (*positive DEP*) or low (*negative DEP*) field [24]. That is, if the particle is more polarizable than the solution, it will move towards the region of high field, and viceversa [25], thus following the electric field gradient or opposing to it. In applications involving biomolecules, positive DEP could cause the damaging of the molecules, due to a strong attraction force towards high-field region. That is why in bioanalytical applications the use of negative DEP is more desirable.
Nevertheless, designing and fabricating integrated microsystems that can fulfil the whole range of requirements for application to the life-sciences is still an open challenge. The main reason for this is that the outstanding forces at the microscale (e.g. surface tension, friction, electrostatic interactions between molecules or between a molecule and a substrate, etc. . .) are different from those playing in macroscale systems and are often more complex to manage and control for a specific purpose [18]. An additional and ineludible source of complexity is represented by the peculiarities of the handled objects. Molecules and cells have specific features and structures that determine their functionalities in a biological macrosystem. Alteration of such properties should be avoided, since it would negatively interfere with the physiological role of such objects. This is another important reason for working out specific solutions at the microscale. Several state-of-the-art examples of the most popular applications of these technologies are given in the next paragraph.

2.3 Examples of application of microfluidics to molecular diagnostics

Current standard techniques/instruments for biomolecular analysis include, among others: chromatography, gel electrophoresis, mass spectrometry. All these techniques involve procedures that require several steps before the completion. And, for each one of these steps, a particular technology/instrument is required, together with a large amount of time spent and usually high volumes of samples that are wasted at the end of the whole operation.
For this reason, the rapid growth and spreading of bioMEMS-based technologies will help in overcoming such drawbacks and in improving both quality and reliability of the results of biomolecular and genomic analysis.
MEMS (Micro-Electro-Mechanical-Systems) is the term usually employed for referring to a set of miniaturized devices, made up by electro-mechanical components fabricated with processes and technologies typical of the semiconductor industry. BioMEMS is the term used for distinguishing devices

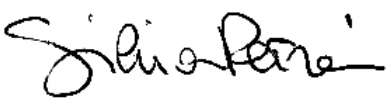

specifically developed for applications in the biomedical field (e.g. diagnostics, drug discovery, drug delivery, etc...). Some of the main applications of bioMEMS are illustrated in figure 2.3. BioMEMS include:

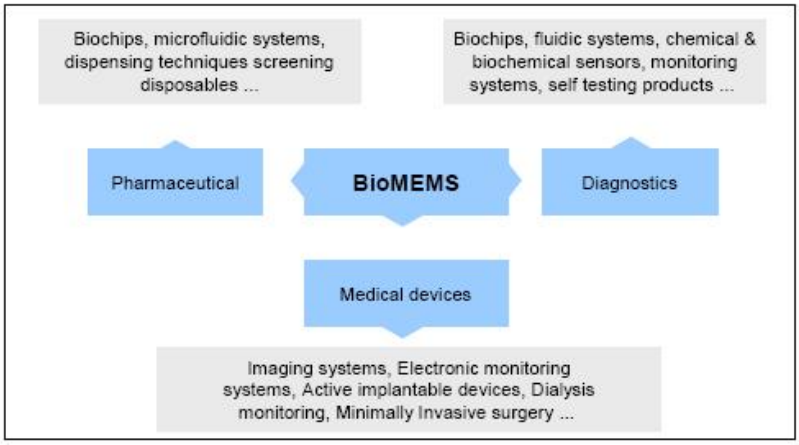

Figure 2.3: Definition and fields of application of BioMEMS according to NEXUS.

- single components (active or passive): e.g. components for micro-flow such as pumps, valves, μchannels, μchambers, etc...;
- devices encompassing several components onto a single chip: these can be μarray systems - where a solution is flown over a surface covered with arrays of molecular probes - or the so-called μTAS (micro Total Analysis Systems) or lab-on-a-chip systems, that include all the steps required for an analysis procedure, such as sample preparation, treatment and detection. In this case, the solution containing the molecules of interest flows in the system through μchannels, in order to pass from a step to the following one.

Indeed, these systems are being deeply investigated both because of the growing interest in rapid large-scale genomic sequencing [26, 27], and for overcoming the aforementioned drawbacks, allowing for an easier management of the analysis.
The basic idea of the analysis techniques that employ μarrays is that small quantities of known biological samples (usually DNA fragments) are dispensed or synthesized onto a solid micromachined surface (see figure 2.4). A portion of unknown DNA is then eluted over the surface. In this way it is possible to detect binding events, since only complementary DNA binds to the sample. Bound DNA is detected by fluorescence methods: sample DNA is usually fluorescently marked and emits light only when the sample hybridizes to the complementary probe strand [28, 29]. The readout is usually

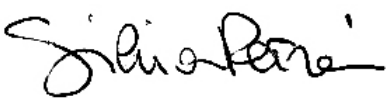

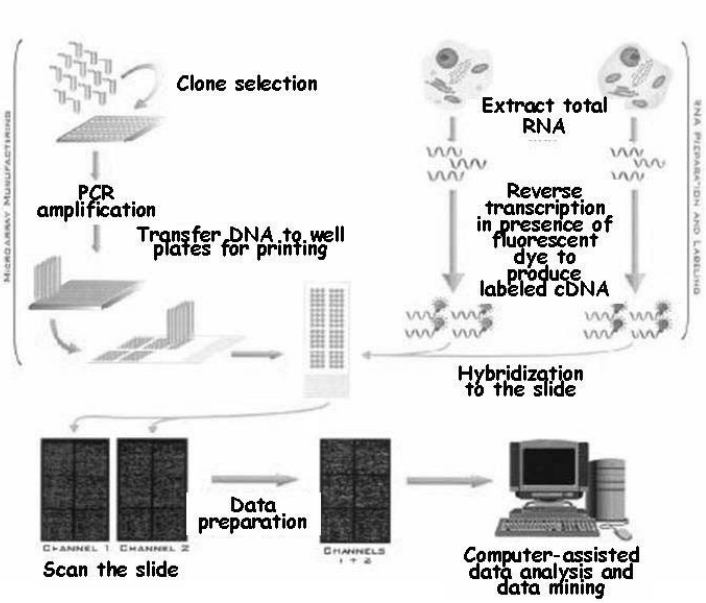

Figure 2.4: Microarray procedure: RNA is extracted from the cell of interest and it is reversed to cDNA; know DNA strands are deposited onto a solid support and the cDNA is eluted over it in order to be hybridized; then the slide is scanned with fluorescence and results are read (image taken from [2]).

performed with a laser scanning. These microsystems provide several advantages, the main one being the opportunity for high information density when performing many parallel analyses [30]. They also allow for a very low sample consumption and consequent cost savings [31, 32].
Microarrays can be manufactured in two ways: synthesizing molecules directly on the support, one residue at a time, after activation of the solid slide by a photolithographic mask; or directly delivering the molecules onto the substrate, by using microdispensers (arrayers) [33, 34]. In this last case, accurate molecules manipulation and precise dosing is the major matter of the whole process. The equipment needed for performing the delivering of samples is usually made up by a Cartesian robot (known as arrayer), provided with a spotter that moves along a workbench on which hundreds of solid supports are placed (see figure 2.5). The solid support is usually a silicon plate, containing an array of wells. Modern arrays can contain up to 10^5 wells for DNA hybridization. The spotter delivers known quantities of samples, employing different dispensing techniques, based on microfluidics or electrokinetic principles [30, 35, 36]. A schematic classification can be used to sort dispensing techniques, respectively, in:

- *Contact dispensing*: pen tips or mechanical pins use capillarity prin-

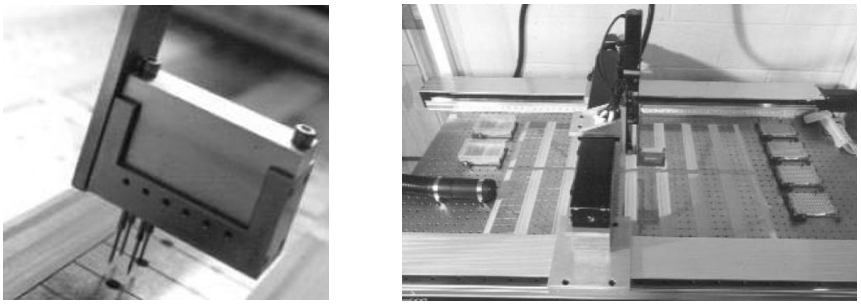

Figure 2.5: The AECOM arrayer print-head, equipped with four of the 12 possible stainless steel pen tips (left). The AECOM workstation, with the wash stations and the dryer on the left and the micro-plates on the right (right). Image taken from [30].

ciples for dispensing quantities of samples (*solid-solid contact*) [5]; alternatively, liquid droplets may be generated inside a microchannel by electrowetting or thermocapillarity before their actual dispensing (*liquid-solid contact*) [20]).

- *No-contact dispensing*: droplets are produced by piezoelectric compression of a small deformable cavity; otherwise a heater in the printhead superheats the liquid so that a vapour bubble is formed. The bubble pressure rises inside the chamber until it ejects a droplet of liquid through a microfabricated nozzle [34].

Each spotted droplet is about $100 - 150\mu m$ in diameter. The high number of samples that can be analyzed at the same time makes this technology the optimal solution for obtaining high information density with a reduced sample consumption.
Several examples of arrayers can be found at research level. One of the early research institutes that built an arrayer is the Stanford University: the Stanford arrayer was designed and developed by J.L. DeRisi and P.O. Brown, who made available on their lab site a complete guide to easily and cheaply build an arrayer (http://cmgm.stanford.edu/pbrown/mguide/index.html). They built gene microarrays for investigating gene expression profiling [37, 38, 39].
One of the most critical issues in the spotting process is to ensure a good level of repeatability, meaning that each pin has to deliver equal volumes of solution onto each spot, in order to generate valid data and provide reliable results. By using contact dispensing techniques the spots dimensions depend both on the moving speed of the pen tip and on the surface features of the slides. Since surface tension is the key mechanism, spot shape and volume strictly depend on the pin material, shape and diameter.
As an alternative to the standard pen tips, Belaubre and co-workers deve-

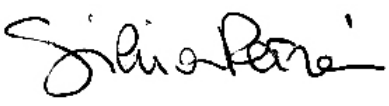

loped and fabricated some silicon-based microcantilevers for sample deposition [27]. The microcantilevers are built using standard microfabrication techniques. Spots of about $10-30\,\mu m$ in diameter have been obtained. One of the main drawbacks of the microcantilever deposition method is that spot size and shape are closely connected with the intensity of the contact force, that lacks of an effective control system. So this was not the optimal solution for gaining a good repeatability.
As we already mentioned, the most conventional no-contact dispensing techniques consist in forming a liquid droplet inside a chamber, and then ejecting it through an orifice by piezoelectric or thermal actuation onto the support. Beyond giving a good level of repeatability, these dispensing techniques result more suitable for being applied even in low-cost applications. The most well-known example of this, is the use of commercial standard ink-jet printers for dispensing biomolecules. In commercial print-heads, in fact, ink ejection may be driven either by piezoelectric actuators or by bubble-jet (thermal) technology.
Roda and co-workers developed a dispensing system by adapting a commercial piezoelectric ink-jet printer for dispensing proteins and other biological samples in droplets of about $200\,\mu m$ in diameter with a good repeatability [40].
Goldmann and Gonzalez used a commercial inkjet printer to deliver DNA segments onto solid supports for high density microarrays [41].
Xu and colleagues recently used a commercial thermal inkjet head for dispensing mammalian cells and motoneurons [42]. After operating several modifications on the printer, they showed that it is possible to deliver living cells onto a support without excessive damage: less of 10 % of the cells resulted damaged. They found that this technique has several drawbacks when used with biological molecules. For instance exposing DNA to temperatures as high as $200\,^{\circ}C$ [43] may cause the molecule denaturation and the loss of its properties. The same can be said in case of exposure of the molecule to high shear stresses.

Beyond the μarray field, many other solutions are currently under investigation concerning μTAS, with the aim of developing more and more automated devices for performing molecular analyses onto a single chip, mainly to reduce operation time, sample volumes, and the complexity of the procedures that at present are employed.
This class of devices may be fabricated using different materials: silicon or glass (typical of the microelectronics industry), polymers or biological material [44]. In particular, among polymers, the most employed is the (poly)dimethylsiloxane (PDMS), thanks to its properties that include [45]: optical transparency in the UV and visible; possibility of being used in rapid prototyping techniques such as soft lithography, that do not require highly controlled environments (e.g. cleanroom); low-cost; and possibility of

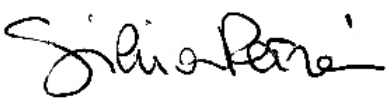

being sealed (either reversibly or through an irreversible plasma oxygen) to silicon, glass and PDMS, thus allowing fabrication of more complex structures [46, 47].
Also due to the growing number of possibilities offered by new materials and technologies for fabricating such kind of devices, research is rapidly stepping forward in the development of more and more miniaturized systems, encompassing all the main analysis capabilities that a molecular analysis lab has. On the whole, a common trend can be identified, that could be defined "lab-on-a-chip-oriented": the basic idea is to exploit the advantages of both microfluidic techniques and miniaturization technologies for developing a system that could be used even for self-testing directly from patients.
As an example, several clinical studies in literature show how the presence of a polymorphism in a specific nucleotide (Single Nucleotide Polymorphism, SNP) may be an indicator for several pathologies, e.g. cardiovascular diseases or several classes of cancer [48]. For this reason, many current investigations aim at developing devices for detecting such mutations, in order to perform a very early self-diagnosis, thus offering the opportunity for developing, as an example, extremely targeted or preventive therapies.
Indeed, great improvements could be achieved in this field with the development of a portable and completely automated system, that, starting from a simple biological sample (e.g. a blood drop), detects the presence of such mutations. Such a system should implement several procedures onto a single chip. A typical sequence of steps for this kind of analysis could be as follows: DNA extraction and amplification through PCR, hybridization, laser scanning and fluorescence readout. A possible conceptual scheme of this sort of device is shown in figure 2.6.
As an example, a couple of commercial systems can be found, that are simi-

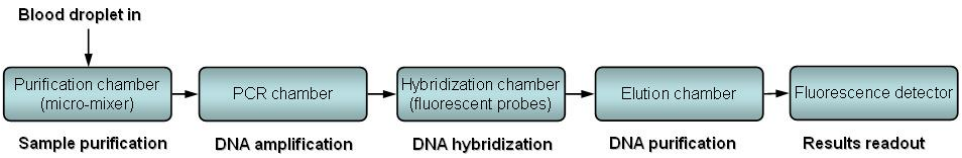

Figure 2.6: Possible conceptual scheme of a μTAS: the analysis steps go from sample extraction to results readout on-chip.

lar in structure to the aforementioned one [49]: the Biosite (http://www.biosite.com/) diagnostic kit device (see figure 2.7, left), that is able to diagnostic a heart attack condition in 10-minute time, only by automatically processing a blood drop; and the i-STAT device, marketed by Abbott Laboratories (http://www.i-stat.com/), that in few minutes can provide several kinds of blood analyses starting from few blood droplets (see figure 2.7, right).
Several solutions can also be found in the literature, concerning both the

Figure 2.7: The Biosite (left) and I-stat (right) diagnostic kits.

single step and the development of integrated lab-on-a-chip systems that perform the whole analysis procedure. The development of miniaturized integrated systems embedding several parallel operations onto a single automated chip to be applied for molecular diagnostics has been a much investigated research theme for almost two decades in the field of life-sciences, especially due to the possible impact on population quality of life [1, 50, 51]. In most cases, for performing analyses starting from a biological sample such as a blood drop, several operations of sample pre-treatment are needed. Such operations often consist of molecule extraction and purification, reagent mixing, and sample amplification. The so-obtained DNA molecule can then be labelled with fluorescent dye and moved to the hybridization chamber, where there are DNA probes that link only to their complementary strand (*hybridization*). After a purification step, they pass through a laser source, in such a way that fluorescence of bound strands is detected (only hybridized strands emit light).
As it can be found in the literature, extraction and purification of nucleic acids can be carried out either performing sorting through capillary electrophoresis (CE, especially for DNA strands) [52], either inside a microfabricated chamber, where samples undergo a mixing operation with other reagents. Such reagents may be introduced through a network of microchannels, and they cause cellular membrane lysis first, and, through subsequent reactions, the isolation of the molecule of interest [53].
DNA amplification must be performed through thermal cycling of molecules, as in conventional PCR systems. An example of microfabricated PCR chamber can be found in [54] (see figure 2.8). The solution is flown through a microfabricated serpentine-like channel, that is placed upon regions kept at different temperatures. By passing through these regions, the fluid performs the desired thermal cycling, and the DNA is amplified as many times as the number of completed cycles.
Hybridization step happens inside a microfabricated chamber, where probe

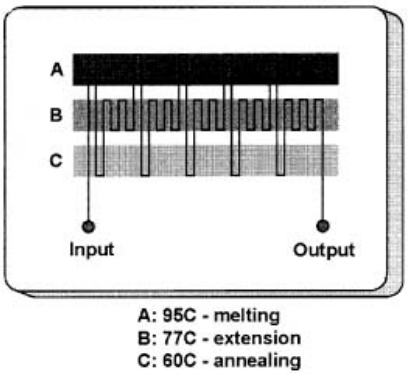

Figure 2.8: The serpentine-like channel used for performing PCR cycle. Image taken from [54].

strands are immobilized, as in the standard microarray procedure.
The readout of the results is usually performed with fluorescence scanners, but several other techniques are currently under investigation. As an example, magnetic nanoparticles may be used instead of fluorescent markers, and an on-chip readout can be performed by using magneto-resistive sensors that measure the magnetic field produced by the hybridized probes [55]. Another solution is to employ conductive particles (e.g. gold or silver) for measuring hybridization through current measurements (Direct Current Electrical Detection, DCED) [56].

From the reported literature analysis, the liveliness of research activity in the field of bioMEMS clearly emerges. This is because microfluidics and miniaturization technologies offer several advantages with respect to traditional procedures, the main ones being saving of sample volumes, reduced analysis time, increased reliability and quality of results, and possibility of lowering costs. Moreover, with the use of polymeric materials and rapid prototyping techniques the development of rapidly marketable devices could also be obtained.
The majority of the solutions so far developed is aimed at performing large scale high-throughput and parallel analyses, with a high level of automation, onto a single μsystem. It is clear that such technology trend is going to be applied more and more frequently in fields such as molecular diagnostics, genetic screening and new drugs development.
The main issues that still remain open, and could be better referred to as future challenges, are: the development of an effective power source easily integrable in a miniaturized system, to allow a real portability of such systems; moreover, the aforementioned electrokinetic principles still bring several drawbacks, being strongly dependent both on the fluid and on the

solid (channel) properties; in addition, electrolysis bubbles may occur near the electrodes, thus lowering pumping efficiency; Last but not least, a high level of biocompatibility must be guaranteed, either for bioMEMS that are going to be implanted in the human body (e.g. for drug delivery), and for systems that do not have to work inside the body, but have to treat biological material, that cannot be altered in properties during the analysis procedure.

2.4 Novel technologies for bioassays

In the following two sections two feasibility studies are reported, that we carried out in our lab, concerning the development of novel microfluidic technologies for bioassays.
The first case can be defined an "incremental" innovation, because an existing technology is modified and adapted to be employed with biological materials. The second work concerns a completely novel technique, whose feasibility is investigated through modelling and simulation operations, that can be used for performing thermal cycling of biological samples in a microfabricated chamber, as a first step in a completely automated lab-on-a-chip , similar to the one described in the previous section in figure 2.6.

2.4.1 Low-cost dispensing technologies for biomolecules

Taking into account that annual sales for immunoassay reagents and supplies are valued about 2 billion dollars in the US and 7 billion dollars worldwide, developing microfluidic immunoassays is a strongly pursued trend in bioanalytical research [57].
As already cited in the previous section, commercial ink-jet printers are low-cost systems which enable the rapid dispensing of few-picoliter droplets (less than $20\,pl$) at a high rate rate ($>\ 10\,kHz$ per nozzle) [58, 59]. Their dispensing flow-rates are on the order of $350\,\mu l/min$. Therefore it is worth investigating whether commercial heads, relying on a well-assessed and well-established technology, could be adapted for the assembly of low-cost and high-performance biomolecules dispensers.
For this reason, as other research group did (as cited in section 2.3), in our group we adapted two commercial printers, a piezoelectric and a thermal one, for the dispensing of immunoglobulines onto an ELISA (Enzyme-Linked ImmunoSorbent Assay) plate [60]. The aim of the study was to compare these two technologies to find out which one, if any, is more suitable, in terms of hardware modifications, for the dispensing of this class of bio-molecules. It must be underlined that the shear and thermal stresses caused by the droplets ejection mechanisms could be a possible source of biomolecules damaging. Therefore, it is also necessary to test the functional activity of

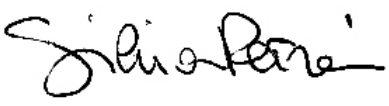

the bio-molecules after their dispensing, and the ELISA assay was also used to evaluate such activity on the ejected biomolecules.
ELISA [61] is one of the most widely used analytical techniques for the detection of antigens or antibodies in a sample. The ELISA protocol uses two antibodies, one of which is antigen-specific while the other is coupled to an enzyme. The latter one, referred to as conjugate, gives the assay its *enzyme-linked* name, and induces a chromogenic or fluorogenic substrate to produce a color change in the solution.
Two commercial ink-jet printers were used: a HP Deskjet 5740, based on thermal technology, and an EPSON Stylus C46, based on piezoelectric technology. These two models were chosen because, according to the Manufacturers' specifications, they have similar flow rates, which was confirmed by experimental measurements. As previously said, the working principle of the thermal technology is based on the generation of vapor bubbles by heating the liquid, which is confined in a series of micro-chambers. The heat is produced by resistors, having a typical size of few tens of microns, located beneath the floor of the chambers. As vapor bubbles expand, the liquid is pushed away and droplets are expelled from the nozzle [62]. Piezoelectric printheads, instead, expel ink droplets by means of piezoelectric crystals, whose deformation pressurizes the fluid contained in a series of chambers, thus expelling droplets through the nozzles [63].
Both the printers underwent only hardware modifications, i.e. the drivers were kept unmodified and the dispensed solutions were not altered in their wetting properties.
In the thermal printer the polyurethane sponge soaked with ink contained inside the cartridge was replaced with a clean one; then the paper feeding mechanism was removed, in order to place the ELISA plate under the printhead; the paper feeding optical sensor was also removed; eventually, a proper signal, produced by a MATLAB routine, was sent to the printer motherboard, emulating the signal produced by the paper detector during a regular printing session, thus allowing the continuous dispensing without further modifications to the drivers.
The hardware of the piezoelectric printer was modified as follows: an external feeding kit was used, with four reservoirs (for black and colour inks) and feeding tubes connected to clean print cartridges (EPSON T036); again, the paper feeding mechanism was removed and two supports were built and fixed to the printer to hold the ELISA plate under the printhead; the paper sensor could not be removed as it also sensed the home position of the printhead; and again, a proper square signal was produced by a MATLAB routine and sent to the printer motherboard, thus allowing a continuous dispensing process.
The two printers after modifications look as shown in figure 2.9.
For each test 7 wells of a standard ELISA plate were filled: three wells contained the Positive, Negative and Cutoff Control, while 4 wells contained

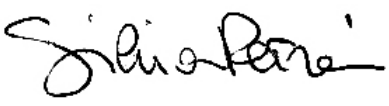

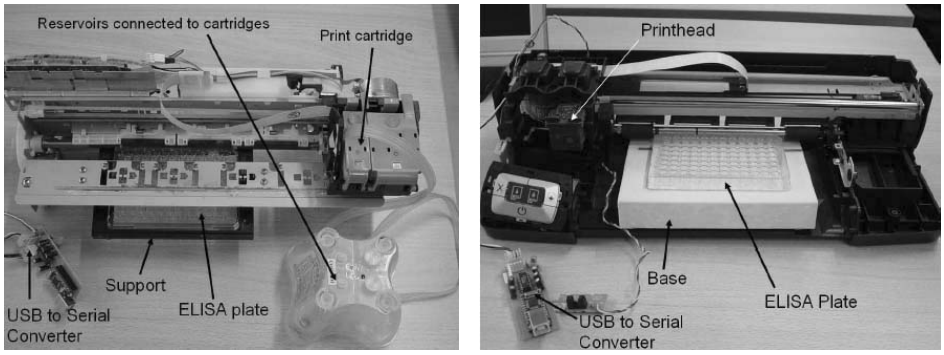

Figure 2.9: The piezoelectric (left) and thermal (right) printer after hardware modifications, ready for the dispensing of immunoglobulines onto the ELISA plate.

serums from 4 patients. The test procedure includes the following steps:

1. dispensing of controls and pre-diluted patient samples into the wells;
2. incubation for 30 minutes at room temperature $(20 - 28\,^{\circ}C)$;
3. the contents are discarded and the wells are washed 3 times with $300\,\mu l$ of washing solution;
4. dispensing of $50\,\mu l$ of enzyme conjugate solution into each well;
5. incubation for 15 minutes at room temperature;
6. the contents are discarded and the wells are washed 3 times with $300\,\mu l$ of washing solution;
7. dispensing of $100\,\mu l$ of substrate solution into each well;
8. incubation for 15 minutes at room temperature;
9. adding of $100\,\mu l$ of stop solution to each well and incubation for 5 minutes at room temperature;
10. reading of the optical densities at $450\,nm$ and calculation of the results.

All these steps were performed manually with a micropipette, except for the enzyme conjugate solution dispensing, which was performed with the printers. The optical densities were read using a DAS Plate Reader (DAS s.r.l, Palombara Sabina, Rome).
Results are shown in figure 2.10.

While the piezoelectric head was able to dispense an enzyme conjugated solution, giving results comparable to those achieved by manual dispensing, the thermal head often underwent clogging phenomena which prevented it

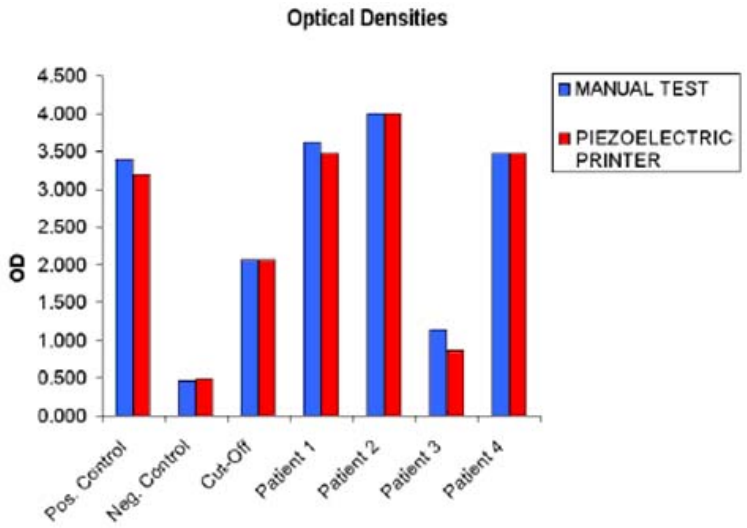

Figure 2.10: Results of the ELISA test: the optical densities of different samples are compared, as results of a manual (blue) or piezoelectric dispensing (red).

from dispensing the solution.
As it can be seen from the results, the optical densities values show no significant difference between the manual test and the one performed with the piezoelectric printer, proving that the dispensed immunoglobulines did not lose their binding ability after the dispensation.
From these analysis we can conclude that the qualitative outcomes of the two tests are identical. But, what is more interesting, the differences in ODs are small enough not only as to preserve the outcome of the tests but also in absolute values. In particular, the % OD difference in the two tests for the three controls and two patients (1 and 4) are around 6%, a value very close to the coefficient of variation 2 of the test, as reported in [64]. This not trivial result indicates that the binding ability of piezoelectrically dispensed immunoglobulines are not significantly altered by the deposition process. Therefore the shear stress during drops ejection is not sufficient to cause important molecules damaging. This conclusion, which can be drawn for each of the seven samples, is statistically significant.
Last but not least, each deposited sample is generated by a large number of droplets ejections: being each droplet about $6\,pl$ in volume, about $8 \cdot 10^6$ droplets are required to deliver $50\,\mu l$ of solution. This also confirms the excellent level of repeatability in the spotting process.

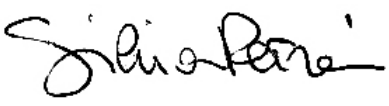

2.4.2 On-chip sample amplification technologies: a feasibility study

Beyond performing PCR thermal cycling through a microfabricated serpentine-like channel with different temperature zones, another possible solution for the amplification step onto a μTAS can be derived from the motion of fluids through the Rayleigh-Bénard convection together with the use of electrokinetic principles.
Rayleigh-Bénard convection is caused by buoyancy-driven instability in a confined fluid layer heated from below [65]. The dimensionless Rayleigh number Ra expresses the interplay between buoyant forces driving the instability and diffusive restoring forces acting in opposition. Convection occurs when Ra rises beyond a certain critical value (that is, around 2000).

$$Ra = \frac{\text{buoyancy force}}{\text{viscous force}} \cdot \frac{\text{heat transport by convection}}{\text{heat transport by conduction}}$$

Starting from this phenomenon, since PCR consists in performing thermal cycling among three different temperatures, in order to amplify DNA strands, we studied the feasibility of a microfabricated system for performing PCR based on Rayleigh-Bénard convection, by controlling only two temperatures, respectively, a hot one, at the lower base of the chamber, and a cold one, at the top base of the chamber.
However, since such convection occurs only for a certain value of Ra, that depends, among others, also on the temperature difference between hot and cold wall, and since PCR needs three specific temperatures (i.e. around $95-60-75\,^{\circ}C$) for correctly performing DNA amplification, what is needed is a sort of "driven" convection. That is, it should be possible, by keeping two chamber walls at two desired temperatures, to move the fluid, in order to drive it through the desired temperature zones.
A similar operation was performed by Gonzalez, Green and co-workers [66, 67, 68]. They used electrokinetic principles for moving a certain amount of fluid, with electrolytes inside, in a microfabricated chamber as follows: two coplanar electrodes are placed at the bottom of the chamber (see figure 2.11), separated by a small gap; by applying an ac voltage to such electrodes the fluid starts moving with electroconvective whirling motion, as shown in figure 2.12. This fluid motion is observed only at low frequencies, that is, well below $1\,MHz$. An electric double layer is formed between the solid base and the liquid layer. The force induced by the electric field set the liquid in motion, in a direction that is always from the electrode edge, onto the surface of the electrode (i.e. parallel to the electrodes and directed away from the gap), towards the chamber side walls. The magnitude of the fluid velocity is frequency dependent, tending to zero at low and high frequency limits.
Figure 2.13 shows the whirls produced in [68], together with the simulations,

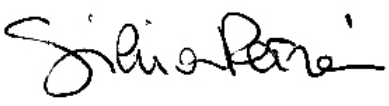

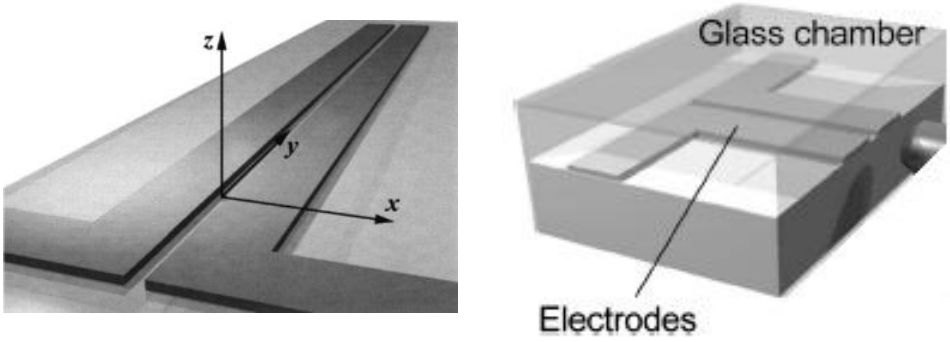

Figure 2.11: The two coplanar electrodes (left) and a view of the microfabricated chamber (right). Image taken from [67, 68]

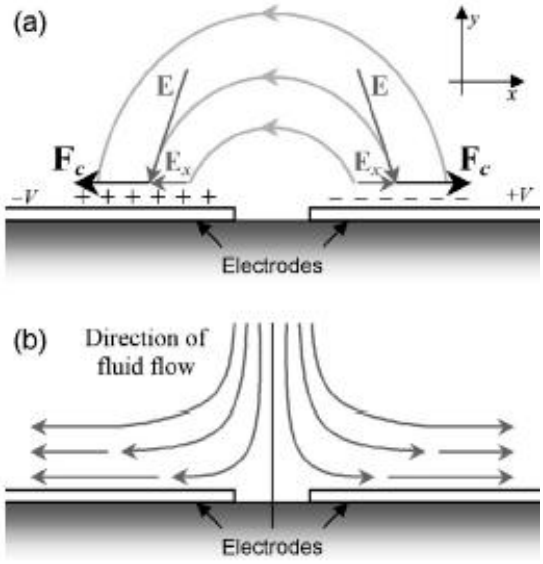

Figure 2.12: The electric field applied at the electrodes (a). The streamlines of the fluid set in motion by the ac applied voltage. Images taken from [68]

for different frequency values.

If the lower base is kept at a high temperature, the fluid is heated, its density lowers, and it is pushed up to the top cover. Here there is the cold wall, so the liquid density increases again, and the fluid is pushed down towards the electrodes. Once inside the electrical field effect, the liquid whirl starts again, until the field is applied.

As a feasibility study we applied the same approach found in [66], and already applied in [69], to a chamber where the hot and cold wall are ,

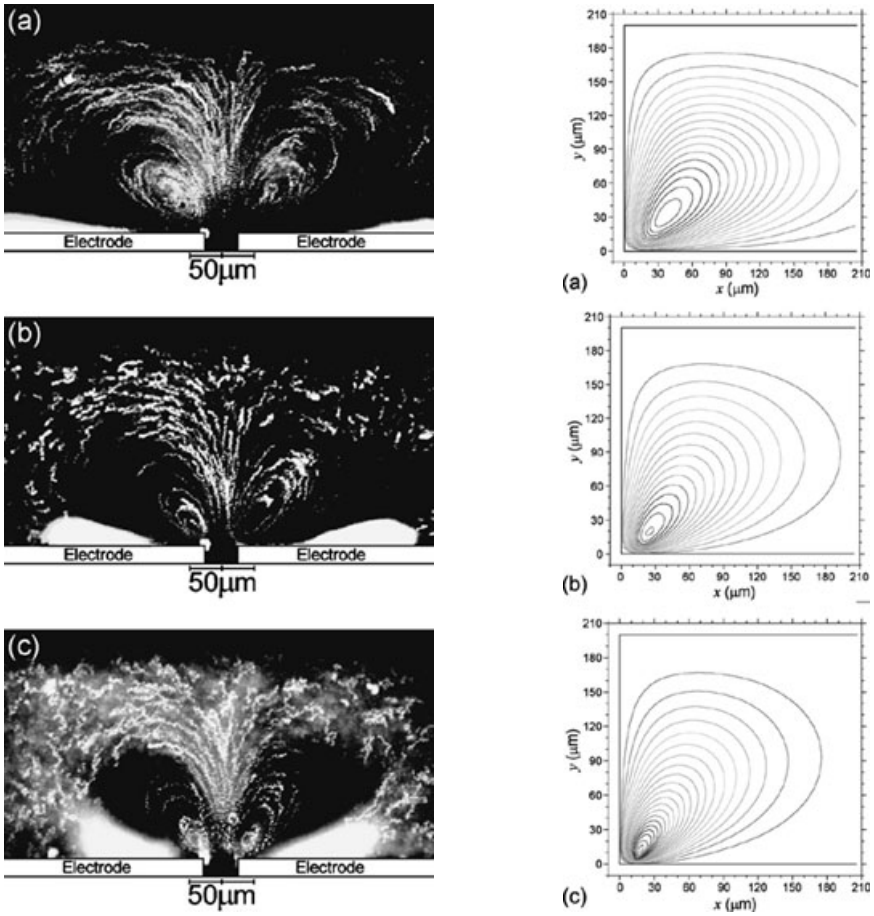

Figure 2.13: The whirling motion of fluid inside the micro-chamber (left). A simulation of electroconvective fluid motion in one-half of the chamber (right). Images taken from [68]

respectively, the minimum and maximum temperature values of the PCR cycle. We used a software for multiphysics modelling (COMSOL Multiphysics, www.comsol.com) of the whole system.
Following the hypotheses made in [66], we designed a 2-D rectangular chamber with dimensions $225\,\mu m$ (base) and $100\,\mu m$ (height). The electrode length is $200\,\mu m$ and the gap is $25\,\mu m$.
At first, we decided to keep the hot wall at $99\,^{\circ}C$ and the cold wall at $67\,^{\circ}C$. We coupled thermal and fluidic problems, by using conductive and convective heat transfer equation, and Navier-Stokes equation for incompressible fluids. Chosen boundary conditions were [66]:

- y-axis symmetry;
- constant temperature T_h and T_c for the hot and cold walls, and heat insulation for the side walls;

- no-slip condition on the side and top walls and on the gap;
- slip velocity on the electrode derived from the Helmoltz-Smoluchowski equation and equal to [66]:

$$U = -\frac{\epsilon V_0^2}{16\eta}\Lambda\frac{\partial}{\partial x}\left|F\left(\Lambda\frac{\epsilon\omega x}{\sigma\lambda_D}\right)\right|^2, \tag{2.8}$$

  where ϵ is the fluid permittivity, V_0 is the amplitude of the applied voltage, η is the dynamic viscosity of the fluid, Λ is a dimensionless number, indicating diffusivity properties of the double layer, ω is the angular frequency, σ is the electrolyte conductivity, λ_D is the Debye's length;
- the applied voltage at the electrodes has the following expression:

$$V = V_0 \cos\omega t,$$

  where the amplitude varies between $1 - 2.5\,V$ and the frequency is also varied in different simulations, since on it depends the fluid velocity (as it is shown in figure 2.14).

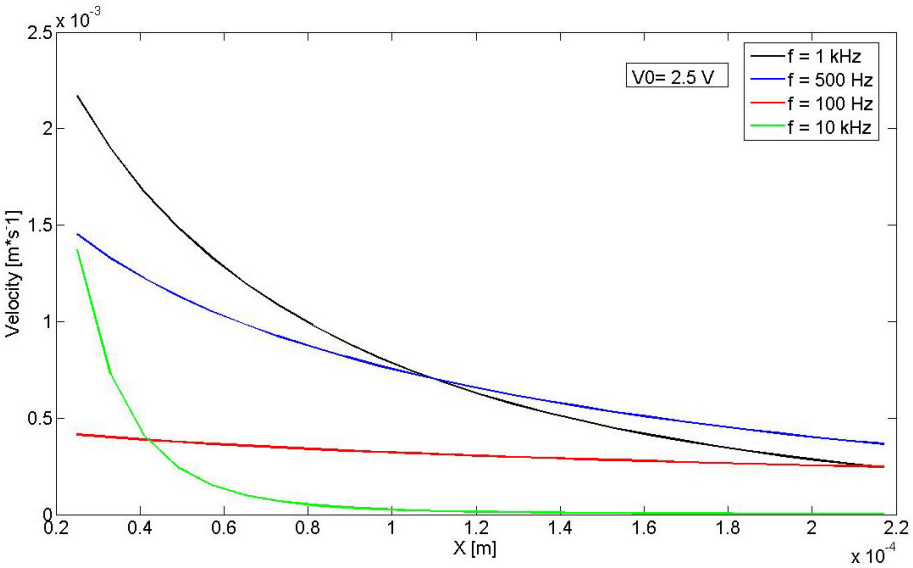

Figure 2.14: Fluid velocity trend along the electrode for different frequency values (source: our simulation).

Due to the y-axis symmetry of the problem, we only studied the behaviour of one half of the chamber, on one electrode and on half the gap (that in [66] is $50\,\mu m$), since the obtained results can be easily extended to the left half

of the chamber.
Moreover, we assumed to work with only water, since, for diluted solutions, fluid properties are not significantly different from water.
Figure 2.15 shows the whirling motion of fluid in the chamber, as resulting from our multiphysics analysis.

In order to evaluate the actual portion of fluid performing the whole cor-

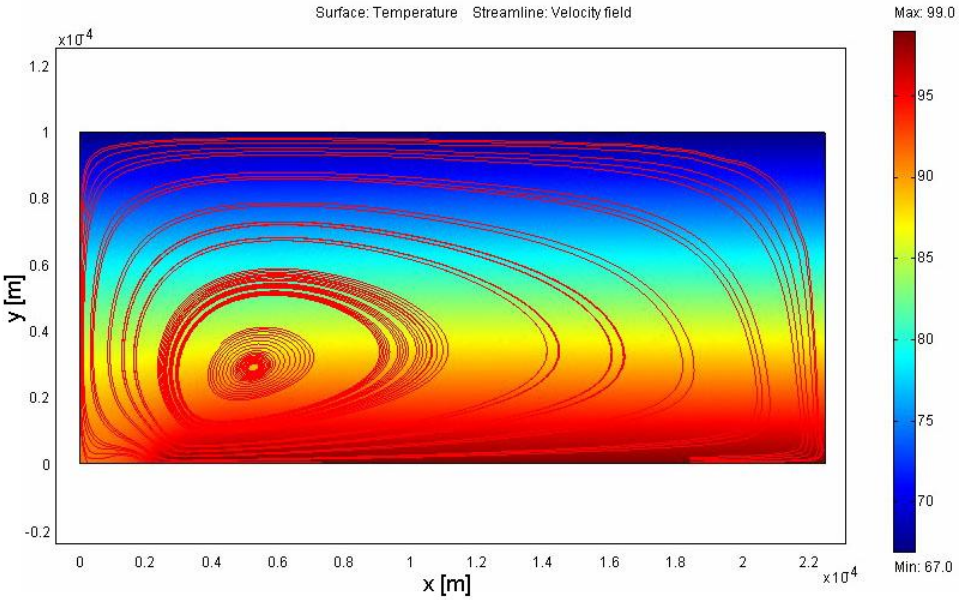

Figure 2.15: Simulations results, showing the fluid whirlpools streamlines inside (half) the micro-chamber. The temperature gradient is also shown on the background.

rect thermal cycling, we exported a grid of velocity values from COMSOL to Matlab; here, through linear interpolation, we found velocity values for other unknown coordinates values; every found velocity value was integrated in order to find the coordinates of the fluid trajectory. An example of performed trajectory is shown in figure 2.16 (A). All the y-trajectory components were subsequently associated to a temperature value, since in the chamber, the temperature y-gradient is uniform, in order to obtain the performed thermal cycle. Results are shown in figure 2.16 (B).
After finding fluid trajectories, we had to evaluate the portion of fluid passing through the three right temperatures, in order to perform the PCR thermal cycling. All the fluid whirls passing through these temperatures were selected, and the percentage on the total fluid volume was then evaluated.
As a first result we found that, with a $\Delta T = 99 - 67\,^{\circ}C$, no fluid was found

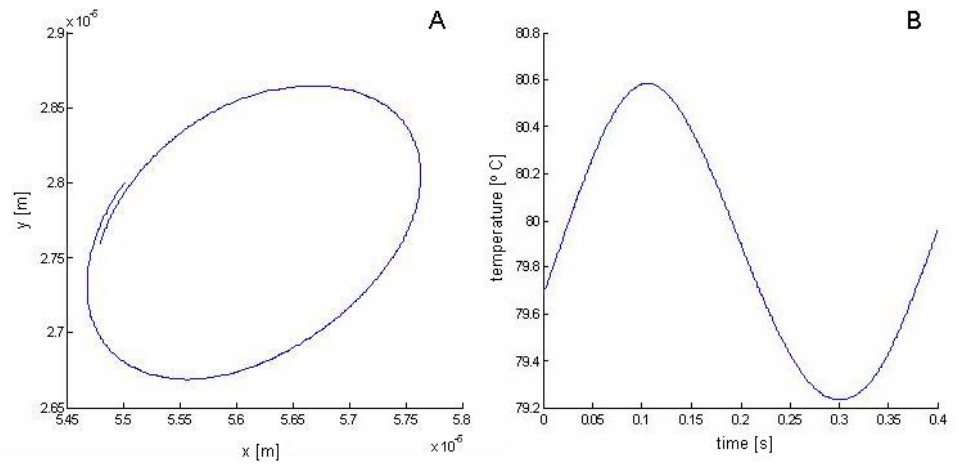

Figure 2.16: Trajectory performed by a fluid particle having initial point $x = 5.5 \cdot 10^{-5}$ and $y = 2.8 \cdot 10^{-5}$ (A). Temperature values crossed by such particle (B).

performing the desired thermal cycle. For this reason, we had to optimize the temperature difference, in order to obtain as much fluid as possible performing the PCR cycle. In doing this, we acted only in reducing the temperature of the cold wall: as a matter of fact, we could not increase hot wall temperature, since at $100\,°C$ there is water boiling. Several results of different ΔT are shown in table 2.1.

As it can be seen, the highest percentage of fluid passing through the de-

Table 2.1: Percentage of fluid volume passing through the desired temperatures with respect to different temperatures values of the cold wall.

Temperature $[°C]$	**% Volume**
66	0 %
61	0%
56	0%
51	5.96 %
46	10.13 %
41	9.28%
36	18.26%
31	6.92%

sired temperatures is obtained for a $\Delta T = 99 - 36\,°C$, and is equal to 18.26%.

On the whole, our feasibility study ended with the following conclusions:

- It is possible to perform a PCR-like thermal cycling inside a miniaturized structure by using electrokinetic principles, such as electroosmosis, for moving the fluid.
- Even after the optimization of the ΔT inside the chamber, only a small percentage of the total volume (i.e. 18.26 %) performs the whole cycle.
- Another possible way for increasing the volume of fluid performing PCR could be acting on chamber geometry.

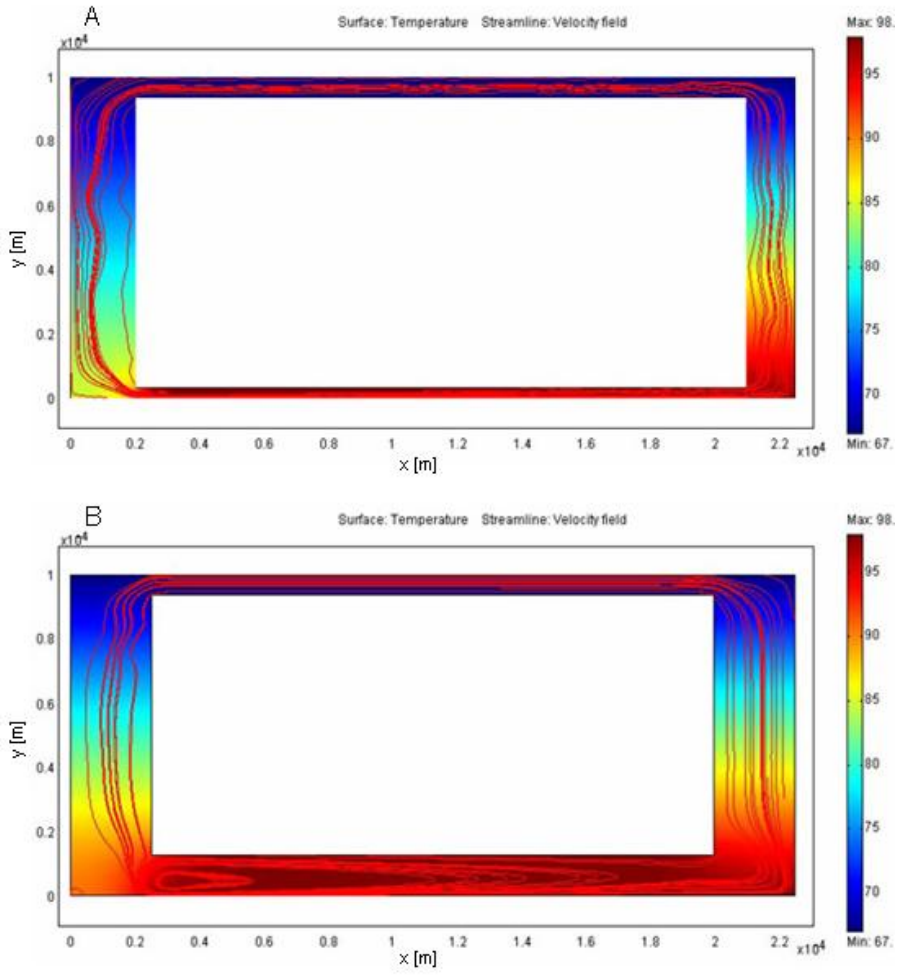

Figure 2.17: Simulation results after geometry variation, through the insertion of a conductive bar. The fluid is forced to perform larger whirlpools, thus passing through the desired temperatures.

As an example, simulations were performed after inserting a conductive bar inside the chamber, in order to force all the contained liquid to pass only through certain temperature zones (i.e. the desired ones), performing larger whirls, as it is shown in figure 2.17.

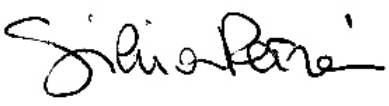

Chapter 3

Biomechatronic design and development of a novel system for drug delivery to the brain

As stated in the introduction, within the investigation on microfluidic applications to the biomedical field, this chapter relates to the design and development of a novel drug delivery device, specifically intended for the cerebral compartment.

3.1 Introduction and state of the art: drug delivery to the CNS

Administration of chemotherapeutic agents to the Central Nervous System (CNS), and in particular to the brain tissue, is at present a not completely fulfilled target and brain tumours are still a major cause of death. The American Cancer Society estimates that in 2002 there were 189,485 new cases of cerebral and nervous system tumours all over the world, and 141,650 of them were fatal. Incidence of this kind of tumour is of 3.7 males and 2.6 females every 100,000 inhabitants, with higher values in the most developed countries [70].
The difficulty in the treatment of such kind of pathologies is due to several reasons. First of all the anatomic location is very sensitive and difficult to treat with a drastic surgical removal of the affected tissue: for this reason relapses can often be fatal. Secondly, affected tissues are highly vascularized and their internal pressure is higher than that of the surrounding healthy tissues, and this prevents drugs from effectively penetrating

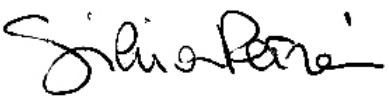

into the core of the tumour [71]. Besides, the whole intracranial compartment is protected by a group of physiological mechanisms, collectively called *Blood-to-Brain Barrier* (BBB), that prevents the brain tissue to be reached by any kind of substance coming from the systemic circulation out of the nutritional ones [72, 73, 74, 75] (i.e. glucose, oxygen and carbon dioxide).
Beyond the standard treatments used for cancer, i.e. surgery, systemic chemotherapy, radiotherapy and stereotactic radiosurgery (SRS), research in this area is at present focused on two fields: the research of new drugs and the development of novel ways for administering them. Concerning the ways for administering drugs two main possible solutions are at present under investigation, that differ on the way the drugs are carried into the brain tissue. The first one is based on diffusive transport and uses implantable polymers charged with drug that is released as the polymer degradation goes on. The second is a mainly convective transport, accomplished with an implantable infusion system, made up of a reservoir and a pump that drives the drug through a flexible catheter into the site of injection.
Since it is shown that penetration depth is significantly enhanced with high-flow convection-based drug delivery [76] (see figure 3.1), and since implanted polymers are out of the aim of this work, we will focus on convective drug infusion through implantable devices.
The early human implants of infusion devices were in the middle Seventies

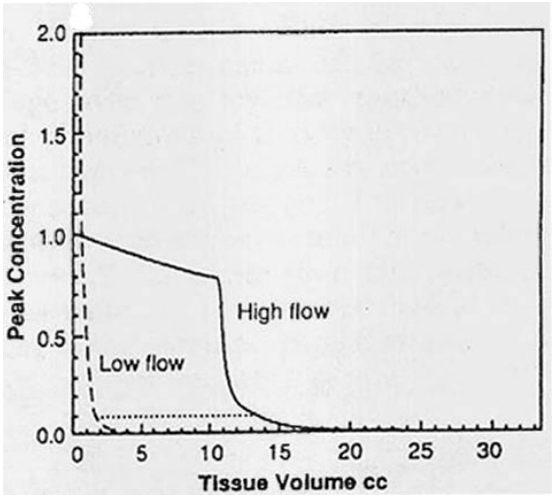

Figure 3.1: Comparison of penetration depth between low-flow and high-flow drug delivery. Image taken from [76].

and had been developed for systemic infusion of heparin [77]. After a few years Medtronic Inc. developed and marketed implantable systems for site-specific drug delivery [78].
A standard implantable drug infusion device consists of five main parts:

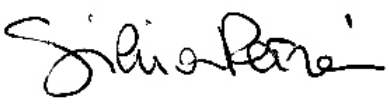

- a reservoir filled with drug;
- an actuation mechanism (usually a pump, or a chamber with pressurized fluid);
- a catheter to connect the outlet of the pump with the needle;
- a needle for the infusion into the tissue;
- electronic circuitry, involving the power supply and the controller.

As an example, figure 3.2 shows the latest model of the Medtronic Synchromed implantable infusion pump, that is used for intrathecal drug administration for chronic pain treatment or for administering chemotherapy to liver metastases or kidney carcinoma, or in the management of severe spasticity.

The early developed infusion devices were provided with constant flow

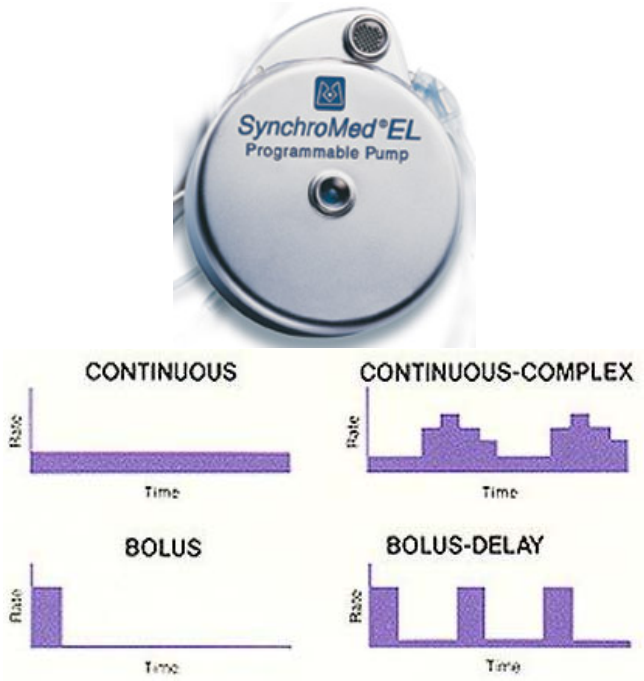

Figure 3.2: Medtronic Synchromed implantable infusion pump and the infusion modes that can be set on the pump.

pumps, that pumped a pre-programmed constant quantity of drug. At present most of the implantable drug delivery devices are equipped with a programmable variable-flow pump (http://www.medtronic.com). The reservoir and the pump are usually contained inside a metal case, equipped with an inlet port for the syringe needle used to fill the reservoir from the outside.

Table 3.1: Functional and safety issues related to direct drug infusion into the cerebral tissue.

Functional limitations	**Safety limitations**
Lack of effective penetration depth (only about $0.5\,cm$)	Lack of intracranial pressure control
Lack of infusion uniformity in administering the drug	Lack of compliance and adaptability to the cavity left after tumour resection

However, at present, a specific application of such class of devices to the administration of drugs into the cerebral tissue is still lacking [71], and standard implantable drug delivery devices do not work effectively with brain tumours. The main limitations related to the use of standard drug delivery devices into the brain tissue can be classified as functional and safety issues and are summarized in table 3.1. Since marketed devices do not fulfil the requirements of table 3.1, we propose the development of an innovative drug delivery system, specifically devised for the brain tissue, having the following features:

- high-flow infusion to enhance penetration depth (up to $2-3\,cm$);
- multiple needles to guarantee an uniform infusion;
- active control of ICP using direct pressure measurements;
- compliant catheters and needles.

A functional diagram of the proposed device is shown in figure 3.3.

As a first step, a modelling procedure has been carried out, that involved first a modelling of the infusion device, then a modelling of the cerebral dynamics. Finally, the two models were coupled together, drug infusion was simulated and system responses were analyzed. Simulation results helped in the dimensioning of several components for the infusion system. Moreover, with the modelling of the cerebral dynamics, we could define all the components for a simulator, which we are up to use for an early *in vitro* testing of the device prototype, that replicates the behaviour of the intracranial compartment.

In the next section the procedure for modelling the system architecture is presented, following a biomechatronic design approach [79].

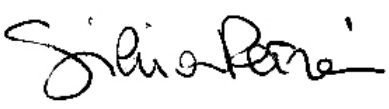

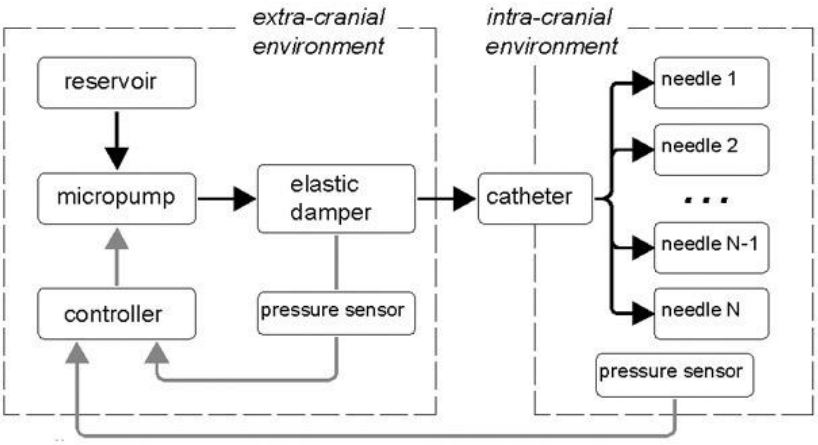

Figure 3.3: Functional diagram of an implantable drug delivery device specifically intended for the cerebral compartment. As it can be seen, system architecture has been chosen following a biomechatronic design approach.

3.2 Modelling of the device architecture

Following the biomechatronic design approach the structure of a device, that is specific for the cerebral compartment, is illustrated in figure 3.4 [79].

The starting point for our modelling procedure is the architecture of a conventional implantable drug delivery system, that basically encompasses the components mentioned in the previous section.

Physiological constraints imposed by the interaction with this anatomic compartment, together with several specifications given by neurosurgeons on drug doses and on the value of some important biological parameters were taken into account when defining the system architecture. As an example, there is a strong limitation that must be considered when dealing with drug delivery into the cerebral tissue, that is the trend of the Intra-Cranial Pressure (ICP) during and after the infusion. Following the Monro-Kelly theory [80] the intracranial compartment constitutes a partially compliant system, that can withstand only moderated volume variations without significant rises in the ICP, thanks to mutual changes in the different tissues properties. For this reason particular care must be given to intracranial pressure control.

As listed in the previous section, a drug delivery system for brain therapy has to fulfill several requirements, the main ones being: uniformity of drug distribution inside the tissue, flexibility of the components inside the surgical cavity, high-flow infusion for effective therapeutic action and direct monitoring of the ICP trend during drug infusion.

Concerning drug flow-rate, the value of $10\,\mu l/min$ comes from an analysis

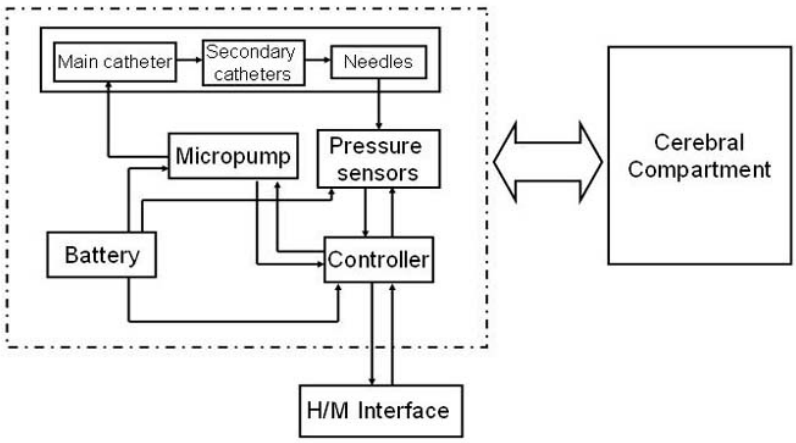

Figure 3.4: Another schematic of the architecture of a biomechatronic implantable drug delivery device.

on rat brain [81], taking into account the flow rates for which reflux has been observed and that rat brain is almost 30 times smaller than human one. The maximum allowable value for the ICP for safety issues comes from the analysis of the *elastance curve* (see figure 3.5 [82]), that is the curve describing the relationship between ICP and intracranial volume. Beyond a certain value, for minimal volume increases, significant and no more tolerable ICP increases occur [80]. Moreover, although a constant average flow-rate must

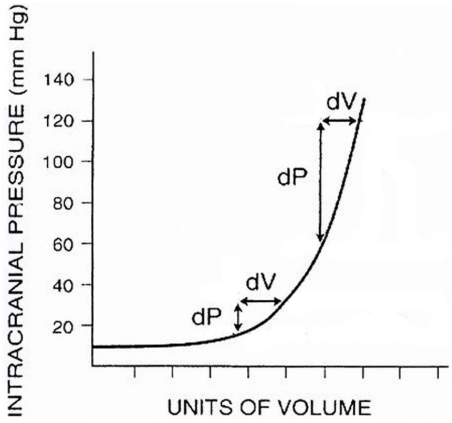

Figure 3.5: The elastance curve, representing the relationship between ICP and ICV (intra-cranial volume) in the PV plane (image taken form [82]).

be assured, battery life should be preserved by operating the pump only when strictly needed.

For increasing the uniformity of drug distribution, as proposed by Bouvier and colleagues [83], the infusion will be made through several outlet ports (needles). Catheters will be made using proper materials and shape in order to obtain the desired compliance. Eventually, two pressure sensors will be inserted in order to perform direct and indirect pressure measurements (as it will be discussed later on in this work).
In order to investigate the behaviour of the whole system, encompassing the drug infusion device and the brain, and to analyze the system response during the infusion, an electrical analogy approach has been used. The system has been translated in electric terms following a similar methodology as in [84].
Considering conventional diameters of catheters and needles, the small value of the flow-rate used in the current clinical practice ($10\,\mu l/min$) leads to low Reynolds' numbers ($Re < 1$), which assure a linear fluidic behavior. Hence, flow-rates and pressure drops are proportional via a constant coefficient, called fluidic resistance, which can be quantified by Poiseuille's law. Liquid inertia is electrically equivalent to an inductance but, because of the small typical Reynolds' number, inertia can be neglected. Therefore, the equivalent electric network is just a RC circuit.
In the electric analogy the infusion pump becomes a current source. The main catheter, that runs from the pump to the brain, is modelled as a purely resistive (fluidic resistance) and capacitive component. The capacity takes into account volume changes due to elasticity, which allows the internal radius of the catheter to change as an effect of internal pressure, so that the total volume of liquid contained within the catheter may vary. Infusion needles are solely resistive components, as their flexibility can be neglected, as it can be confirmed by simple calculations.
As regards the brain, it is a delicate compartment with complex physiologi-

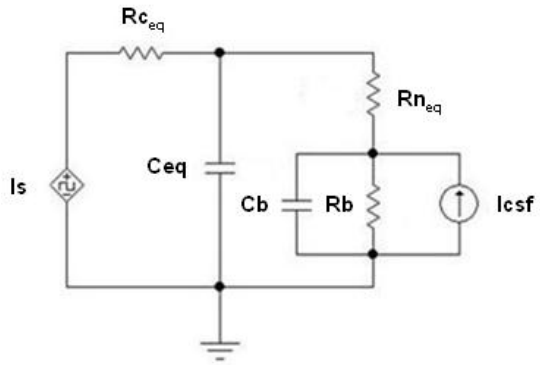

Figure 3.6: Electric analogy, encompassing the drug delivery device and a simplified model of the brain.

cal mechanisms. For an early analysis we assumed a simplified model, taking into account only tissue elasticity, drain mechanism and the Cerebro-Spinal Fluid (CSF) production. For further operations we used a more detailed cerebral model, as we will show in the following sections. The three equivalent components of the simplified model are a capacitor (brain elasticity), a resistor (drainage) and a constant current source (CSF production). Figure 3.6 shows the resulting electric analogy.
The values calculated for all the components are listed in table 3.2. Keeping

Table 3.2: Values of equivalent electric parameters

Component	**Value**	**Description**
I_s	$1.7 \cdot 10^{-10}\, A$	Infused flow-rate
R_c	$5.8 \cdot 10^{11}\, \Omega$	Main catheter resistance
R_{c_i}	$5.8 \cdot 10^{10}\, \Omega$	Secondary catheter resistance
R_{n_i}	$2.3 \cdot 10^{11}\, \Omega$	Needle resistance
R_{i_i}	$1.6 \cdot 10^{14}\, \Omega$	Infusion resistance
C_c	$2.6 \cdot 10^{-11}\, F$	Catheter compliance
I_{CSF}	$5 \cdot 10^{9}\, A$	CSF production
R_b	$2.7 \cdot 10^{11}\, \Omega$	Cerebral tissue resistance
C_b	$5.9 \cdot 10^{-9}\, F$	Cerebral tissue compliance

all units within the S.I., the translation of mechanical quantities into their electric equivalent is straightforward, as shown in table 3.3. The numerical

Table 3.3: Electric quantities equivalent to mechanical ones

Mechanical quantity	**Electrical equivalent**
Flow-rate, $Q\left[\frac{m^3}{s}\right]$	Current, $I\,[A]$
Pressure, $P\,[Pa]$	Voltage, $V\,[V]$
Fluidic resistance, $R\left[\frac{Pa \cdot s}{m^3}\right]$	Resistance, $R\,[\Omega]$
Elastic compliance, $C\left[\frac{m^5}{N}\right]$	Capacity, $C\,[F]$

values of the resistive components of the catheters are calculated through Poiseuille's law:

$$\frac{\Delta P}{Q} = \frac{32 \mu L}{S d^2} \tag{3.1}$$

where μ is the water dynamic viscosity at body temperature:

$$\mu_{H_2O} = 8.9 \cdot 10^{-4}\, \frac{N \cdot s}{m^2},$$

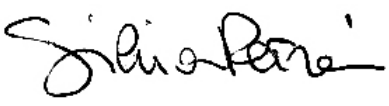

while d and L are the internal diameter and the length of the catheter and are respectively equal to $0.5\,mm$ and $1\,m$. The fluidic resistance of the secondary catheters is calculated in the same way, but in this case it is assumed $L = 10\,cm$. The same is done for the calculation of the needles resistance, by setting $d = 0.2\,mm$ and $L = 1\,cm$. At the end of the needle the fluid meets a further resistance in entering the cerebral tissue. Its value can be evaluated using Darcy's Law, from which the following relation comes:

$$\frac{\Delta P}{Q} = \frac{1}{4\pi r k} \tag{3.2}$$

where r is the needle radius and k is the hydraulic permeability of the cerebral tissue. An acceptable value for k is found to be [85]:

$$k = 5 \cdot 10^{-9}\,\frac{cm4}{dyne \cdot s}$$

The catheter compliance to internal pressure can be found using Hooke's law for cylindrical hoses. The compliance is defined as a volume variation over pressure variation: $\Delta V/\Delta P$. The calculation is made only for the main catheter, because the length of the secondary hoses is negligible with respect to it. The chosen material is a silicone rubber with Young modulus $E = 1\,MPa$ and Poisson ratio $\nu = 0.45$. The constant current source is evaluated by physiological data about the CSF production, that is generally equal to $0.3\,ml/min$ [80]. By turning this quantity into its electrical equivalent, one can find the current supplied by the source. The tissue resistance is calculated with Ohm's law, with the hypothesis that, in absence of any infusion, the ICP is kept constant at about $10\,mmHg$ and the only current that flows through the resistance is the one supplied by the constant current source.
Particular care must be taken in the evaluation of the intracranial compliance. This is well represented by a capacitor, connected in parallel to the other two brain components. In order to find a value for the capacitance it is possible to refer to the work of Marmarou [86], who showed that the relation between brain pressure and volume can be written as an exponential function (elastance curve [82]), as it is shown in figure 3.5. At each point of the curve the intracranial compliance is the inverse of the local slope. An acceptable value of compliance in case of glioma affected patient, after a surgical removal of part of the tumour, is found to be $C = 0.79\,ml/mmHg$. Thus the capacitor value is equal to $C_b = 5.9 \cdot 10^{-9}\,F$.
The resulting equivalent electric network shown in figure 3.6 is obtained by calculating equivalent series and parallel resistances of needles and catheters and by observing that the infusion resistance is much larger than needle resistance so that, being in series, the latter can be neglected. A first model has been carried out taking into account four infusion ports, but the same procedure can be adopted with a different number of needles.

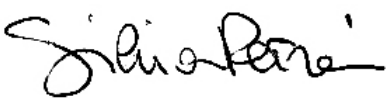

In order to define a proper architecture for the system, beyond taking into account the properties of the anatomic compartment, a careful evaluation of the power burnt off by the pump is mandatory to find the best way to preserve battery life and to guarantee a working time of the device as long as possible. This evaluation has been carried out starting from Parseval's theorem and implemented in a Matlab environment. The results have shown that there are three main parameters that can significantly affect the value of the power: the period T (inverse of the frequency, f) of the square wave (i.e. the waveform chosen for the infusion), the duty cycle DC and the capacitance value C_{eq} of the whole system, that in this case is given by the catheters elasticity. In figure 3.7 the power consumption vs. system compliance for two duty cycles and three different periods is shown. As it can be

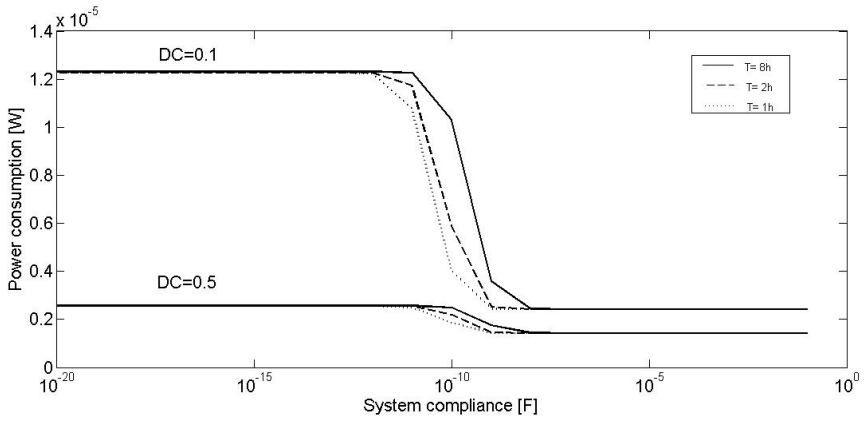

Figure 3.7: Power consumption as a function of system compliance. The curves have been plotted for various durations of the period.

seen the power requested by the pump increases as the duty cycle is reduced from $DC = 1$ (that is equivalent to a continuous supply) to $DC = 0.1$. However, by analyzing the power vs. the value of the capacitance, it is clear that, as the value of C raises, the power requested decreases. There is a threshold value of capacitance beyond which important energy saving occurs. But, analyzing the graph, the proper value of capacitance is found to be at least two orders of magnitude larger than the actual value guaranteed by the compliance of the catheters. This justifies the introduction of an additional elastic component aimed at raising the compliance of the whole system. Actually, there are two main reasons for this choice:

- an elastic component allows for dampening undesired and unexpected pressure spikes that may be generated by the infusion pump and that, otherwise, would propagate inside the brain, thus becoming dangerous for patient's safety;

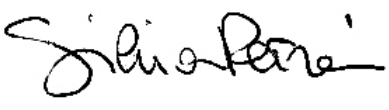

- by inserting a pressure sensor inside the chamber it is possible to perform indirect measurements of ICP, since there is a mechanical connection (i.e. the fluid-filled catheters) between the pressurized chamber and the cerebral tissue.

Strictly speaking, the first reason could be referred to as a "passive safety" criterion, meaning that the only presence of the elastic chamber is needed for meeting such safety requirement. On the other hand, the second issue can be considered an "active safety" criterion: as previously said, in this way it is possible to link the trend of the pressure inside the chamber with the trend of the ICP and, by measuring the chamber internal pressure, it is possible to indirectly control the ICP keeping it always below the maximum allowable safety value.
Basically, this solution allows for de-coupling the insertion of a liquid volume from the outside (the *cause*), from the ICP increase (the *effect*). Without the proper elasticity, all the liquid volume supplied by the pump would be infused into the tissue with the same waveform. In this way it would not be possible to control the pressure value upstream (i.e. at the needles). With the elastic chamber one can obtain, at the needles' tip, an infusion profile that depends both on the pressure difference between the chamber and the ICP and on the chamber compliance. In this way it is possible to control the ICP by controlling the chamber internal pressure.
The final architecture of the system should be as shown in figure 3.3, where the chamber is inserted right after the pump.
Early simulations have been carried out using Matlab/Simulink, in order to preliminarily evaluate system response. For an early dimensioning of the damper, we chose a compliance value of $C_{eq} = 10^{-9}\,F$, that is the value beyond which power consumption significantly drops. System equations include the device and the simplified cerebral dynamics and are as follows:

$$\begin{cases} \frac{dV_{eq}}{dt} = -\frac{V_{eq}}{R_{s_{eq}}C_{eq}} + \frac{V_b}{R_{s_{eq}}C_{eq}} + \frac{I_s}{C_{eq}} \\ \\ \frac{dV_b}{dt} = \frac{V_{eq}}{R_{s_{eq}}C_b} - V_b\left(\frac{1}{R_{s_{eq}}C_b} + \frac{1}{R_bC_b}\right) + \frac{I_{CSF}}{C_b} \end{cases} \tag{3.3}$$

As it can be seen from figure 3.8, the insertion of an additional compliance in the system helps in dampening pressure oscillations.

Anyhow, before the development of the system can start, additional effort is needed on brain modelling. This early model was useful for defining the main components of the device, but a more complete modelling of the cerebral compartment, that takes into account the many physiological phenomena and parameters that contribute to the dynamics of the system, is mandatory. The main reason for this is that early experimental tests are necessary in order to validate all the simulation results and, in order to

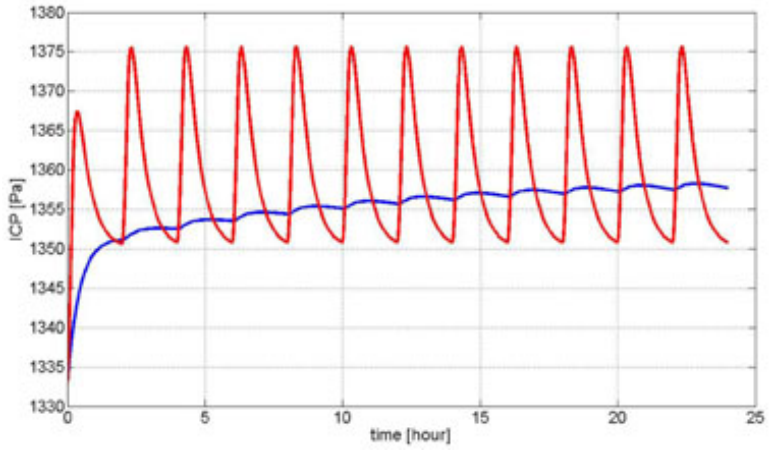

Figure 3.8: ICP trend vs. time during drug infusion. Flow-rate: $10\,\mu l/min$. Red curve: system response without elastic chamber. Blue curve: system response with the elastic chamber.

perform these test, a proper simulator has to be set, that replicates all the physiological features of the cerebral compartment. In this way an early prototype of the device can be fabricated and validated with bench-tests on the mock-up simulator.
In the next section a more detailed model of the cerebral dynamics, adapted from the literature, is proposed, and further simulations are performed, showing the interaction of the device model with such model of the intracranial compartment.

3.3 Modelling of the cerebral dynamics

As previously said, the skull and its content form a half-open system, where the overall volume must be kept constant. When a volume is inserted from the outside, as an example, all the internal components in the system may undergo slight mutual variations in volume, in order to counterbalance the addition of the external volume and to prevent the ICP from raising beyond a certain safety value (Monro-Kelly theory) [80]. Such a property is called intracranial compliance and it is described by the so-called *elastance curve* in the Intracranial Volume (ICV) vs. Intracranial Pressure (ICP) plane (see figure 3.5). The main compartments that act in the regulation of the intracranial environment are the brain tissue (80%), the vascular compartment (12%) and the CSF circulation (8%), and are illustrated in figure 3.9. As it can be seen, pressure within the intracranial compartment is determined by

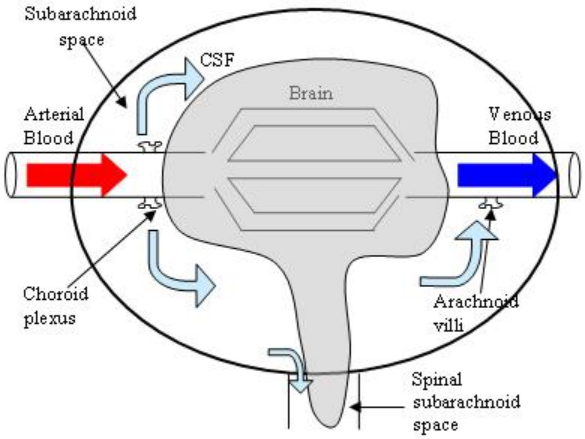

Figure 3.9: The main mechanisms that act in regulating cerebral dynamics.

three factors:

- brain's blood supply (arterial and venous);
- cerebral tissue;
- CSF production and absorption.

The arterial volume is given by the oxygenated blood supply to the brain via the arterial system, while the venous volume is the volume of blood and other constituent matter leaving the brain system through the venous vascular bed. The brain tissue encompasses the brain parenchyma (nerves and extracellular fluid) and the cerebral capillary system. The final contribution is given by the cerebrospinal fluid (CSF), a clear bodily fluid, produced in the cerebral ventricles. Cerebral blood flow (CBF) represents 15% of resting cardiac output (about $750\,ml/min$). The CBF remains constant over a wide range of arterial pressures (between 60 and $150\,mmHg$) since arterial resistance adjustments modify the caliber of arteries and arterioles. The CSF occupies the subarachnoid space in the brain (the space between the skull and the cerebral cortex -more specifically- between the arachnoid and pia layers of the meninges). It acts as a "cushion" or buffer for the cortex thus realizing a mechanical protection for the brain itself. The CSF also occupies the ventricular system of the brain and the spinal cord. CSF is mainly produced by the choroid plexi of the cerebral ventricles and it is reabsorbed into the venous system through the arachnoid villi in the subarachnoid space between the brain and the skull. The total amount of cerebrospinal fluid that the skull can contain is about $150\,ml$, and about $500\,ml$ are produced every day.
Normal values for ICP are between 8 and $15\,mmHg$ in adults. Since the

skull is incompressible, any increase in the volume of one component (i.e. blood, CSF or brain tissue) must be counterbalanced with a decrease in the volume of another component. In the early stages, adjustment is made to maintain ICP within normal range. That is, if there is an increase in the volume of either the brain or blood, the initial response is a reduction in CSF volume within the skull. CSF is forced out into the spinal subarachnoid space. Thus the ICP is initially maintained. If the pathological process progresses with further increase in volume, venous blood and more CSF is forced out of the skull. However, such mechanisms (i.e. the intracranial compliance) can withstand only limited volume increases. As it can be seen in figure 3.5, beyond a certain threshold, the more volume is added, the higher ICP rises.

The most important contribution on cerebral modelling is, by far, the one given by Ursino and his group [87]. They provided a mathematical model of the cerebral hydrodynamics, together with a scheme of both, an electrical and a mechanical analogy. The two schemes of their model are shown in figure 3.10. The main aforementioned cerebral mechanisms are taken into account. The arterial-arteriolar cerebrovascular bed is modelled with an unique variable lumped arterial compliance C_a, which has been assumed to be equal to the sum of the compliances of all the large intracranial arteries, and with a hydraulic resistance R_a, that is variable too. The venous cerebrovascular bed is described by means of two hydraulic resistances R_{pv} and R_{dv}. The blood enters the skull at the systemic arterial pressure P_a. CSF production and reabsorption processes are modelled as passive mechanisms depending on the *transmural pressure* (i.e. the difference between cerebral arterial pressure and intracranial pressure) value. At capillary pressure P_c there is the resistance R_f for the CSF production with a flow rate of q_f. The blood pressure falls to venous pressure P_v (that is assumed equal to the intracranial pressure P_{ic}), and the blood leaves the skull at the sinus venous pressure P_{vs} (that is kept constant in the model). At this point, the CSF is reabsorbed through the resistance R_o with a flow rate q_o. C_{ic} is the intracranial compliance and I_i represents an external infusion flow (in our model this contribution is replaced with the drug infusion flow coming from the implantable device model).

C. Ying and colleagues [88] also simulated the cerebral dynamics, by using a model similar to the one proposed by Ursino. However, we mainly based our modelling procedure on the model proposed by Ursino since, as an example, experiments by Ying and colleagues were carried out on dog brains, and the values of several anatomical parameters were significantly different from human ones. We also modified the equations by integrating this model with the one of the device previously developed [79].

In their work, Ursino and Lodi took as a starting point the equation that indicates that the overall intracranial volume, given by the aforementioned

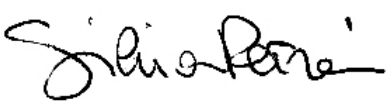

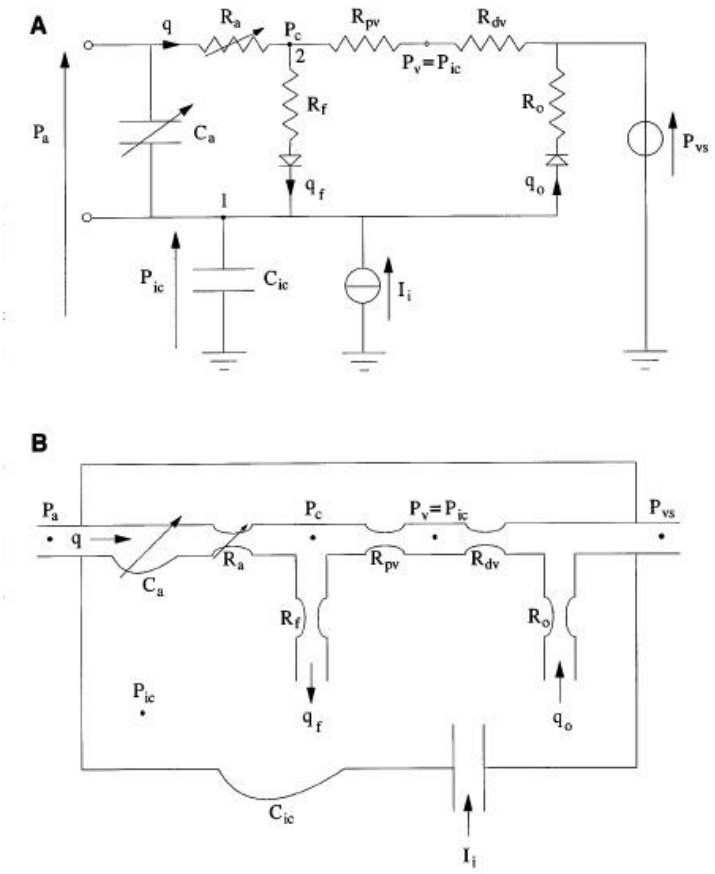

Figure 3.10: Model of the cerebral dynamics proposed by M. Ursino and C.A. Lodi. Electrical equivalent (A) and mechanical model (B). Image taken from [87].

compartments (see figure 3.9), must be kept constant:

$$V_b + V_{ic} + V_{CSF} + V_i = const \tag{3.4}$$

where V_b is the cerebral blood volume, V_{ic} is the cerebral tissue volume, V_{CSF} is the CSF volume and V_i is the external injected volume. V_b is composed both by the arterial (V_a) and venous (V_v) blood volume. Anyway, V_v can be considered as constant, so the equation becomes:

$$\frac{dV_a}{dt} + \frac{dV_{ic}}{dt} + \frac{dV_{CSF}}{dt} + \frac{dV_i}{dt} = 0 \tag{3.5}$$

The most important parameter in evaluating cerebral dynamics is the ICP (P_{ic}). So the equation above must be expressed in terms of this parameter. By examining the circuit in figure 3.10, and by imposing the mass

preservation at node 1 we can write:

$$C_{ic}\frac{dP_{ic}}{dt} = \frac{dV_a}{dt} + \frac{P_c - P_{ic}}{R_f} - \frac{P_{ic} - P_{vs}}{R_o} + I_i$$

They defined C_{ic} as:

$$C_{ic} = \frac{1}{k_E P_{ic}} \tag{3.6}$$

where k_E is defined as the elastance coefficient of the craniospinal system, and its value is $k_E = 0.11\, ml^{-1}$. This expression for C_{ic} is adopted by Ursino from the work of Marmarou et al. [89, 90], where they assumed C_{ic} to be inversely proportional to ICP, following the exponential relation holding between pressure and volume in the intracranial space.
They also found the expression for $\frac{dV_a}{dt}$ by considering the filling arterial volume as proportional to the transmural pressure $(P_a - P_{ic})$:

$$V_a = C_a(P_a - P_{ic}), \tag{3.7}$$

thus obtaining:

$$\frac{dV_a}{dt} = C_a\left(\frac{dP_a}{dt} - \frac{dP_{ic}}{dt}\right) + \frac{dC_a}{dt}(P_a - P_{ic}) \tag{3.8}$$

The two terms on the right part of the equation 3.8 indicate that the arterial blood volume changes according to a rate depending on two terms: the first one being a passive change, due to the transmural pressure variations; the second one being an active change, due to changes in the arterial compliance because of the presence of autoregulation mechanisms. Such autoregulation mechanisms have also been identified by Ursino and Lodi. They found out that C_a variations can be written with the following equation:

$$\frac{dC_a}{dt} = \frac{1}{\tau}\left[-C_a + \sigma(G \cdot x)\right], \tag{3.9}$$

where

$$x = \frac{q - q_n}{q_n}$$

Here τ is the time constant of the regulation, σ is a sigmoidal static function with upper and lower saturation, G is the maximum autoregulation gain, q is defined as the CBF entering the skull each instant, and q_n is the basal value of the CBF. q_n is calculated through the analysis of the circuit in figure 3.10, and is equal to:

$$q = \frac{P_a - P_c}{R_a}$$

They also defined the sigmoidal function σ as:

$$\sigma(G \cdot x) = \frac{\left(C_{an} + \frac{\Delta C_a}{2}\right) + \left(C_{an} - \frac{\Delta C_a}{2}\right) \cdot exp\left(\frac{G \cdot x}{k_\sigma}\right)}{1 + exp \cdot \left(\frac{G \cdot x}{k_\sigma}\right)} \tag{3.10}$$

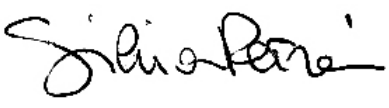

with C_{an} and ΔC_a being, respectively, the central value and the amplitude of the sigmoidal curve. ΔC_a and k_σ are chosen as follows:

$$\begin{cases} \text{if } x < 0 \text{ then } \Delta C_a = \Delta C_{a1};\ k_\sigma = \frac{\Delta C_{a1}}{4} \\ \\ \text{if } x > 0 \text{ then } \Delta C_a = \Delta C_{a2};\ k_\sigma = \frac{\Delta C_{a2}}{4} \end{cases}$$

The main reason for this choice, authors say, is that, if CBF decreases below the basal value q_n, a vasodilatation occurs, and the compliance rises. The opposite (i.e. vasoconstriction) happens when the CBF goes beyond the basal value. But, the increase in blood volume due to vasodilatation is higher than the decrease in volume due to vasoconstriction: this explains why the sigmoidal function is not symmetrical. Of course, a change in the arterial compliance, involves a change also in the arterial resistance R_a, that is expressed as follows:

$$R_a = \frac{k_R C_{an}^2}{V_a^2} \tag{3.11}$$

In order to find an expression for P_c, the mass preservation can be imposed at node 2 of the circuit in figure 3.10, and the following equation can be written:

$$\frac{P_a - P_c}{R_a} = \frac{P_c - P_{ic}}{R_f} + \frac{P_c - P_{ic}}{R_{pv}}$$

However, Ursino and Lodi consider that the production of CSF, i.e. the first term on the right of the equation above, is negligible with respect to the CBF, so the expression for P_c becomes:

$$P_c = \frac{P_a R_{pv} + P_{ic} R_a}{R_{pv} + R_a} \tag{3.12}$$

After the definition of all these equations and parameters it is possible to write the equation of the ICP dynamics:

$$\frac{dP_{ic}}{dt} = \frac{k_E P_{ic}}{1 + C_a k_E P_{ic}} \left[C_a \frac{dP_a}{dt} + \frac{dC_a}{dt}(P_a - P_{ic}) + \frac{P_c - P_{ic}}{R_f} - \frac{P_{ic} - P_{vs}}{R_o} \right] \tag{3.13}$$

In order to generate the arterial pressure waveform (P_a), a lumped parameters mechanical model of the left heart and the aorta has been implemented. The output of the model is the aortic pressure, which is approximately equal to cerebral arterial pressure. The waveform of the arterial pressure, as it comes out of the model is shown in figure 3.11. With such an input the cerebral dynamics has been simulated and validated. The final equation system that has been implemented in Matlab/Simulink for simulation is the

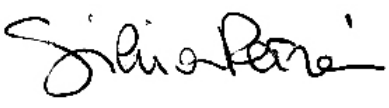

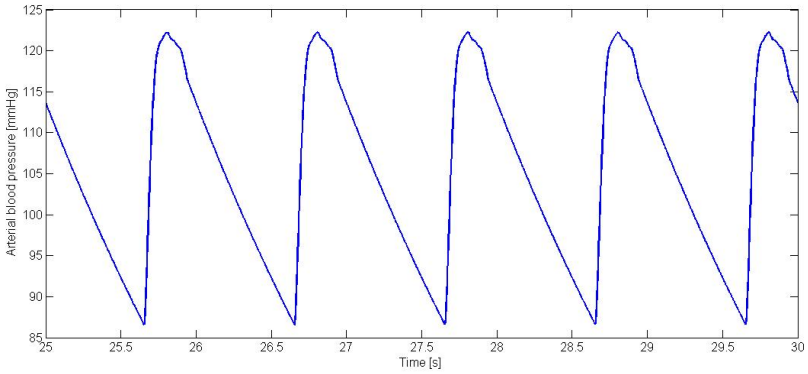

Figure 3.11: The waveform of the arterial pressure, as it comes out of a model of the left heart previously developed, and here employed for generating the P_a trend as an input to the Ursino model of the cerebral dynamics.

following:

$$\begin{cases} \frac{dP_{ic}}{dt} = \frac{K_E P_{ic}}{1+C_a K_e P_{ic}} \left[C_a \frac{dP_a}{dt} + \frac{dC_a}{dt}(P_a - P_{ic}) + \frac{P_c - P_{ic}}{R_f} - \frac{P_{ic} - P_{vs}}{R_o} \right] \\ P_c = \frac{P_a R_{pv} + P_{ic} R_a}{R_{pv} + R_a} \\ R_a = \frac{k_R C_{an}^2}{V_a^2} \\ V_a = C_a (P_a - P_{ic}) \end{cases} \tag{3.14}$$

Other parameters used by Ursino and Lodi are listed in table 3.4. In the equation describing P_{ic} we do not take into account the term I_i, because, as previously said, it accounts for a liquid infusion from the outside. In this case we are just simulating the cerebral dynamics in absence of infusion.

As it can be seen from figure 3.12, in normal conditions the ICP oscillates around an average value, correctly matching the normal behaviour. In the next paragraph we will couple this more detailed model of the intracranial dynamics with the model of the device previously developed. We will carry out simulations during infusion in order to analyze system response and in order to correctly dimension both the device prototype and the simulator for the *in vitro* tests.

Table 3.4: Value of parameters and model input quantities in basal conditions

Parameter	**Value**
R_o	$526.3\,mmHg \cdot s \cdot ml^{-1}$
R_{pv}	$1.24\,mmHg \cdot s \cdot ml^{-1}$
R_f	$2.38 \cdot 10^3\,mmHg \cdot s \cdot ml^{-1}$
ΔC_{a1}	$0.75\,ml/mmHg$
ΔC_{a2}	$0.075\,ml/mmHg$
C_{an}	$0.15\,ml/mmHg$
k_E	$0.11\,ml^{-1}$
k_R	$4.91 \cdot 10^4\,mmHg^3 \cdot s \cdot ml^{-1}$
τ	$20\,s$
q_n	$12.5\,ml/s$
G	$1.5\,ml \cdot mmHg^{-1} \cdot 100\%\,CBF\,change^{-1}$
P_a	$100\,mmHg$
P_{ic}	$9.5\,mmHg$
P_c	$25\,mmHg$
P_{vs}	$6\,mmHg$

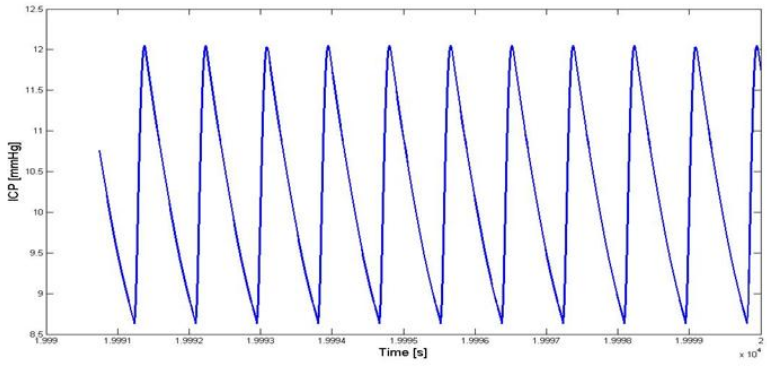

Figure 3.12: ICP trend as an output of the model of the cerebral dynamics implemented in Matlab/Simulink following the Ursino modelling procedure.

3.4 Cerebral system response during infusion: simulation results

The overall system, encompassing both the infusion device and the model of the cerebral dynamics, has been implemented in Matlab/Simulink. The block diagram built for performing simulations is represented in figure 3.13,

where the green block is the subsystem of the implantable infusion device, the red blocks are the signal sources representing the arterial pressure and its derivative and the remaining blocks and subsystems represent all the modelled mechanisms of the cerebral dynamics. The new equations describing

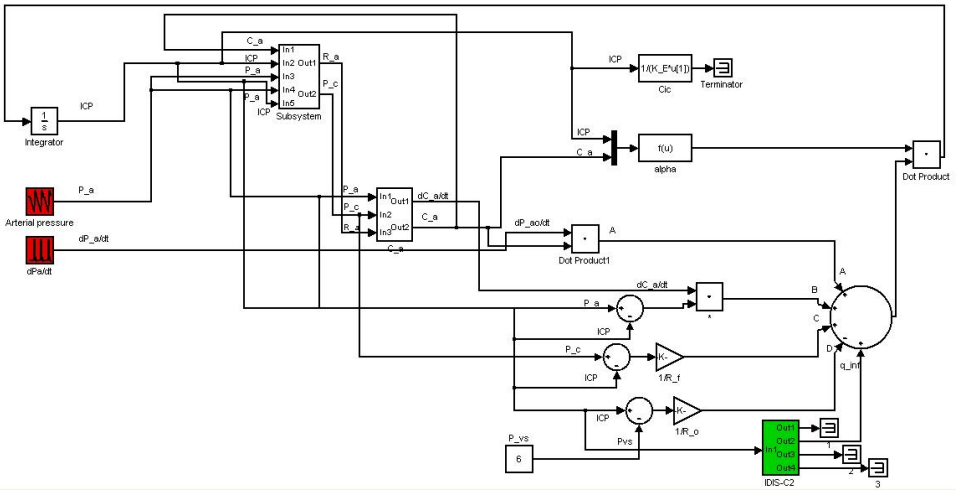

Figure 3.13: Simulink model encompassing the infusion device (green block) and the cerebral dynamics.The red blocks are the arterial pressure and its derivative.

the complete model in terms of mechanical quantities results as follows:

$$\begin{cases} \frac{dP_{ic}}{dt} = \frac{1}{C_a+C_{ic}} \left(C_a \frac{dP_a}{dt} + \frac{P_c - P_{ic}}{R_f} - \frac{P_{ic} - P_{vs}}{R_o} + \frac{P_{eq} - P_{ic}}{R_{tot}} \right) \\ \\ \frac{dP_{eq}}{dt} = -\frac{P_{eq} - P_{ic}}{R_{tot} C_{eq}} + \frac{I_s}{C_{eq}} \end{cases} \tag{3.15}$$

where P_{eq} is the pressure inside the elastic chamber, I_s is the infusion flow-rate, coming from the infusion device.
In figure 3.14 the ICP trend in normal conditions (top image) is compared with the trend of the ICP during an infusion of $5\,\mu l/min$ (bottom image). As it can be seen, during the infusion phase the oscillations amplitude increases as the average pressure value does, that in normal condition was set to $10\,mmHg$. These results show that a control system is necessary, in order to be able to infuse the desired drug flow-rate (i.e. $10\,\mu l/min$) without increasing ICP beyond a safety value.
Based on the simplified model of the cerebral dynamics coupled with the model of the device developed in [79], a preliminary feedback on-off control scheme had been developed. Such control takes into account only the ICP value. Two threshold values have been set: the first one is the minimum

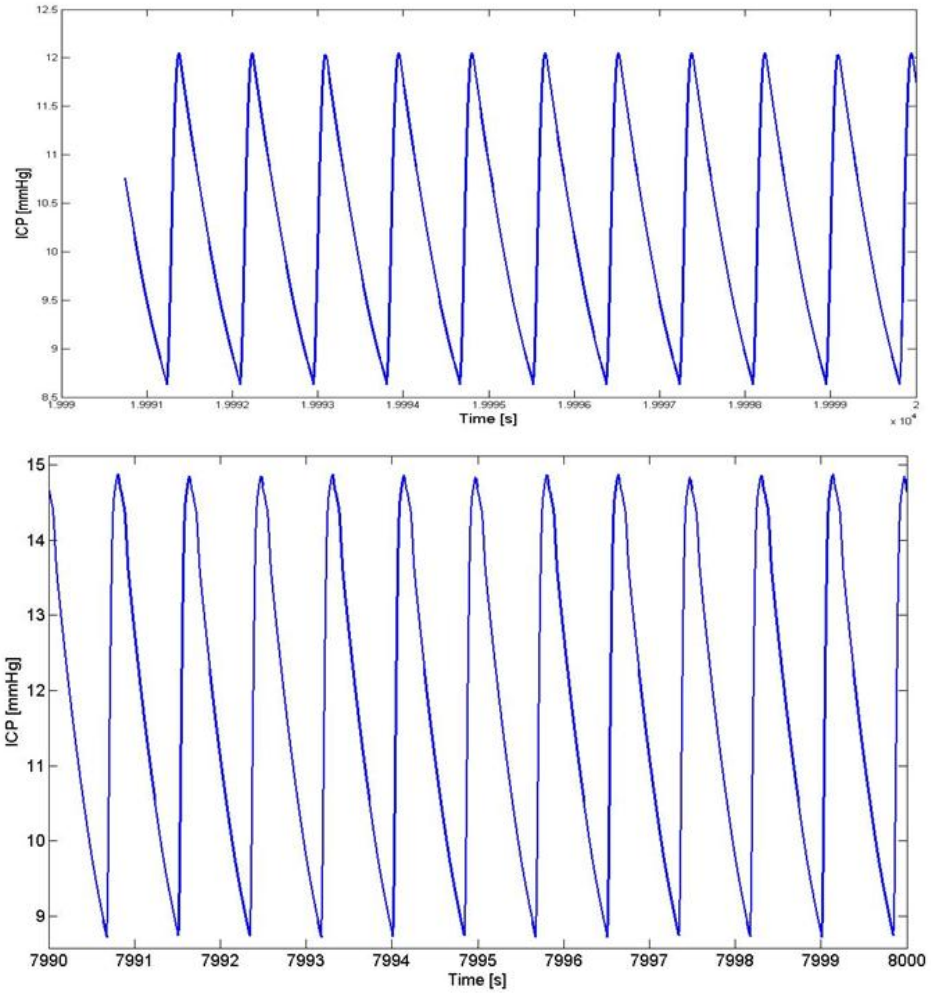

Figure 3.14: ICP trend in normal conditions without infusion (top image); ICP trend during an infusion of $5\,\mu l/min$ (bottom image).

ICP value below which the pump can be turned on to infuse drug, and the other one is the maximum value beyond which the pump must be turned off, for safety issues, until the ICP falls again below the minimum value. As previously said, the ICP can be measured by calculating it once the pressure in the elastic chamber is known or by directly inserting a pressure sensor in the cerebral cavity. For redundancy, it is safer to use both sensors, as it is shown in figure 3.3. This provides additional information on the fluidic resistance of secondary catheters and needles, which may be obstructed by scar tissues. Figure 3.15 shows that, once two convenient threshold values have been chosen, it is possible to turn the pump on only five times in a day in order to have the desired flow-rate, that is $10\,\mu l/min$ in value (around

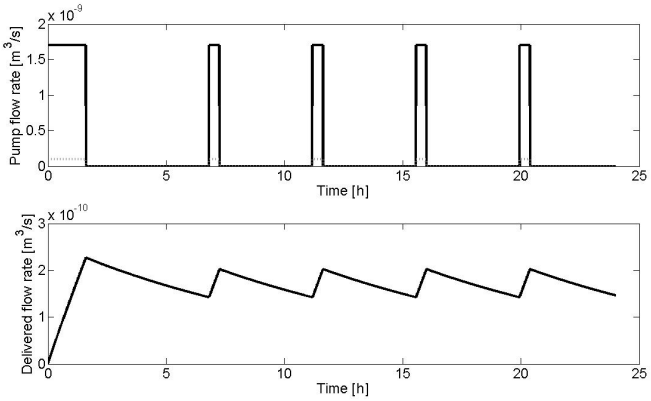

Figure 3.15: Pump flow-rate (top image) and infused flow rate (bottom image) regulated by the on-off control system with the ICP set as the only control parameter.

$1.7 \cdot 10^{-10}\, m^3/s$).
However, the effectiveness of the whole modelling procedure needs to be tested onto a real system, in order to validate our design choices or to make the necessary adjustments. For this reason, in the following sections, we describe the design, fabrication and assembling procedures of both the infusion device and the testing platform.

3.5 Definition of the testing platform architecture

As previously said, one of the aims of this research project was to design and fabricate a sort of "active" platform to be used for realistic in vitro testing of the developed drug delivery device. The Ursino model has been considered the most exhaustive for our purposes, because every physiological mechanism is taken into account and plainly modelled as a hydraulic/electrical component (see figure 3.10).
An early design of the simulator is shown in figure 3.16, where the skull is represented as a plexiglas box and every mechanism modelled by Ursino is translated into a hydraulic component. We conceptually divided this platform into three subsystems: the first one replicating the skull and the cerebral tissue properties; a second one, that is basically a hydraulic circuit, representing the cerebral blood vascular bed, i.e. arteries, capillaries and veins, each one bringing their own pressure drops; the last one, that is a hydraulic circuit itself, and acts as the CSF production-reabsorption mechanism. The P_{vs} can be represented with a reservoir, placed at a certain

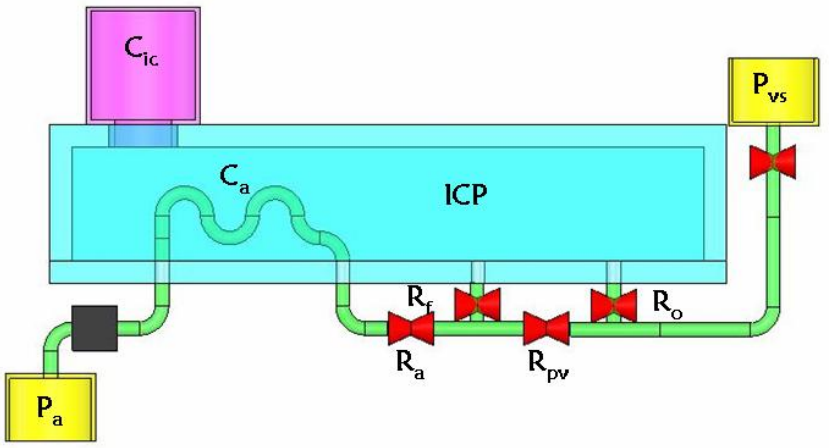

Figure 3.16: Early design of the platform simulating the cerebral dynamics: in this case all the components of the model by Ursino are straight translated into a mechanical component.

height with respect to the rest of the system, in order to give the desired constant pressure through a hydrostatic column.
All the resistances are designed to be represented through electric valves or taps, set following the value given by Ursino in his model. The desired resistances values have been obtained by adjusting valves/taps opening. This has been carried out by using a setup made up by a fluid reservoir placed at a known height, a chronometer, a precision scale, tubes with known dimensions and the tap to be adjusted. A quantity of fluid has been flown through the tubes and the tap for a given time: the resistance of the tap has been calculated as the ratio between the pressure difference between the inlet and the outlet of the tube (that is equal to the hydrostatic pressure given by ρgH, where ρ is the fluid density and H is the height of the tube) and the measured flow-rate. The right opening of the tap has been measured with a goniometer, in order to define the correct opening angle to obtain the corresponding resistance value.
Two different procedures have been chosen for the dimensioning of the two compliances. At first, to represent the C_a, a calculation for using a flexible tube has been made. Unfortunately, from the Ursino model, the C_a has a mean value of $0.1855\,ml/mmHg$. This leads to a tube that is either extremely long or with a excessive diameter to be easily inserted in a box that is about $30x30x30\,cm^3$ in volume.
For the C_{ic} a different solution has been used. That is, inserting a volume of a compressible gas (e.g. air) inside a cylinder placed above the main plexiglas cube and in communication with it, in such a way that it is possible, in the experiments, to set different values of C_{ic} and regulating intracranial

pressure. Variations of C_{ic} and ICP are made possible through driving a piston upward and downward along the cylinder, as it is shown in figure 3.17. We also found the law linking the desired values of C_{ic} and ICP to the values of the initial and final volumes, V_0 and V_f respectively, of the cylinder. Our starting point was considering air as a perfect gas, thus undergoing the perfect gases law:

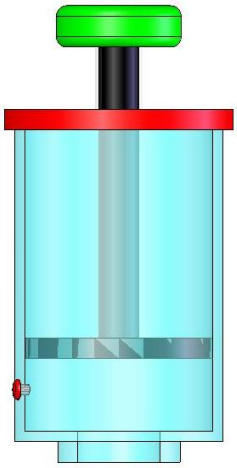

Figure 3.17: Figure shows the cylinder to be placed above the plexiglass cube representing the cerebral compartment,that, filled with air, gives a value for the intracranial compliance.

$$PV = nRT \tag{3.16}$$

All the experiments are assumed to be conducted in isothermal conditions, so the equation becomes:

$$PV = nk$$

From the above equation the expression for P is obtained:

$$P = \frac{nk}{V} \tag{3.17}$$

by differentiating equation 3.16, taking into account that compliance C has the following expression:

$$C = \frac{dV}{dP}, \tag{3.18}$$

and combining the resulting equation with equation 3.17, we obtain:

$$C = \frac{V^2}{nk} \tag{3.19}$$

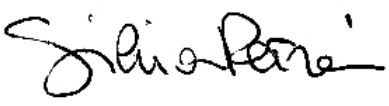

The final two-equation system that we take into account to obtain the initial and final volume V_0 and V_f of the cylinder is the following:

$$\begin{cases} C = \frac{V^2}{nk} \\ \\ P = \frac{nk}{V} \end{cases} \tag{3.20}$$

Starting from such equation system we want to write the expressions for the initial and final volume of the cylinder. As it can be seen from figure 3.17, the cylinder is provided with a hole, that connects the air inside to the atmospheric pressure when the hole cap is not inserted. Let's suppose that we are at atmospheric pressure (cap not inserted), with the piston placed at a certain height, that determines an initial volume, say V_0. Equation 3.16 can be written as follows:

$$P_{atm}V_0 = nk$$

and n, that is the moles' number contained inside the volume V_0, can be written as:

$$n = k'V_0$$

where

$$k' = \frac{P_{atm}}{k}$$

By substituting the expression for n in the equation system we obtain the expressions for the initial and final volume that must be, respectively, set and reached in order to have the desired intracranial compliance and intracranial pressure values inside the plexiglas cube:

$$\begin{cases} V_0 = \frac{P_{fin}^2 C}{k'k} \\ \\ V_{fin} = CP_{fin} \end{cases} \tag{3.21}$$

Anyway, such solution carries a big drawback: the pressure to account for is not only the air pressure, but also the liquid/vapour equilibrium pressure must be taken into account.
For this reason, and for the difficulty in representing also the arterial compliance C_a, we decided to test a second possible solution: we reduced the cerebral compartment to a box with a compliance and a pump (see figure 3.18): the compliance is equal to the C_{ic} coming out of the Ursino model, while the pump should supply a flow equal to the algebraic sum of all the flows produced inside the skull (i.e.: $q_{tot} = q_{C_a} - q_{R_o} + q_{R_f}$). A following step in the development of the best solution was considering that the behaviour of the intracranial dynamics can be reproduced by using the same structure as before (i.e. the box with the compliance and the pump), but giving a

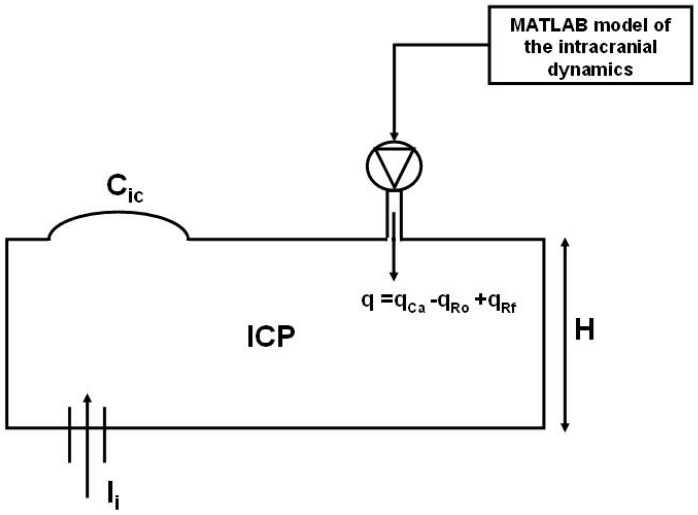

Figure 3.18: A possible second version of the testing platform. Here the cerebral compliance is represented through a flexible membrane and there is only a pump infusing a flow-rate that is the sum of all the flows produced and reabsorbed inside the cerebral compartment.

different value to the compliance. That is, the compliance is different in value from the C_{ic} and, consequently, the flow that the pump has to supply will be different from the one resulting from the sum of the flows produced inside the intracranial space. The scheme of figure 3.18 becomes the one in figure 3.19. This choice gives a big advantage, meaning that the dimensioning of the compliance can be easier, since one can choose the shape, size and the material without being forced to reproduce the C_{ic}. The final behaviour of the simulator will be the same as the one of the intracranial compartment, due to the fact that we designed the following working mechanism for the system (see figure 3.20):

- a flow-rate q_i is set on the pump of the infusion device to be tested, and the actual flow is read by a flow-meter placed inside the box;
- the read value is sent as an input to a computer where the implemented Simulink model of the intracranial dynamics and of the infusion device is loaded, in order to start a simulation;
- the simulation gives as an output the desired ICP value that should be inside the box in response to the infusion;
- such desired value is compared inside a control system with the actual pressure value inside the box, that is continuously read by a pressure sensor;

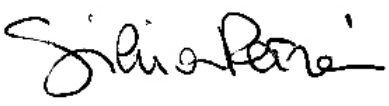

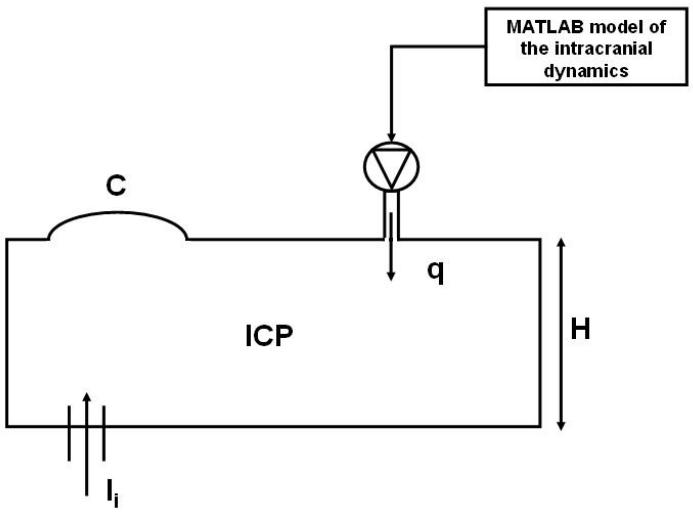

Figure 3.19: Final version of the simulator: the components do not have the values of the corresponding biological component/mechanism, but the resulting behaviour of the box is in accordance with the simulated cerebral dynamics.

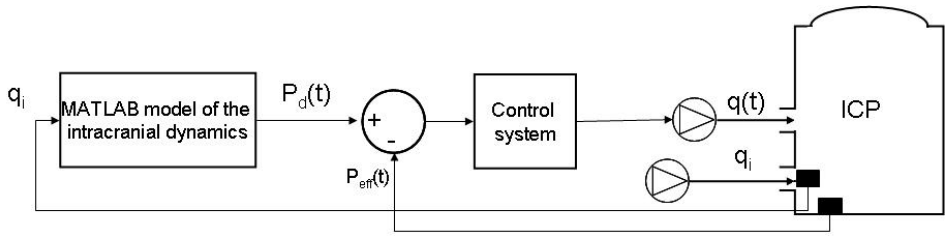

Figure 3.20: Working mechanism of the final testing platform, including the control system.

- the output of the control system is an instruction to another pump (not the one in the infusion device) that has to supply/drain the right liquid volume to pressurize the box with the desired pressure.

This means that the pressure inside the plexiglass box (i.e. the ICP) is determined by the Ursino model implemented in Matlab.
After defining the optimal architecture of the simulator, in the next section the fabrication procedure of the "sensorized box" is shown.

3.6 Simulator fabrication

For easiness of fabrication we chose a cylindric shape for the plexiglass box, and we decided to place the carbon-steel membrane on the lower basement of the cylinder. In this way we could use the upper side for the tubes and pumps connections. A drawing of the cylindric box is shown in figure 3.21. Some pictures of the simulator box after fabrication are shown in figures 3.22- 3.25.

In particular, figure 3.25 shows two modules that have been fabricated for varying the dimensions of the membrane surface in contact with the liquid. The flow-rate range that the pump has to supply/drain for pressurizing the plexiglas cylinder is linked to the ICP variation through the compliance given by the membrane:

$$q = C \cdot \frac{dICP}{dt} \tag{3.22}$$

by varying such compliance it is possible to work with different flow-rates.

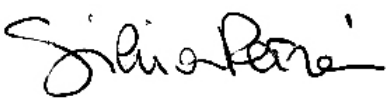

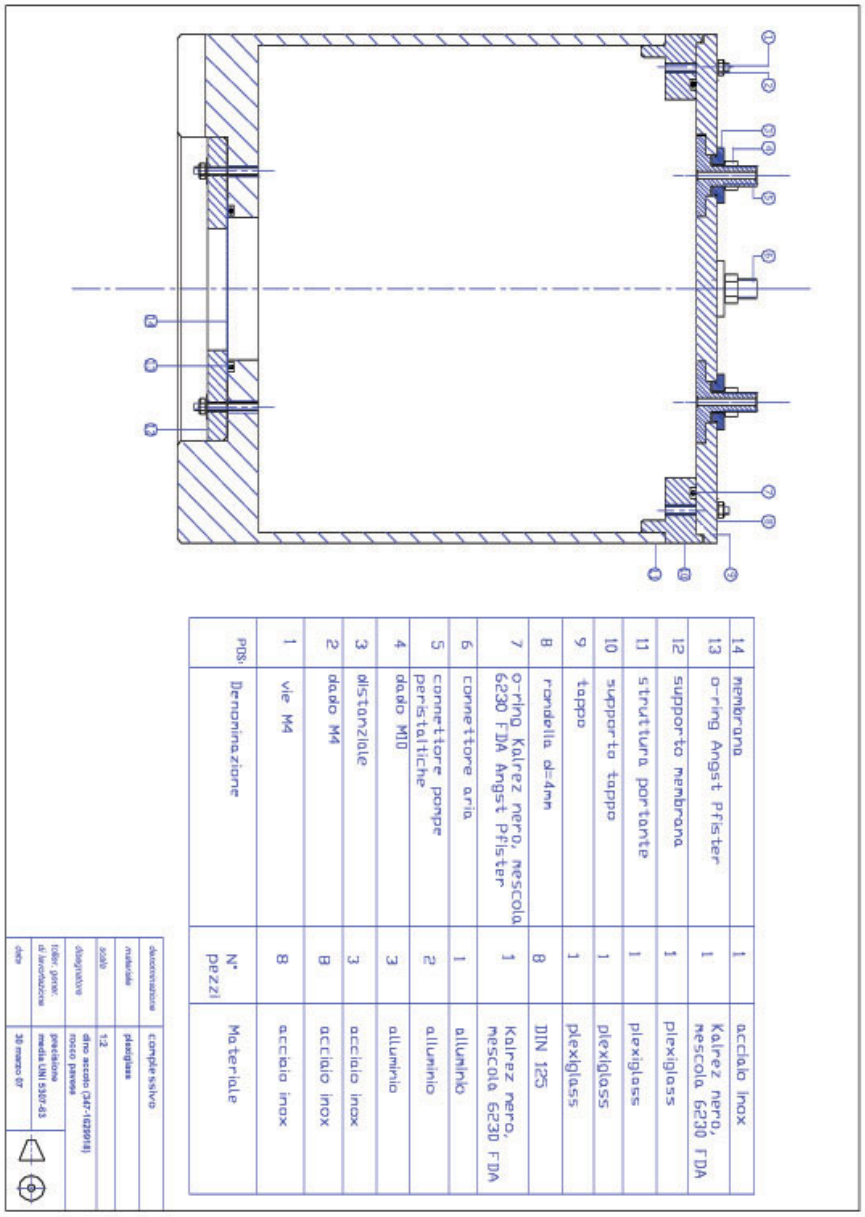

Figure 3.21: Mechanical drawing of the cylindric box.

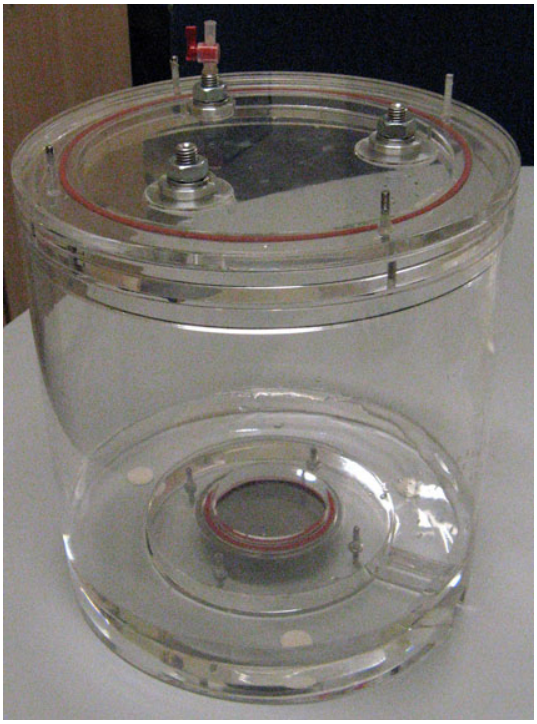

Figure 3.22: The plexiglass box after fabrication and assembling. At the lower base of the cylinder the flexible membrane can be seen, while on the cover all the connections for the catheters are placed.

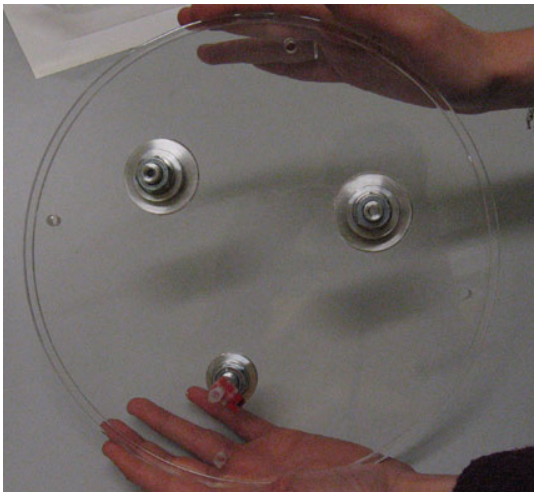

Figure 3.23: The plexiglass cover in detail.

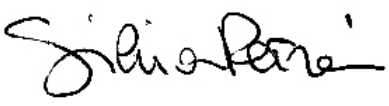

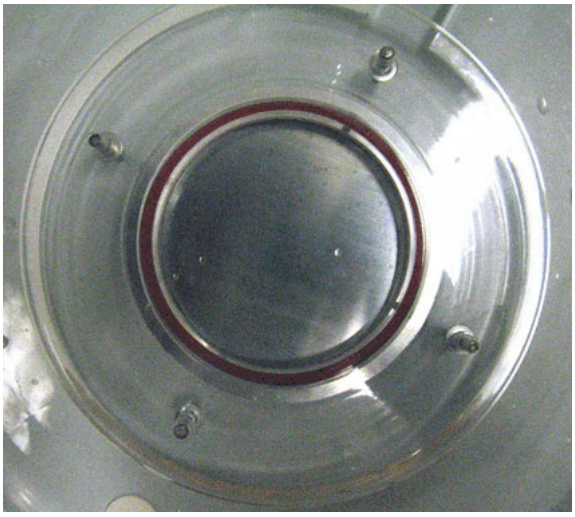

Figure 3.24: The flexible membrane in detail.

Figure 3.25: Two plexiglass modules that have been fabricated in order to vary membrane dimensions and, therefore, system compliance

In order to assemble the setup for the bench tests on the infusion device we also used several other components:

- a pump for generating ICP inside the plexiglass box (Watson-Marlow, 102 FD/R, 65rpm);
- catheter with 1.6 mm ID connected to the ICP pump;
- a reservoir for the ICP pump (phleboclysis-sac);
- an optical sensor (OSRAM SFH 9201) that is used as a pressure sensor in conjunction with the steel membrane at the basement of the plexiglass box for measuring the ICP.

The Watson-Marlow peristaltic pump (see figure 3.26) is equipped with a 12 V DC motor and, in the version of 65 rpm, which is the one we used for ICP generation, connected to a catheter that is 1.6 mm in ID, it can provide flow-rates up to 14.0 ml/min.
An illustration of the optical sensor, taken from the datasheet, is shown in

Figure 3.26: Image of the Watson-Marlow peristaltic pump, model 102 FD/R (www.watson-marlow.com/).

figure 3.27. The optical sensor is centered below the membrane for detecting the membrane strains, in order to link them to a pressure variation.
In the following section the assembling of the infusion device is presented, together with a detailed description of all the components employed.

3.7 Assembling of the infusion device

In order to test to which extent the hypotheses we made on the system architecture, followed by extensive simulations, are confirmed, an early pro-

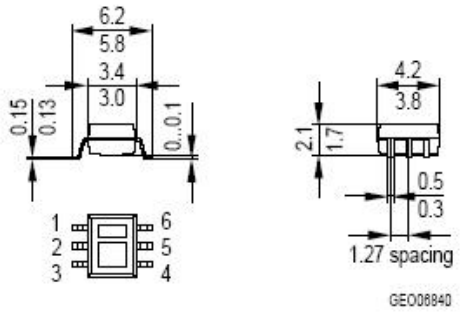

Type	1	2	3	4	5	6
SFH 9201	Anode	–	Emitter	Collector	–	Cathode

Figure 3.27: Schematic drawing of the OSRAM SFH 9201 optical sensor, with indication on the dimensions and on the electrical connections.

totype of the infusion device has been built, to be tested on the active platform representing the behaviour of the cerebral compartment. Most of the components used for the infusion device are commercially available products, that have been chosen as fulfilling the general requirements listed in section 3.1. But, on the other hand, their dimensions, on the whole, are not suitable for being implanted inside the human body. This evident drawback is justified by the need we have, given the early stage of development of the device and its novelty, to experimentally verify that the overall architecture (including mechanics, hydraulics, sensors and control schemes) does achieve the project goals.
Following the chosen architecture, the components constituting the prototype of the infusion device are:

- infusion peristaltic pump (Watson-Marlow, 102 FD/R, 4rpm);
- liquid reservoir (phleboclysis-sac);
- main catheter with 0.8 mm ID;
- hydro-pneumatic storage cell (damper);
- pressure sensor (Freescale, MPX2300);
- infusion sources (Alzet Infusion Kits).

The Watson-Marlow peristaltic pump (see figure 3.28, left image) is equipped with a 12 V DC motor and, in the version of 4 rpm, which is the one we used for drug infusion, connected to a catheter that is 0.8 mm in ID, it can provide

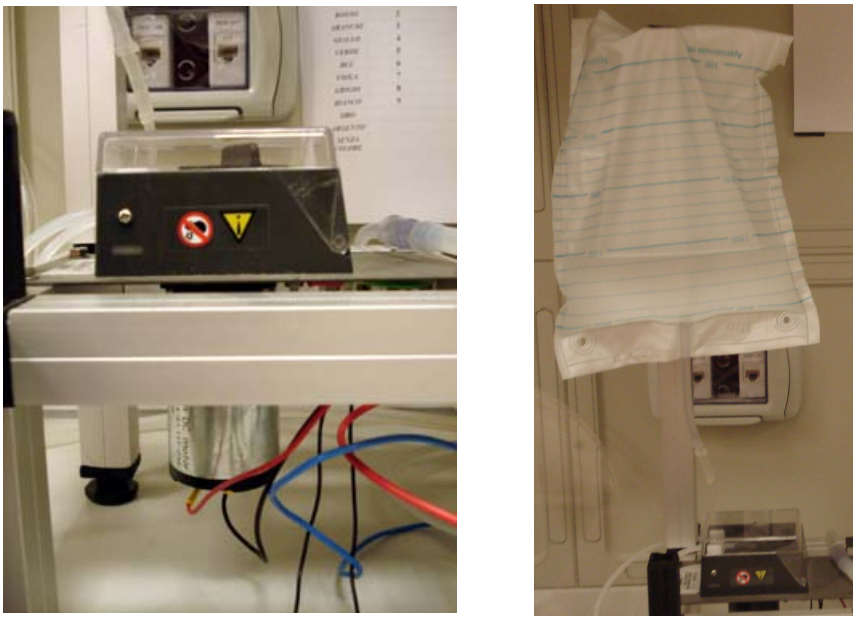

Figure 3.28: Left: the peristaltic pump with the $12\,V$ DC motor mounted on a metal structure used for pumps allocation in the experimental setup. Right: the pump connected to its reservoir.

flow-rates up to $0.20\,ml/min$. The pump is also connected to the reservoir as shown in figure 3.28, right image. The component with the role of elastic chamber is a commercial component too (see figure 3.29).

Saip srl (a small italian enterprise) fabricated such damper based on our

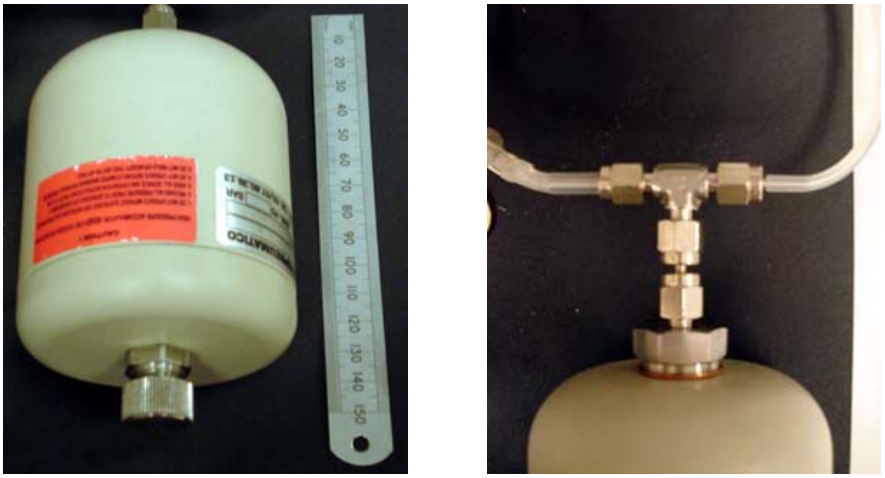

Figure 3.29: Left: the outside part of the elastic damper fabricated by Saip srl (www.saip.it/). Right: detail of the Parker fluid connector used for connecting the damper with the rest of the hydraulic circuit.

specifications, i.e. the component must ensure a compliance value equal to $C = 0.05\,ml/mmHg$. The damper is connected through a Parker fluid connector (see figure 3.29, right image) between the pump and the infusion system.
The pressure sensor is placed in the hydraulic circuit upstream of the damper (see figure 3.30).

The $MPX2300$ sensors (see figure 3.31) have been designed for biome-

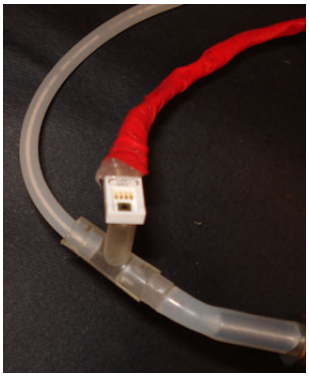

Figure 3.30: Detail of the $MPX2300$ pressure sensor mounted upstream of the damper.

Figure 3.31: The MPX2300DT1 Freescale pressure sensor front (left) and back (right).

dical applications, and are made of biomedical approved materials. Their pressure range is between $0 - 300\,mmHg$ $(0 - 40\,kPa)$. The sensors are purposely intended to be used with liquids (i.e., blood, drugs, extracellular liquid). Their sensitive part is a membrane placed on one side of the sensor (see figure 3.32, A), that can be kept in contact with the liquid.

For assembling the prototype of the infusion sources the Alzet (www.alzet.com) infusion kits have been used, consisting in polyethylene tubes attached to a

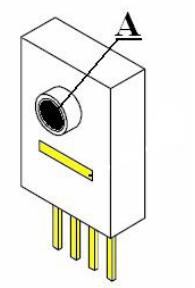

Figure 3.32: View of the Freescale MPX2300DT1 pressure sensor.

special needle (see figure 3.33). In order to reach the desired flexibility for the tubes to be inserted inside the resection cavity we heated the tubes and gave them a spring shape (see figure 3.34). Then we inserted the needles and connected the so obtained "hydraulic dispenser" to the cover of the plexiglass box (see figure 3.35).

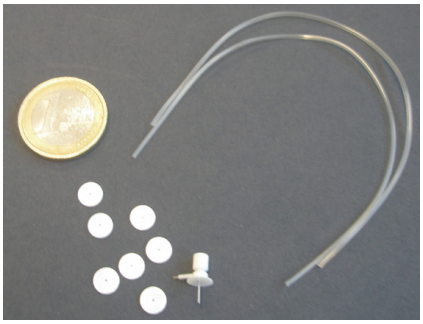

Figure 3.33: Components of the Alzet infusion kits.

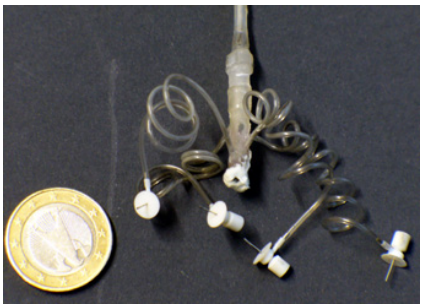

Figure 3.34: The spring-shaped tubes with the needles.

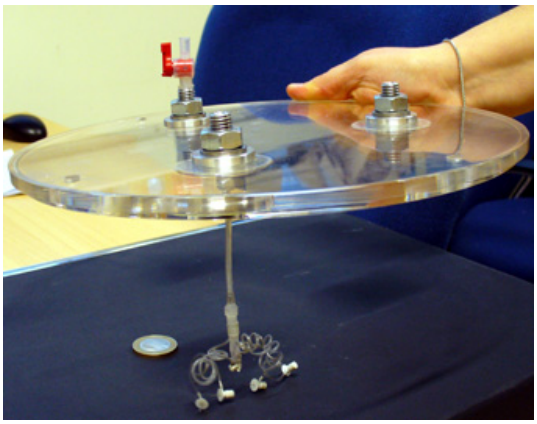

Figure 3.35: The spring-shaped tubes with the needles attached to the cover of the plexiglass box.

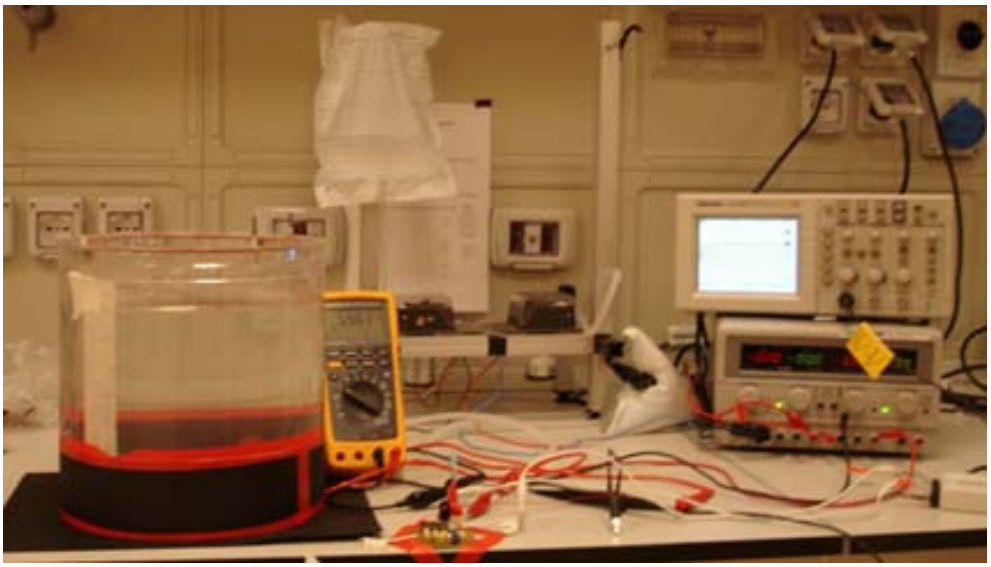

Figure 3.36: The whole setup for the *in vitro* tests.

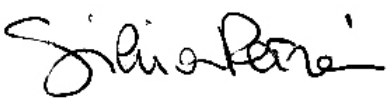

Figure 3.36 shows the overall system, encompassing the infusion device and the testing setup.
In the following sections the calibration of several components and the control systems developed are briefly presented, and some results are provided, after some validation tests made on the system.

3.8 Development of the control systems

Given the solution adopted for realizing the testing platform, it is clear that the overall system needs two different kinds of control, and that the previously described on-off control system is not enough for guaranteeing working safety and effectiveness.
The first control scheme is related to the infusion system, i.e., it is the one that switches the pump off when pressure inside the skull or inside the elastic chamber rises beyond a certain safety value. More precisely, the infusion pump must be turned off until physiological ICP values are restored. The second control is necessary in order to have, inside the plexiglass box, the ICP established from the model of the system running in Matlab.
Moreover, we need to guarantee a certain value of flow-rate infused into the cerebral tissue, and, such instantaneous flow-rate, depends on the difference between the pressure in the elastic damper and the ICP, according to the following equation:

$$Q(t) = \frac{P_{ch} - ICP}{R_{tot}} \tag{3.23}$$

where P_{ch} is the pressure inside the elastic chamber and R_{tot} is the total hydraulic resistance, encompassing catheters, needles, and the tissue. Anyhow, since in our experimental tests the tissue is not modelled, we neglect the tissue resistance, though being aware that it is a very important contribution. In addition, for this reason, pressure inside the damper needs to be lower than a maximum threshold, in order to avoid excessive pressures and infused flow-rates which could be dangerous for the patient. On the whole, the control scheme that has been implemented in the model must switch the pump ON or OFF according to data coming from the pressure sensor inside the elastic chamber and the ICP sensor.
Essentially, the control of the infusion pump has three functions:

- to keep the pressure inside the damper between the two nominal values needed to infuse the desired flow rates ($10\,\mu l/min$);
- to stop infusion if the damper internal pressure increases beyond a critical level;
- to stop infusion when ICP increases beyond a dangerous level.

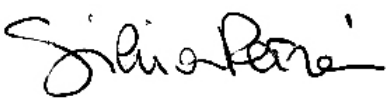

Table 3.5: Possible states of the control signal C

C_{ch}	C_{ICP}	C
1	1	1
1	0	0
0	1	0
0	0	0

The control algorithm of the infusion pump switches the pump on according to an AND operation on two conditions:

- the ICP is below $15\,mmHg$
- the damper internal pressure is below $20\,mmHg$

More precisely, when the ICP raises above $15\,mmHg$ the controller turns off the pump until the ICP falls below $7\,mmHg$. Similarly, when the pressure inside the damper gets to $20\,mmHg$ the infusion pump is stopped, until the pressure falls below $13\,mmHg$. Thus, table 3.5 is produced for the conditions above, where C is the output of the control algorithm (1=pump on; 0=pump off). A simulation of the control on the infusion pump is shown in figure 3.37.

Intracranial pressure is kept oscillating around the desired value. When the damper internal pressure goes beyond a certain threshold, the pump is switched off and is kept off until it falls again below a second threshold. As said before, once the thresholds are properly chosen, it is possible to administer the desired drug flow-rate.

Concerning the pressure inside the skull, it is first simulated by the model implemented in Matlab/Simulink and it is reproduced in real-time inside the in-vitro test system. The working principle of the system is shown in the schematic reported in figure 3.20. Pressure changes into the box according to the flow rate q imposed by the pump and is given by the following equation:

$$\frac{dP(t)}{dt} = \frac{1}{C}q(t) \tag{3.24}$$

where $C = 0.133\,ml/mmHg$ is the measured compliance of the carbon-steel membrane placed on the lower base of the box and $q(t)$ is the instantaneous flow rate of the pump used to generate the ICP inside the box. Pressure inside the box is obtained straightforwardly by integration of equation 3.24. In order to replicate the ICP pressure waveform generated by the ICP model, a proportional-derivative feedback control is designed. The control scheme of the ICP pump is shown in the following block diagram (figure 3.38). The output of the controller V_{pump} is the voltage signal for the ICP pump. Such

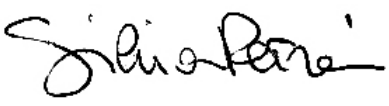

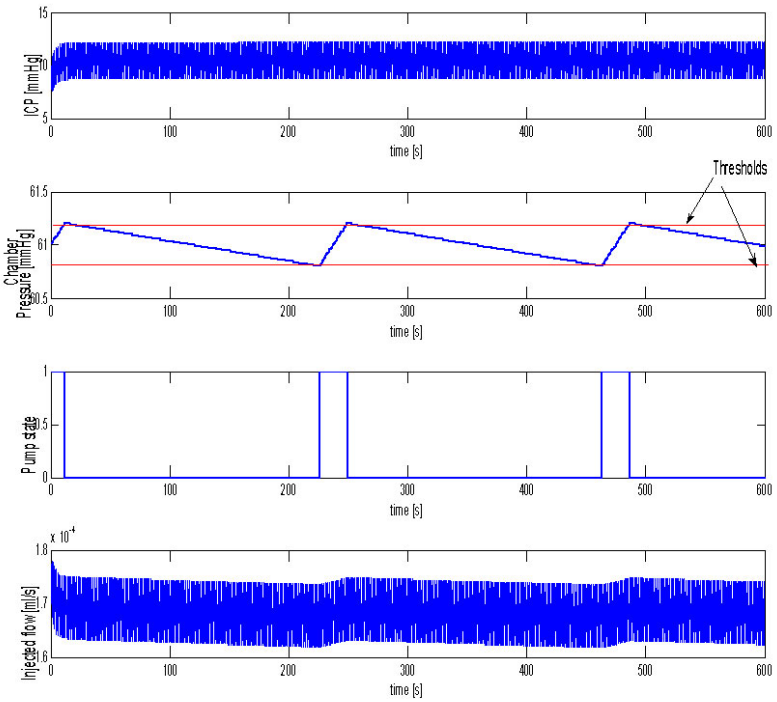

Figure 3.37: Simulation results on the control of the infusion pump. The pump is turned off when the pressure inside the elastic chamber rises beyond a certain treshold.

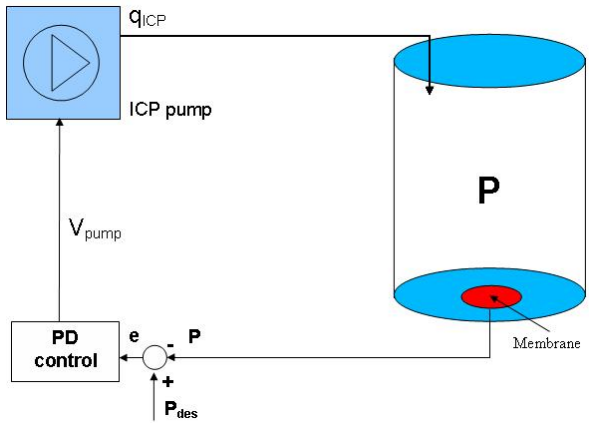

Figure 3.38: Control scheme of the simulator. The pump is switched on or off in order to rise/lower the pressure inside the box for replicating the trend of the ICP inside the skull.

control signal is proportional to the error e between the desired pressure P_{des} and the actual pressure P inside the plexiglas box and to its derivative, as described by the following equations:

$$V_{pump} = K_p\, e + K_d\, \dot{e}$$
$$e = P_{des} - P \tag{3.25}$$

where K_p and K_d are, respectively, the proportional and derivative gain of the control algorithm. Since the control algorithm resides on the PC on which the ICP model is running, a Data Acquisition board (DAQ) is used to convert digital signals into analog signals. Additionally, the signals sent from the PC need to be amplified before feeding the $12V$ DC motor of the ICP pump. The ICP pump outputs a flow rate, which in turns determines a pressure change inside the box according to equation 3.24.

An early test of the control strategy on the real system has been made by

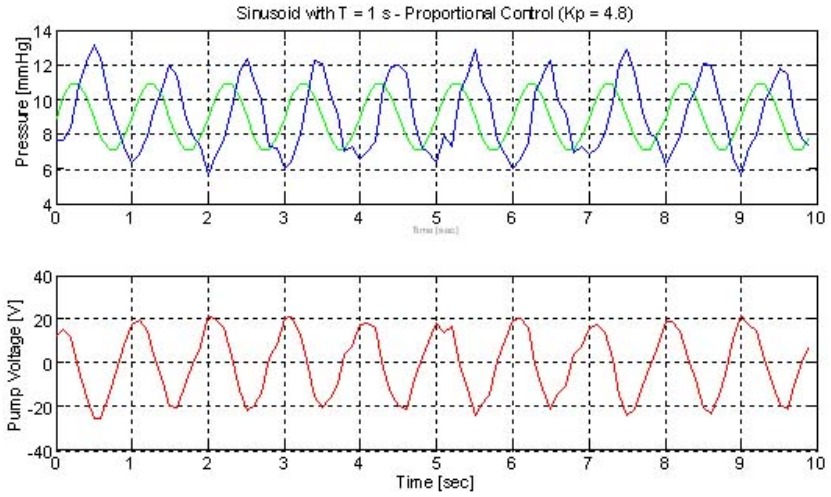

Figure 3.39: Results of an early test of the control system. The system has to replicate a sinusoidal waveform. Here a proportional controller is used.

using a sinusoidal wave ($T = 1\,s$) that must be replicated inside the box. The upper part of figures 3.39-3.40 shows the desired (green) and the actual (blue) pressure inside the plexiglas box (as measured by the optical sensor). The bottom part of the figure shows the voltage signal (red) sent to the pump. Plots in figure 3.39 were obtained using a proportional control, while plots in figure 3.40 have been obtained with a PD control algorithm. As it can be seen, the PD control allows a better tracking of the desired pressure with respect to a simple proportional control.

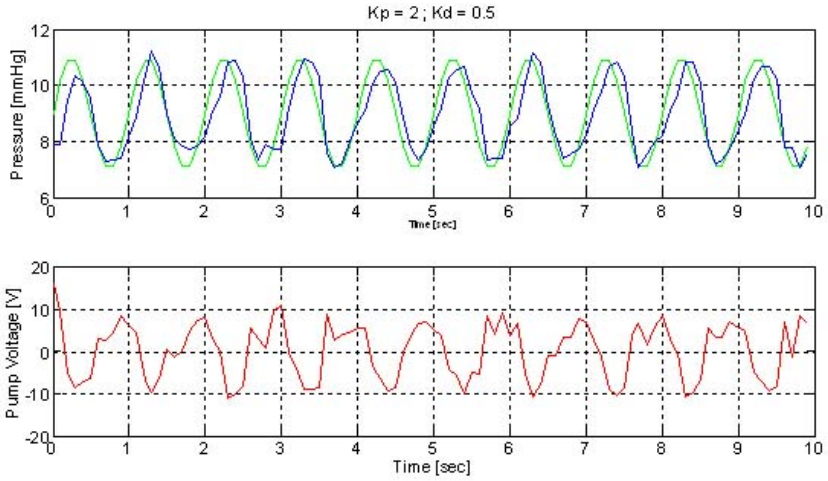

Figure 3.40: Results of a test on the control system. The system has to replicate a sinusoidal waveform. Here a proportional-derivative controller is used.

On the whole, the overall control architecture of the system is shown in figure 3.41.

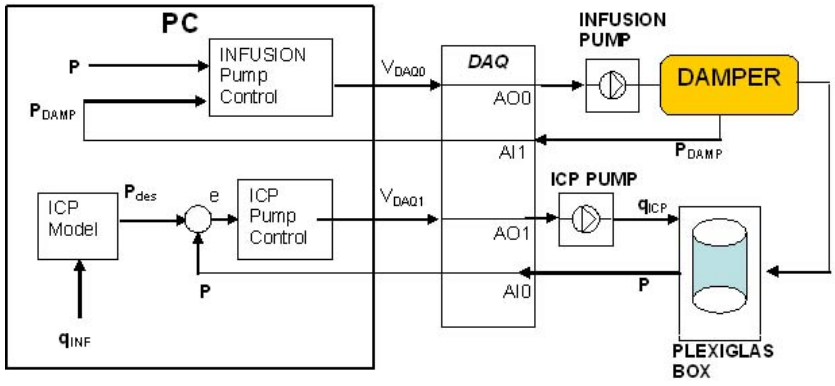

Figure 3.41: Schematic of the hardware components of the system and their interface with the control algorithms and with the ICP model running on the PC. The interface is realized using an USB DAQ card.

After designing the two control systems, in the following section several tests on the prototype are presented, and results are provided.

3.9 Tests on the prototype

These experimental tests are performed in order to check:

- wether the system architecture has been properly chosen;
- that the simulator of the cerebral dynamics actually behaves as the real anatomic compartment;
- that the insertion of the elastic chamber helps in dampening pressure peaks;
- that the control system correctly works, by turning the pump on and off when pressure rises beyond safety level.

Before starting the tests, calibration of the main components has been performed.
Both infusion and ICP pumps have been calibrated by weighing, with a precision scale (EXACTA, A120EC), the amount of water pumped in a certain time for different input voltages. Then, an interpolation has been performed, and the results are shown in figure 3.42, concerning the infusion pump, and in figure 3.43, concerning the ICP pump. The resulting equation for the

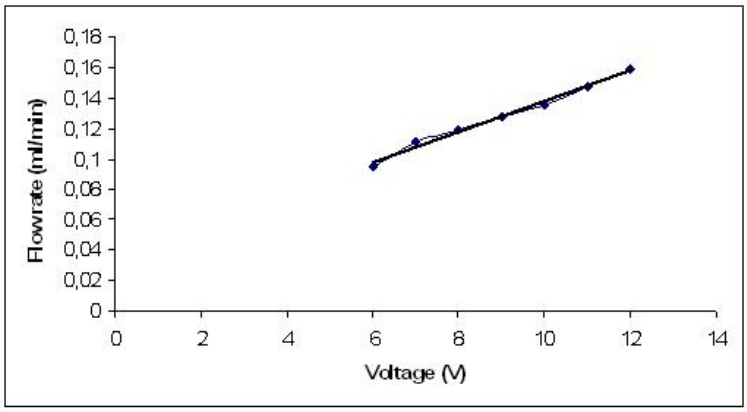

Figure 3.42: Results of the calibration of the infusion pump.

infusion pump is:

$$q = 0.01\,V + 0.0376 \tag{3.26}$$

where q is the output flow-rate and V is the input voltage.

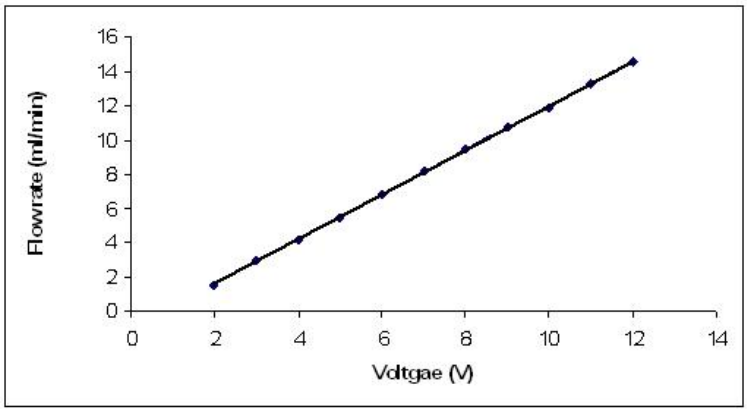

Figure 3.43: Results of the calibration of the pump used for generating the ICP inside the plexiglass box.

The correlation coefficient is $r = 0.9984$, that shows a nearly perfect linear relation between the supplied voltage and the flow rates.
As regards the pump used for generating the ICP, it is as follows:

$$q = 1.29\,V + 0.956 \tag{3.27}$$

with a correlation coefficient $r = 0.9998$, that again shows a nearly perfect linear relationship between the supplied voltage and the flow rate.
Both the pressure sensors have also been calibrated. As previously said, pressure inside the box is monitored using an infrared optical sensor (OSRAM, SFH9201). The sensor reads the strain of the membrane mounted on the bottom of the box. The strain is proportional to the pressure inside the plexiglass cylinder. Calibration of the sensor has been performed by reading the mean output voltage values when known pressures were applied to the membrane. This has been accomplished by filling the box with water at certain known heights. The plot in figure 3.44 shows the linear fitting performed on the measured data. The correlation coefficient here is equal to 0.993, and the resulting equation is:

$$P = 6.664\,V - 12.42 \tag{3.28}$$

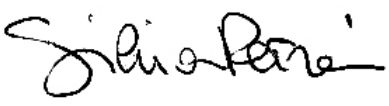

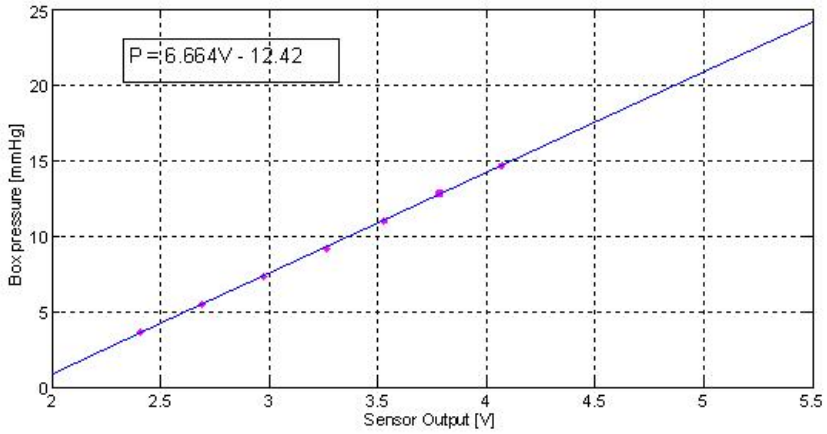

Figure 3.44: Results of the calibration of the optical sensor.

The damper internal pressure is monitored with a piezoresistive pressure sensor (Freescale, MPX2300DT1). The sensor has been calibrated by applying known liquid heights and reading the corresponding output voltage. The resulting linear fitting is shown in figure 3.45, and the corresponding equation is:

$$P = 12.11\,V - 1.252 \tag{3.29}$$

Though in this prototype we use the pressure sensor externally, such sensor,

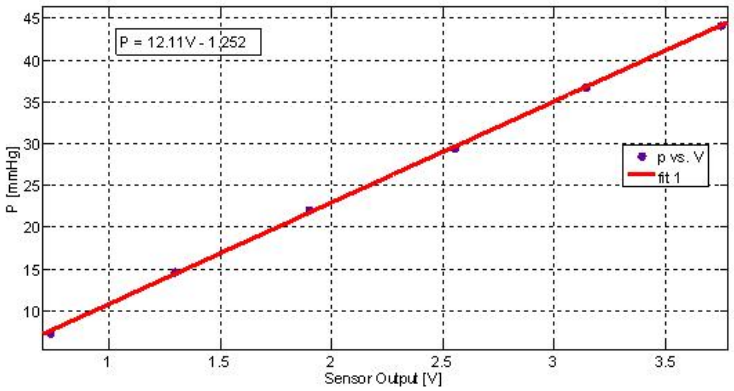

Figure 3.45: Results of the calibration of the piezoresistive pressure sensor.

as stated by the manufacturer, has been purposely designed for biomedical application, and to be used in contact with biological fluids and other materials. Its dimensions can also be suitable for inserting it into the skull, as a future development, to act also as ICP sensor. Obviously, for completely

dipping such component, a proper packaging has to be done, in order to isolate electric contacts from being altered by biological fluids, and also to guarantee a correct functioning after the packaging, without altering sensor properties as they are provided in the data-sheet.
For this reason we covered and sealed the back part of the sensor, that is the one with the electric contacts. A small plastic plate was glued to the back part of the sensor by using an epoxy glue. In this way a small volume of air was trapped inside the sensor cavity, so that the measured values are always referred to the atmospheric pressure. However, the plastic membrane may undergo some strains that, compressing the air inside the cavity, may alter the reference pressure, thus affecting the measurements. For this reason the calibration curve of the packed sensor was also checked. Measures were carried out with the experimental set-up shown in figure 3.46.

The sensor offset resulted equal to $V_{off} = -0.490\,V$, in agreement with

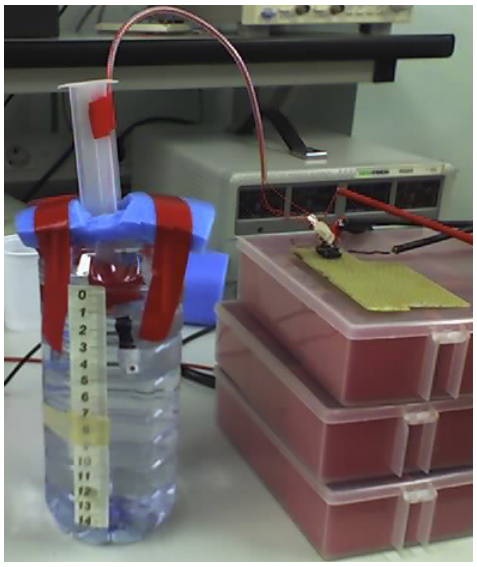

Figure 3.46: The experimental setup used for calibrating the piezoresistive pressure sensor after the packaging.

the range of possible values stated in the data-sheet. Known pressure values were applied to the sensor, by dipping it at known depths inside a liquid-filled reservoir. Measures were repeated three times and the average values were taken. A fitting among these data was done, and the results are shown in figure 3.47. The equation of the linear fitting is:

$$P = 50.2V + 24.1 \tag{3.30}$$

The correlation is equal to $r = 0.9984$, that shows a perfectly linear relation also after the packaging procedure.

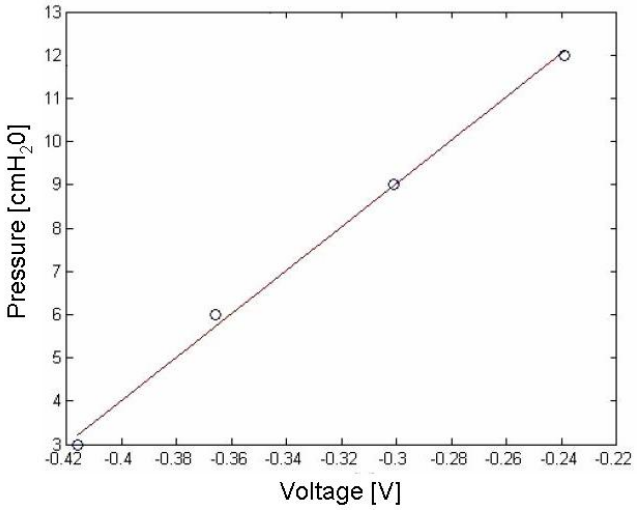

Figure 3.47: Results of the linear fitting for the pressure sensor after the packaging operation.

The first experimental test that is here presented has been performed in order to test whether the damper can reduce the pressure oscillations induced by the peristaltic pump into the catheters. To do so, the infusion pump was intermittently turned on and off and the pressure inside the catheter was measured using the Freescale pressure sensor. Plot in figure 3.48 shows the pressure as measured inside the catheters during such a test. It can be seen that the pressure oscillates between 38 and 46 $mmHg$ when fluid is pumped into the catheters. When the pump is turned off or on, the pressure abruptly changes between the lowest value of 21 $mmHg$ and the highest value of 46 $mmHg$.
On the contrary, as it is shown in figure 3.49, when the damper is connected to the hydraulic circuit, pressure variations due to the pump and to its switching on or off are reduced, because of the added compliance.

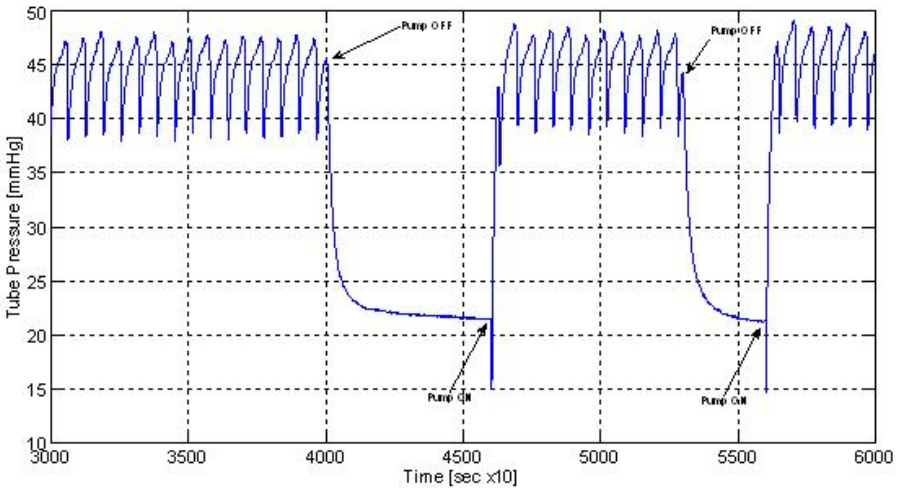

Figure 3.48: Pressure oscillations inside the catheters when the pump is on without the elastic damper.

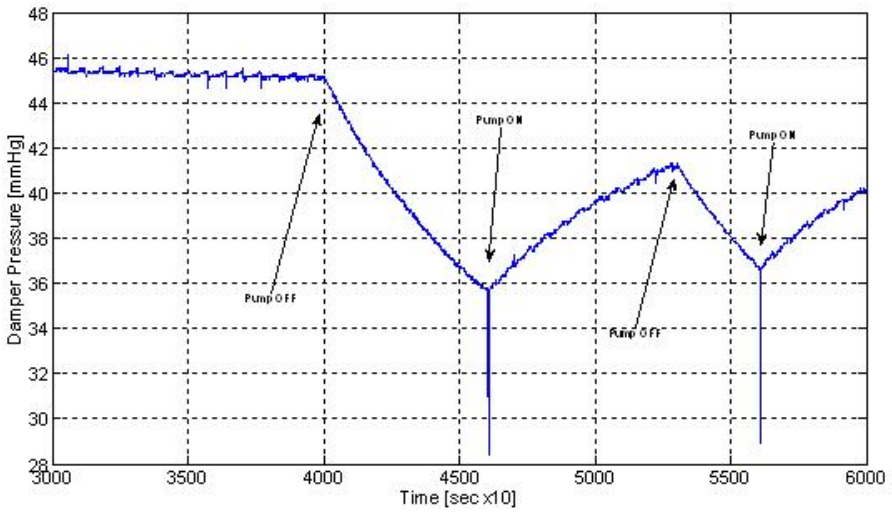

Figure 3.49: Reduced pressure oscillations when the elastic damper is inserted in the circuit.

Secondly, an infusion test has been performed, to test the effectiveness of the control on the infusion pump. Both the ICP and the damper pressure values were monitored during the infusion. If one of them exceeded the maximum allowed value (i.e. $15\,mmHg$ for the ICP, and $20\,mmHg$ for the damper pressure), then the infusion pump was stopped. Figure 3.50 shows the results of this test. The infusion pump is switched on or off according to the pressure inside the damper. As it can be seen, when such pressure exceeds $20\,mmHg$ the pump is turned off and the pressure inside the damper drops. When the damper pressure falls below the minimum value ($13\,mmHg$), the pump is turned on again.

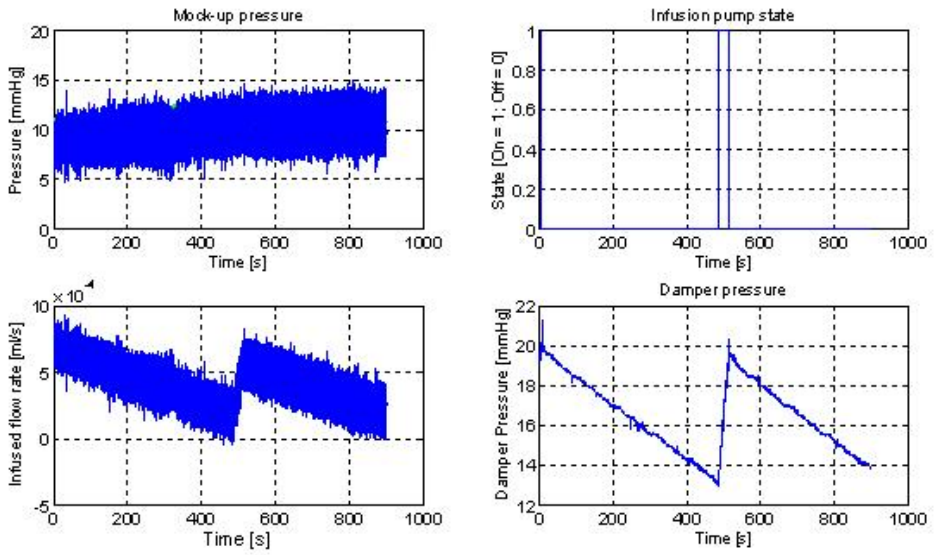

Figure 3.50: Results of an infusion test. Top left: trend of the pressure inside the box (i.e. the ICP). Top right: state of the infusion pump. Bottom left: infused flow-rate. Bottom right: damper pressure.

The last test has been performed to show the effect of a sudden increase of the ICP on the control of the infusion pump. The pressure increase inside the plexiglas box was produced by mechanically pushing on the box. Figure 3.51 shows the results from such a test. As it can be seen, when the ICP exceeds the value of $15\,mmHg$, the infusion pump is turned off until the ICP returns to the value of $7\,mmHg$.

On the whole, these early tests confirmed the correctness of the design approach chosen for the infusion device. Anyhow, they also highlighted the need for going on with the validation procedures and with design refinements, in order to come, as soon as possible, to an implantable and usable solution.

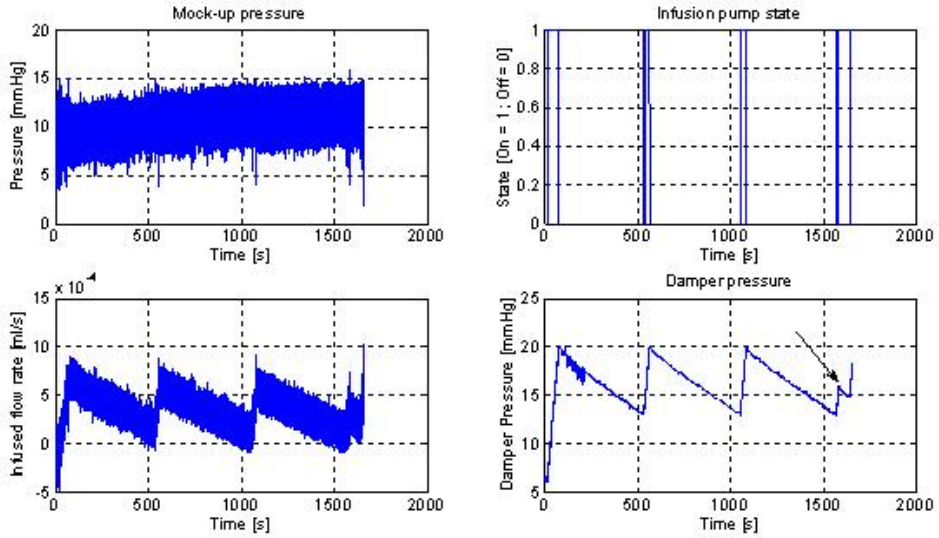

Figure 3.51: Top left: trend of the pressure inside the box (i.e. the ICP). Top right: state of the infusion pump. Bottom left: infused flow-rate. Bottom right: damper pressure.

3.10 Conclusions

The work here presented relates to the design and development of the first prototype of a novel drug delivery system specifically intended for administering drug into the cerebral compartment. Together with the infusion device, a simulator has also been designed and developed, replicating the behaviour of the brain, to be used for *in vitro* tests on the device.
A biomechatronic design approach has been used, that is, both the infusion system, the anatomic compartment and their interaction have been taken into account from the very early stages of development of the idea.
As a first step a modelling procedure has been carried out: we modelled and coupled together the infusion device and the cerebral compartment as electro-mechanical circuits. We performed infusion simulations, in order to test system response, to refine the chosen architecture, and to define a proper control scheme for the whole system.
We assembled a prototype of the infusion device by using almost all commercially available components, and then we fabricated the simulator of the cerebral compartment.
We defined two different control algorithms, one that is specific for the infusion device, and the other one that is necessary for controlling the behaviour

of the testing platform.
From the results of the experimental tests performed on the real system, we found that the chosen architecture for the infusion device could be successfully applied as an effective solution for drug delivery to the cerebral compartment.
In order to guarantee patient's safety and an effective drug administration, pressure is the most important parameter to be controlled: rather, for safety reasons, a control on two different pressures (the ICP and the damper internal pressure) is necessary, as it has been already planned during the design phase. Such control scheme was implemented and tested on the system, and the results were encouraging.
Anyhow, much effort is still due to system development, with the aim of fabricating a device to be fully implanted and used for administering pharmacological therapy to the brain.
Moreover, the simulation platform has to be improved, in order to include cerebral tissue properties, to perform infusion tests on drug penetration depth.
So far, with this work, we have shown how it is possible, by using a biomechatronic approach, to develop systems for targeted and complex biomedical applications such as brain tumours chemotherapy.
It is also worth to underline how the proposed model and the testing platform that we fabricated might be used in several other applications, whenever a detailed analysis of the interaction between the cerebral dynamics and an external system is requested.
Eventually, this design approach may also be enlarged and have a high impact in other applications, i.e., for the design of other biomedical devices interacting with different anatomic locations. The most important issue is to take into account the interaction with a biological environment from the very early stages of the design, with the main aim of avoiding errors that, once the device is fabricated and tested, may be the cause of its uncorrect, unsafe or ineffective functioning, and may bring to its failure, thus having as a consequence a waste of time, resources and, in the worst case, damage for users and patients.

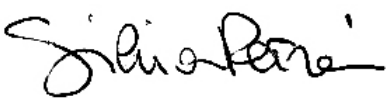

Chapter 4

Health Technology Assessment (HTA) procedures for novel biomedical technologies

As previously said in the introduction, this second part of my PhD dissertation concerns the main results of the activity on Health Technology Assessment (HTA) performed on the technologies I dealt with, that are reported in the first part of this work. For this reason several case studies are presented, each one related to a specific technological field that has already been presented in the first part of this dissertation. Eventually, an additional case study is also presented, that is not closely related to a technology I dealt with during the PhD course, but it concerns another technology at present under development in our Lab, and is another example of how to effectively apply procedures that are typical of HTA to technologies that are in an early stage of development, with the aim of obtaining useful feedbacks from both the technology developers and end-users on how to improve device usability and acceptability, in order to drive a fast device introduction on the market.

4.1 A brief overview on HTA

Several definitions have been given for HTA. Here we briefly report some of the most famous [91], trying to define all the aspects covered in this discipline.
So, HTA is:

> *"... the systematic evaluation of properties, effects or impacts of health-*

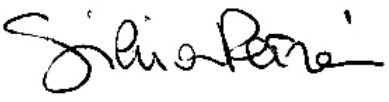

care technology. The main purpose of this assessment is to inform technology-related policy making in healthcare." (C.S. Goodman)

"... any process used for examining and reporting properties of medical technologies used in healthcare, such as safety, efficacy, feasibility, indications for use, cost and cost-effectiveness, as well as social, economic and ethical consequences, wether intended or unintended." (Institute of Medicine)

"... a form of policy research that examines short- and long-term social consequences (for example, societal, economic, ethical, legal) of the application of technology. The goal of technology assessment is to provide policy-makers with information on policy alternatives." (H.D. Banta)

"... a category of policy studies, intended to provide decision makers with information about the possible impacts and consequences of a new technology or a significant change in an old technology. It is concerned with both direct and indirect or secondary consequences, both benefits and disbenefits, and with mapping the uncertainties involved in any government or private use or transfer of a technology. HTA provides decision makers with an ordered set of analyzed policy options, and an understanding of their implications for the economy, the environment, and the social, political, and legal processes and institutions of society" (J.F. Coates)

"... a multidisciplinary field of policy analysis. It studies the medical, social, ethical, and economic implications of development, diffusion, and use of health technology." (International Network of Agencies for Health Technology Assessment, INAHTA)

"... a form of policy research that sistematically examines the short- and long-term consequences, in terms of health and resource use, of the application of a health technology, a set of related technologies or a technology related issue." (C. Henshall)

"... a structured analysis of a health technology, a set of related technologies, or a technology-related issue that is performed with the purpose of providing input to a policy decision." (U.S. Congress, Office of Technology Assessment)

From all the above definitions it clearly emerges that HTA is a multidisciplinary field, involving Economics, Clinical Practice, Engineering and Ethics. More specifically, HTA acts as a linking bridge between technical and decision-making worlds. Every healthcare institution or group of healthcare institutions should be equipped with a HTA team, made up by all of these profiles, working together in order to drive the best choice in terms of

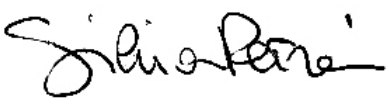

technology use. This same concept has already been expressed in terms of the main HTA objectives, that are [92]:

1. Continuous monitoring of developments concerning new and emerging technologies.
2. For new technologies: assessment of the clinical efficacy, safety, and cost/benefit ratio, including their effects on established technologies.
3. Evaluation of the short- and long-term costs and benefits of alternate approaches to managing specific clinical conditions.
4. Estimation of the appropriateness of existing technologies and their clinical use, identification and elimination of outmoded technologies.
5. Rating of specific technology-based interventions in terms of improved overall value to patients, providers and payers.
6. Guaranteeing continuous uniformity between needs, offerings and capabilities.

At present HTA is a well-established discipline in several countries all over the world: Canada, UK, Australia, USA, Scandinavian Countries, are the leading nations in this field. Here there are several national regulatory agencies (e.g the UK NICE, *National Institute of Clinical Excellence*), that act giving guidelines at national level. There are also some international organizations for HTA, putting together several smaller agencies, as the *International Network of Agencies for Health Technology Assessment* (INAHTA), or the *European Network for Health Technology Assessment* (EUnetHTA), coordinating 35 european organizations.
In this way policy makers of the health care institutions are driven from such guidelines in their decision-making activity.
Italy still suffers a delay in the development of the HTA procedures [93, 94]: there is not a national standard that can be used as a reference. HTA procedures are carried out only in few healthcare institutions, and only at local level. Recently there has been the development, at national level, of a department of the *Istituto Superiore di Sanità* ("Istituto" is a technical arm of the Ministry), called *Technology and Healthcare Department*, whose main aim is the development, experimentation, assessment and use of novel biomedical technologies for diagnosis, therapy and rehabilitation, in order to evaluate effectiveness, safety and quality of the developed solutions. Though being a good starting point, Italy is still a long way behind the HTA leading countries. In 2003, the *Italian Network for HTA* (NI-HTA) was founded, thanks to a project funded by the Italian Ministry of Health. Eventually, a significant step forward was achieved in 2006, when the *"Carta di Trento"* (available at http://www.aziendasanitaria.trentino.it/) was drawn up from the NI-HTA, containing several shared basic principles on HTA activity.

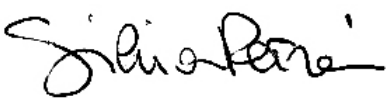

A standard HTA procedure, performed on established technologies, should follow several basic steps [91]:

1. *Identify assessment topics*
2. *Specify the assessment problem*
3. *Determine locus of assessment*
4. *Retrieve evidence*
5. *Collect new primary data*
6. *Interpret evidence*
7. *Synthesize/consolidate evidence*
8. *Formulate findings and recommendations*
9. *Disseminate findings and recommendations*
10. *Monitor impact*

However, such a strategy is not always applicable, especially to new emerging technologies that are still at research level[1]. It is very difficult to define the costs, the impact, and the long-term consequences of such a kind of technology. But, at the same time, it could be very hazardous not to perform assessment at all, until the technology reaches a well-established stage of diffusion. As a matter of fact, there is a high risk of finding out too late that a certain technology is economically disadvantageous, not user-acceptable, or even detrimental [95]. For this reason it could be very useful to perform assessment at each stage of development of technologies. But, in such a case, the traditional HTA methodologies are not suitable.
A possible solution is in the use of *"early HTA"* procedures.
The main reason for this statement is in the fact that the field of novel biomedical technologies and their use in the clinical practice is very high in *risk* and *uncertainties*. While the risk is defined as "the chance of having a

[1]Technologies stages of diffusion have been defined as follows [91]:

1. Future: in a conceptual stage, anticipated, or in the earliest stage of development.
2. Experimental: undergoing bench or laboratory testing using animals or other models.
3. Investigational: undergoing initial clinical evaluation.
4. Established: considered by providers to be a standard approach to a a particular condition and diffuse into general use.
5. Outmoded/obsolete/abandoned: superseded by other technologies or demonstrated to be ineffective or harmful.

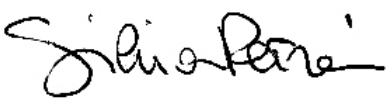

damage" (i.e. something that can be measured and quantified), uncertainties lack of "measurability" [96]. So, if for risk there are several techniques of *risk assessment* and *risk management*, for assessing uncertainties, especially in the biomedical field, we need to adopt the so-called "precautionary approach". In this context, a possible application of this approach is the early health technology assessment. It must be intended as the performing of anticipatory analysis on the technology, before the damaging occurs. This could be done by assessing technologies and risks at the very early steps of technology development [95].
Since methodologies for this early assessment have not been implemented yet, in this second part of my PhD dissertation several case study are presented. Different assessment methodologies have been used for each technology taken into consideration. This choice was due to several reasons: first of all the chosen technologies are all at experimental/investigational stage of development, but at different "sub-stages"; moreover, the same kind of analysis could not be applied to all the technologies, since they have very different features and destination for use. Eventually, as it has been previously said, there is not the optimal early HTA procedure yet, so we still need to try different possible solutions, in order to identify the ones that best fit a certain technology.

4.2 Case study I: Impact of microfluidic systems for molecular and genomic analysis: technological, socio-economic and ethical perspectives

As it has been said in chapter 2, the application of the latest findings in the field of microtechnologies and microfluidics in life-sciences is completely changing the way of performing diagnostics and, in many cases, therapy. In chapter 2 the technology state-of-the-art is presented, concerning several applications of microfluidics in the field of life-sciences. Anyhow, the rapid development of these technologies brings many other implications, covering not only the technological, but also the socio-economical and the ethical-legal fields.
A thorough HTA procedure, as it has been previously said, cannot set aside all these aspects. For this reason in this paragraph we present a HTA case-study, concerning the development of microdevices for molecular diagnostics and their potential applications, by examining the most relevant issues and open challenges concerning the aforementioned fields [97]. After the technology state-of-the-art presented and discussed in chapter 2, some economic data and considerations are provided in order to sketch the market potential of such novel devices and a patent overview is also presented.
Eventually, several considerations about the many important ethical issues

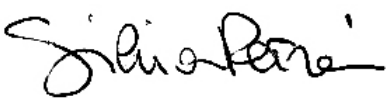

that remain open are provided, with the aim of giving an outline of the main issues that must be faced when dealing with such novel technologies, in order to better evaluate pros and cons of introducing them in the clinical practice, thus supporting the decision-making in a field that is, for a significant portion, full of uncertainties.

4.2.1 Technological and socio-economic trend

Since detailed studies on this subject have not been performed yet, only the preliminary economic aspects are briefly presented, because this is a quite young field and such systems have not largely spread onto the market yet, out of a tiny niche, mainly intended for research applications.
For this reason it is not easy to provide conclusions of general validity about cost-effectiveness of such technologies. However sometimes some preliminary information is available for certain specific devices or applications.
As an example, a cost benefit analysis can be found in the recent literature, comparing a conventional apparatus for DNA analysis through gel electrophoresis with a more compact automated system for capillary electrophoresis [98]. Authors calculated the average costs for a conventional 12-channel gel electrophoresis equipment, comprising all the instrumentation needed for the analysis procedure, and found a value of about $ 25,600. The same 12-channel analysis can be performed with a compact bench-type system at comparable costs. Even though, from this analysis, there are negligible cost savings with the use of a novel device, significant time savings are shown: indeed, while $101 - 191\,min$ are needed for performing a complete analysis with the conventional equipment, the novel device takes only about $10.2\,min$. Moreover, lower costs per sample are needed with the compact system, since it requires only an all-including cartridge, whose cost is significantly lower than for conventional electrophoresis, where lots of consumables must be used for performing the test.

In order to provide a sketch about liveliness of research and innovation in the field concerned, a patent[2] survey is hereafter presented, thus allowing

[2]Indicators of knowledge creation, TrendChart, Innovation Policy in Europe (The European TrendChart on Innovation is an initiative of the European Commission, Enterprise & Industry Directorate General, Innovation Policy Development Unit). Other indicators of knowledge creation are:

- Public R&D expenditures (% of GDP)/EUROSTAT (R&D statistics); OECD
- Business expenditures on R&D (% of GDP)/EUROSTAT (R&D statistics); OECD
- EPO high-tech patent applications (per million population)/EUROSTAT;
- USPTO high-tech patents granted (per million population)/EUROSTAT;
- EPO patent applications (per million population)/EUROSTAT;
- USPTO patents granted (per million population) / EUROSTAT.

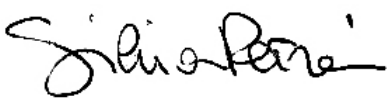

early considerations on the growth and spreading of such technologies both at research level and on the market. The patent survey was carried out on a worldwide patent database (http://v3.espacenet.com), by using several key words and searching them in the patent title or abstract over the decade 1998-2007. The used key words were: genomics, proteomics, microfluidics, microfluidic system, microfluidic device, microarray and DNA microarray. The number of patents containing each term were grouped in three graphs, that are shown in figures 4.1-4.3.

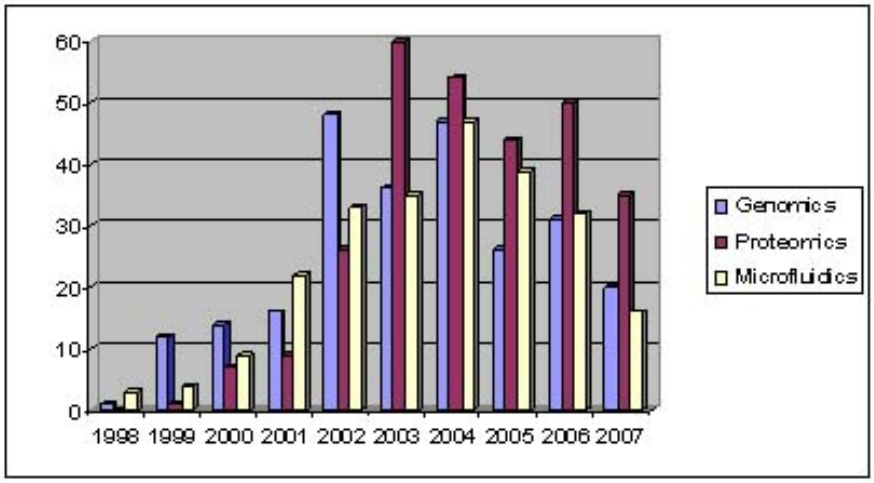

Figure 4.1: The number of published patents in the decade 1998-2007 on the worldwide database of Espacenet (http://v3.espacenet.com) containing in the title or abstract the terms: genomics, proteomics and microfluidics.

First of all, a common trend can be observed for all the key words: the most significant growth has occurred from the 1998 to the years 2002-2003, then a sort of stability can be noted in the number of published patents. Sometimes even a reverse trend is shown in the years 2004-2006, although it is not significant, especially when compared with the tremendous growth of the previous years. However, the majority of the patents has been published since 2002. The terms genomics and proteomics show a peak in the years 2002-2003. The same can be seen for DNA microarray, whose number raised significantly starting from 2002. This trend may be due to the fact that years 2001-2003 were the most important for the progress that brought to the completion of the human genome mapping.

A survey on the scientific literature has also been performed, in order

Innovation Scoreboard, 2004: http://trendchart.cordis.lu/scoreboards/scoreboard2004/indicators.cfm.

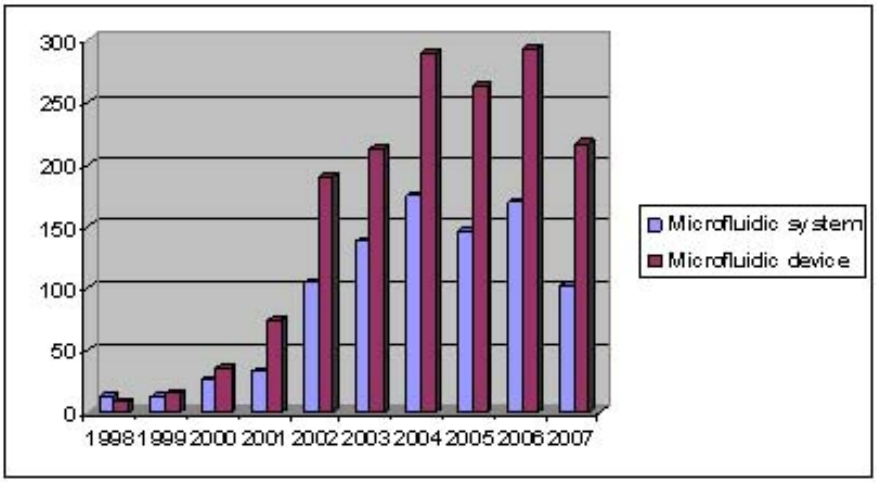

Figure 4.2: The number of published patents in the decade 1998-2007 on the worldwide database of Espacenet (http://v3.espacenet.com) containing in the title or abstract the terms: microfluidic system and microfluidic device.

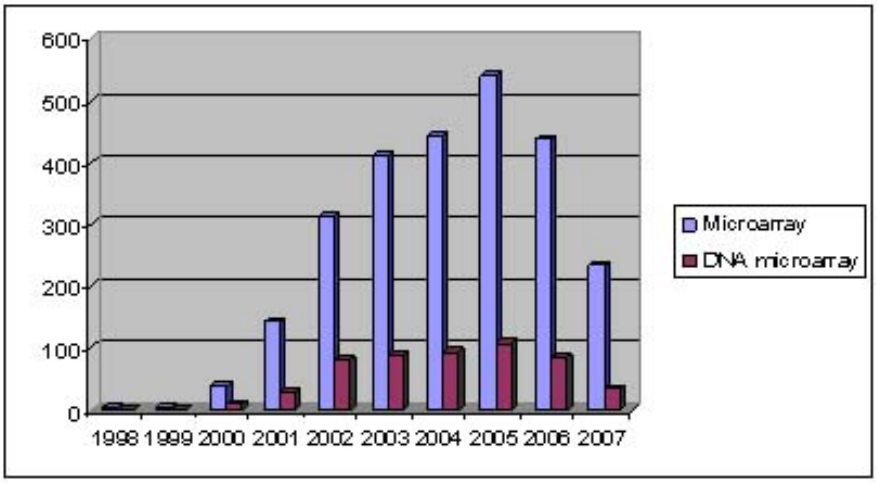

Figure 4.3: The number of published patents in the decade 1998-2007 on the worldwide database of Espacenet (http://v3.espacenet.com) containing in the title or abstract the terms: microarray and DNA microarray.

to help analyzing the general trend of these technologies. The research was made on Pubmed database, taking into consideration scientific publications starting from the year 2000 till 2007. The terms used in the research were: *microarray*, *lab-on-a-chip* and *bioMEMS*. The results are shown in

figures 4.4-4.6. It is worth to highlight that no publications containing the term *microarray* were found on Pubmed before the year 1993; the term *lab-on-a-chip* appeared only after 1996 and the term *bioMEMS* not before the year 2001.

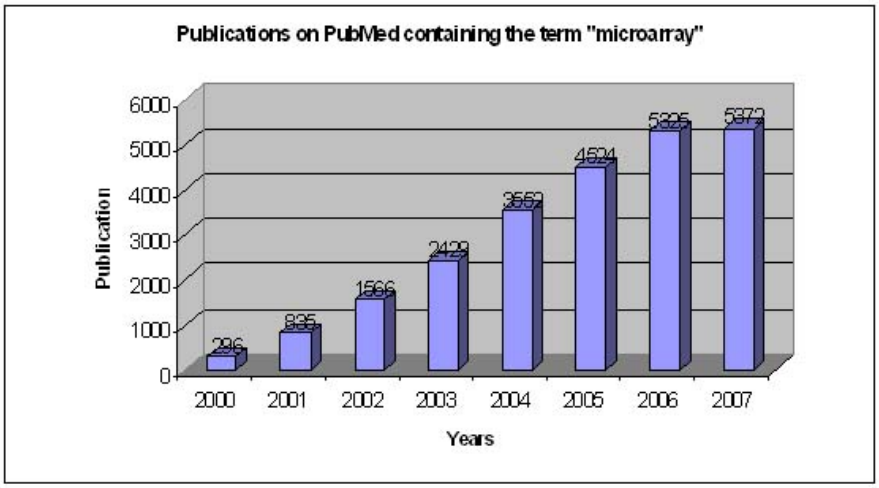

Figure 4.4: The number of publications found on PubMed database in the years 2000-2007 containing in the title or abstract the term *microarray*.

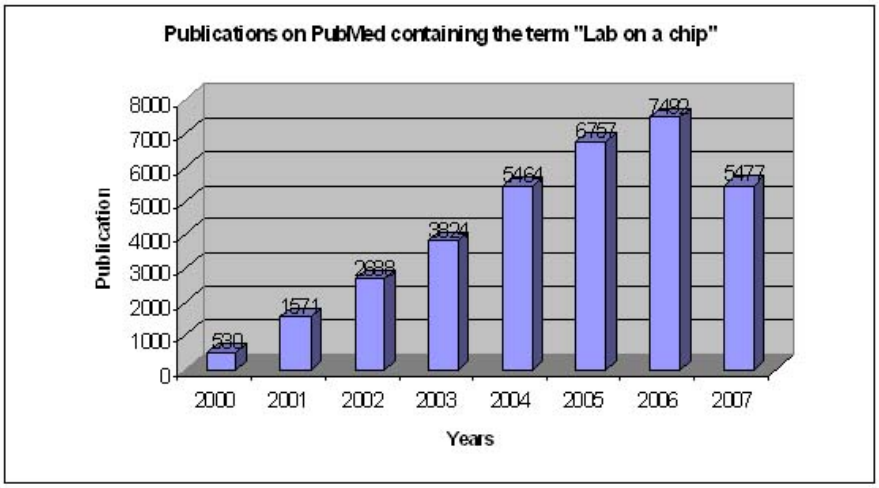

Figure 4.5: The number of publications found on PubMed database in the years 2000-2007 containing in the title or abstract the term *lab-on-a-chip*.

Anyhow, from the overall survey, it is clear that an intensive research

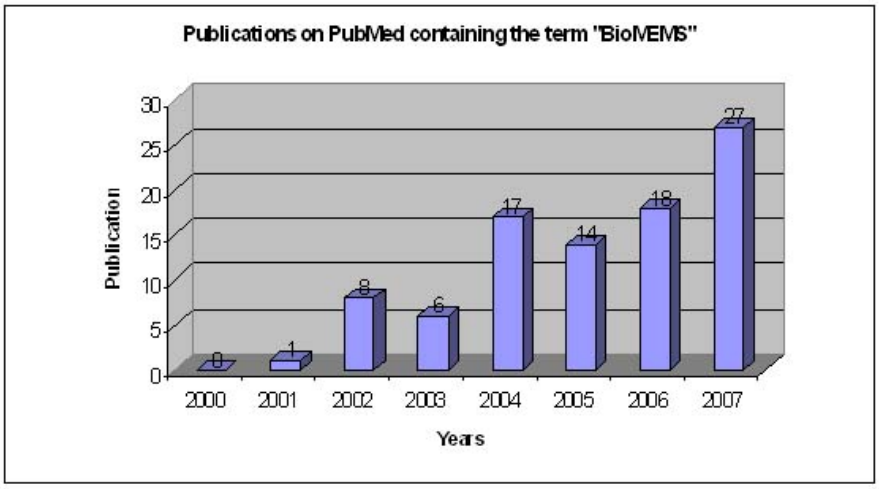

Figure 4.6: The number of publications found on PubMed database in the years 2000-2007 containing in the title or abstract the term *bioMEMS*.

activity is being undertaken in these recent years. This reflects the continuous growing interest of the scientific community towards these technologies, that is aware of the important consequences that such kind of "revolution" may bring to diagnosis and therapy. Several technology roadmaps reflect such trust in the development of such technologies (see, for example, figure 4.7). The near future is in the application of these solutions to predictive diagnostics, to personalized therapy or (even) to early self-diagnosis.
As an example, a recent review paper can be cited on this subject: Sims and co-workers investigated the potential of gene expression profiling by using emerging genomic technologies for predicting response to therapy and risk of recurrencies after therapy in women with breast cancer [100]. They highlighted the main open issues related to the use of high-throughput genomic technologies for delineating tumour subtypes and response to therapy, and for identifying patient characteristics that may influence tumour behaviour, in order not to over- or under-treat subjects that may not respond, or may very well respond to a particular therapy (*"One of the keys to improving breast cancer management is the targeting of treatment to those who will truly benefit, thereby avoiding iatrogenic morbidity in those who will not."* [100]).

4.2.2 Ethical and social open challenges

However, the field of technologies for genomics is still highly controversial. There are two main reasons for this: the first one is that there is not yet

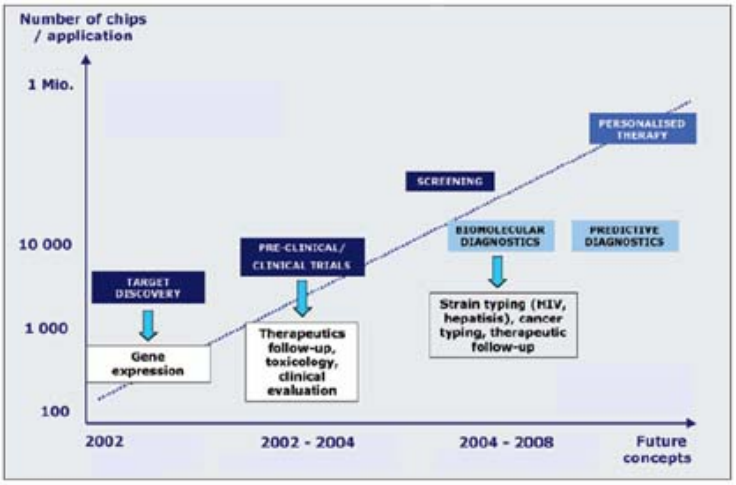

Figure 4.7: An example of technological roadmap concerning the trend of on-chip technologies for gene expression profiling, therapy, diagnosis. A promising future trend is in predictive diagnostics and personalized therapy. Image taken from [99].

a strongly supporting evidence that may confirm or totally discourage the use of these technologies into the routine clinical practice; the second reason is that the consequences that a spread use of these technologies may bring, raise many ethical and privacy-related issues. As a matter of fact, though an earlier detection of pathologies may bring to better outcomes, and also if a disease "subtyping" may bring to a more targeted therapy for a specific disease, still there are issues associated with the development of, for example, tests for disease predisposition: the possibility of early discovering a pathology or a proneness to a pathology, in fact, may bring significant changes in the occupational and also in forensic medicine: as an example, workers' recruitment may be dependent from the results of such kind of analysis, and new regulations might be needed for facing such situations. There is a strong need for anti-discrimination legislative protections, but also regulations are needed regarding data protection, or testing without consent, or even procreative liberty or precautionary abortion.

"...so, for genomic technologies of health, the impact of uncertainty on innovation is still the key feature that avoids a lead to a more favourable clinical experimental outcome for both micro and macroeconomical benefits." [101]

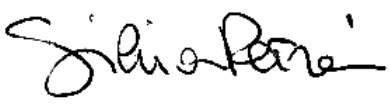

4.3 Case study II: Technological and socio-economical implications in the development of implantable drug infusion systems for brain tumour therapy

As a second HTA case study, following the technological work performed on the drug delivery system for the cerebral compartment in the first part of my PhD course (and given the poor effectiveness of the current standard therapies), here the chances given by the development of novel technologies for drug delivery, both from technological and socio-economical points of view are presented [102]. A possible technological roadmap is also sketched-out, concerning the development of drug delivery systems, that could be helpful for driving future directions in the development of such kind of technology.

4.3.1 Epidemiology of brain tumours

As previously said in chapter 3, cerebral tumours are a heterogeneous group of diseases, that, on one hand, account only for the 1-2% of the newly diagnosed tumours each year, but, on the other hand, they mainly hit young people (i.e. people under the age of 30) and children [103, 104, 105]. As a matter of fact, following leukaemia, they are the second most common class of tumours spread among children aged under 15.
Brain tumours can be classified as primary and secondary or metastatic. Primary brain tumours originate inside the brain, while metastatic tumours are due to metastases that are caused inside the cerebral compartment by tumours originating in other anatomical locations (e.g. lungs, liver, etc...)
The major part of the epidemiological data are available for primary brain tumours, as other data concerning the survival rates or the costs of this pathology.
Estimated new cases of brain tumours in the USA in 2007, based on 1995-2003 incidence rate, are about 20,500, 11,170 being males and 9,330 females [105]. Incidence in Europe in 1995 has been ranging from 4 to 11 every 100,000 inhabitants, with about 50,000 diagnosed cases in 1995 [106]. Even if these numbers seem to be not so high, the most serious thing is that, as it has been said in the introduction, such a pathology has a high mortality rate.
Pathology evolution and outcome significantly depend on several elements, among which the main ones are:

- Kind/subtype of tumour
- Age and gender of the patient
- Location and dimensions of the tumour

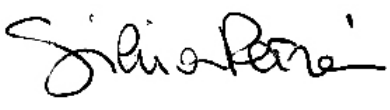

As an example, the poorest prognosis is held by malignant gliomas: one year, with only 25% surviving 2 years. For other types of brain tumours, e.g medulloblastoma, a 50% of affected patients can survive 5 years, and the 40% 10 years [104]. On the whole, for all types of brain tumours, as it can be found in Davis et al., the 5-year survival rate is only 20% [107].
Concerning age and sex, younger people and women show a higher survival rate. In children aged under 14, 5-year survival is estimated to be 72% and women, on the whole, show a better percentage than men [108, 109].
Location of the tumour is also an important element, since on it depends the extent of tolerable tumour resection during a surgery and the possibility for the onset of recurrencies [110, 111].
However, several authors assert that very little progress has been achieved in terms of survival rate since 1970s until today [112]. In [113], as an example, the same average survival rates can be found, for patients following a treatment that included both surgery and radiation therapy.

4.3.2 Overview on cost analysis

Searching literature for economic analysis about brain tumour, only few results were obtained. Mainly *Cost of Illness* (COI) analysis have been performed on the matter, given the fundamental lack of quantitative data. Such a method measures the total costs that must be borne for a certain pathology. It is a descriptive and qualitative method, that takes into account three main cost categories:

- *Direct costs*: these are cost directly paid by the health services and the patients, that mainly involve: costs for surgery, hospital stay, out-patients examinations, pharmacologic therapies and other clinical exams [114, 115].
- *Indirect costs*: these are all the pathology-related costs, due to the loss of productivity, or early retirement, or long-lasting absence from workplace, or early mortality.
- *Intangible costs*: they mainly refer to a decrease in patients' quality of life due to the onset of the pathology. Such intangible costs fall also on patients' families, as an example due to psychological stress or to changes in their everyday life [104, 116].

However, also if it may appear as a thorough cost analysis method, it has several drawbacks, the main one being its qualitative nature that, moreover, does not account for comparisons with, for example, alternative solutions.
The American National Institute of Health (NIH) estimates that, in 2006, the total costs for cancer in the U.S.A. were $ 206.3 billion. On this total amount, about 30% accounted for direct costs, while the left 70% was spent

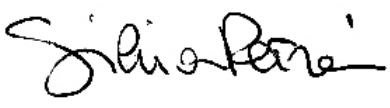

for indirect costs [105].
In particular, for brain tumours, the most recent study is the one by Kutikova et al., that estimate direct costs and their allocation for primary malignant brain tumours in the U.S.A., through a retrospective cohort analysis covering the years 1998-2000 [117]. They estimate that the total cost of care per patient from diagnosis to death is about $ 49,242 (see figure 4.8, top). This corresponds to a monthly cost of about $ 6,364 per patient, with respect to a cost per control of $ 277, that means more than 20 times higher costs for brain tumour affected patients. The biggest part (about the 64%) of such costs is due to inpatient care, and the 21% is due to outpatient exams, visits and other procedures (see figure 4.8, bottom). The monthly costs for some of the standard procedures for cancer treatment were also estimated: about $ 658 for radiation therapy, $ 365 for surgery, $ 105 for visits and drugs.

Very few data are available for Europe. One of the most detailed studies is the one by Blomqvist et al., that performed a COI analysis for brain tumours in Sweden in 1996 [104, 118, 119]. In their work it can be found that indirect costs account for 75% of the total costs for brain cancer. In 1996 $ 150 million were spent as brain cancer indirect costs, while $ 52 million were spent for direct costs. The major part of the direct costs was due to hospital care, while the majority of indirect costs was due to early mortality. The high percentage of these last costs (54%) is due to the fact that cerebral tumours often hit young people, causing an average loss of about 22 years of life expectancy [120]. Blomqvist et al. also estimated that the total cost of brain tumour for each patient in 1996 in Sweden was equal to $ 52,400.
Other not so exhaustive studies have been performed, that can provide several data on costs in other European countries.
A British study estimated the direct costs for hospital treatments of brain cancer patients [121]. The mean total costs were £15,701 per patient, allocated as follows: £442 for preliminary investigations, £2,407 for hospital stay, £2,068 for neurosurgery, £8,832 for radiotherapy, £1,078 for outpatients and £440 for chemotherapy.
Another study evaluated the direct costs for surgery between 1998 and 1999 [122]: the mean total cost for each patient was 15,242 Euros. A comparison was made with stereotactic radiosurgery performed with GammaKnife (http://gammaknife.org/): in this way the total cost was 7,920 Euros. This means that, if proven the greater effectiveness of stereotactic radiosurgery over standard neurosurgery, there could be significant direct costs savings.

4.3.3 Future trends in the treatment of brain cancer

Starting from the standard treatments, the evolutionary pathway of therapies for brain tumours could follow the trends illustrated in figure 4.9.

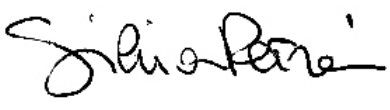

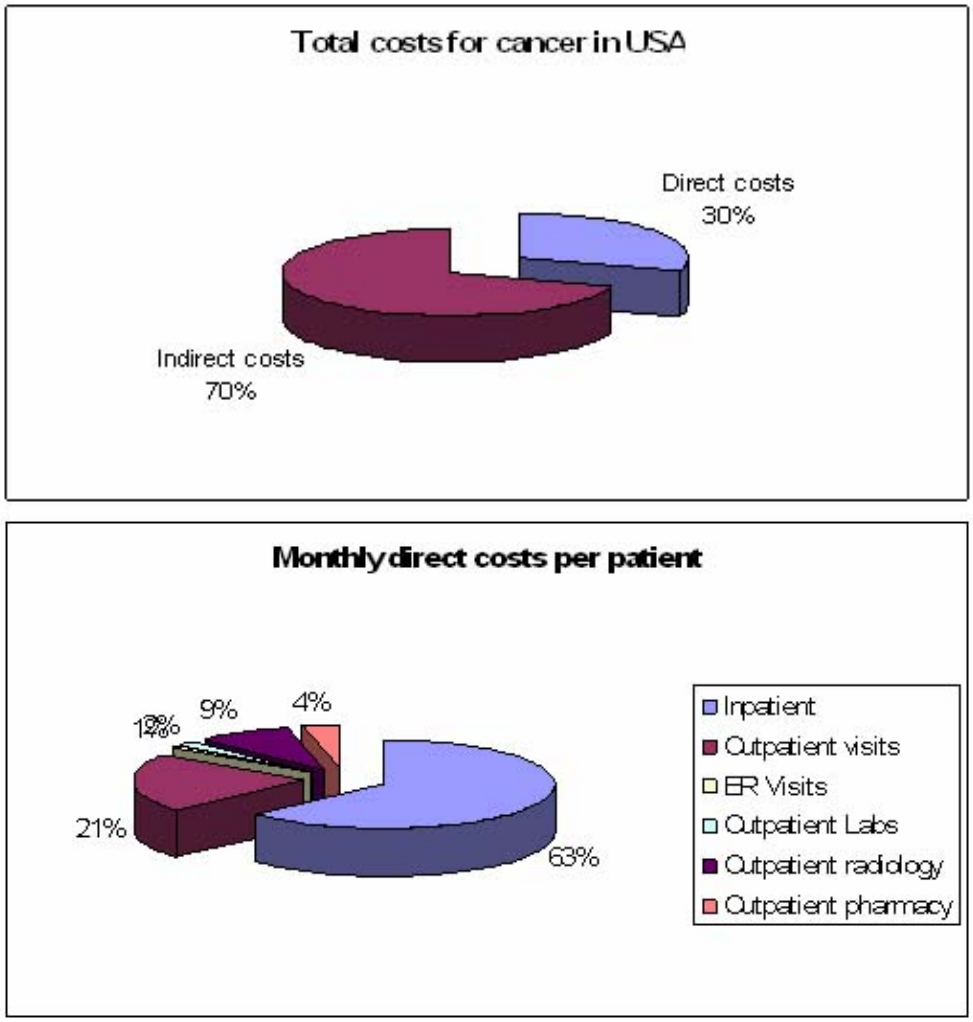

Figure 4.8: Results of the cost analysis performed by Kutikova et al., on direct costs allocation for primary malignant brain tumours in the USA. Monthly costs are indicated in the bottom diagram. Image taken from [117].

Progress could be foreseen in enabling technologies for neurosurgery, such as intra-operative imaging and computer assisted navigation systems, that would reduce the risk of neurological damaging in surgical resection. Morbidity and mortality in the perioperative period (preoperative, intraoperative and postoperative phases) should be reduced accordingly.
Chemotherapeutic drugs proved to improve considerably the median survival rate of patients with brain cancer. A meta-analysis demonstrated a 8-15% prolongation of median survival for patients treated with chemotherapy [123]. Besides, chemotherapy often helps in palliate symptoms, and can improve the patients' quality of life [124]. The difficulties in drug ad-

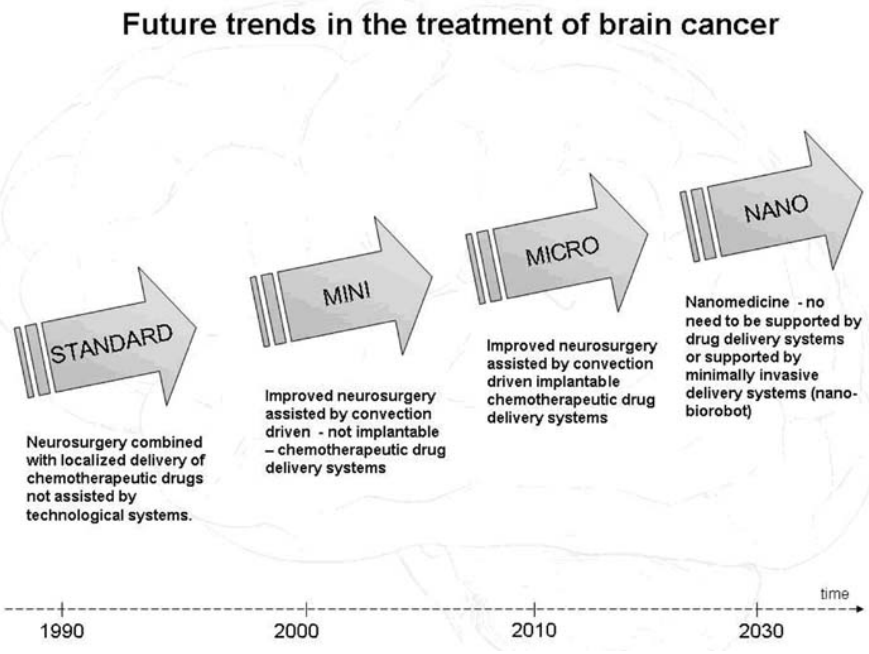

Figure 4.9: A roadmap of possible future trends of therapies for brain tumours.

ministration and penetration constitute a strong roadblock to the effective and extensive use of chemotherapy in the treatment of brain cancer.
More effective strategies for overcoming chemotherapeutic drug resistance would pass through the development of small - not implantable -, smaller and smallest - implantable - devices and systems for localized drug delivery. Nanotechnologies and nano-bio-robots will definitely change the scenario of therapies for brain tumours in the next decades, overcoming the physiological, chemical and mechanical limitations affecting the current treatments.
Based on the data collected from the literature, and taking into account the work that is currently under development in our Lab, we carried out a technological roadmap on the future of the implantable infusion systems for drug delivery, that is shown in figure 4.10.

As it can be seen, implantable drug infusion systems specific for the cerebral compartment are still at their experimental stage of development, so it would be difficult to make comparisons with the standard techniques, but the trend is quite promising.
The cost of standard implantable drug delivery systems currently ranges from $ 1,500 to $ 7,700 [125], but, if the effectiveness of such a solution will be proven, the costs of these devices will well balance the gained advantages, in terms of reduced hospital visits and increased patients' autonomy in ad-

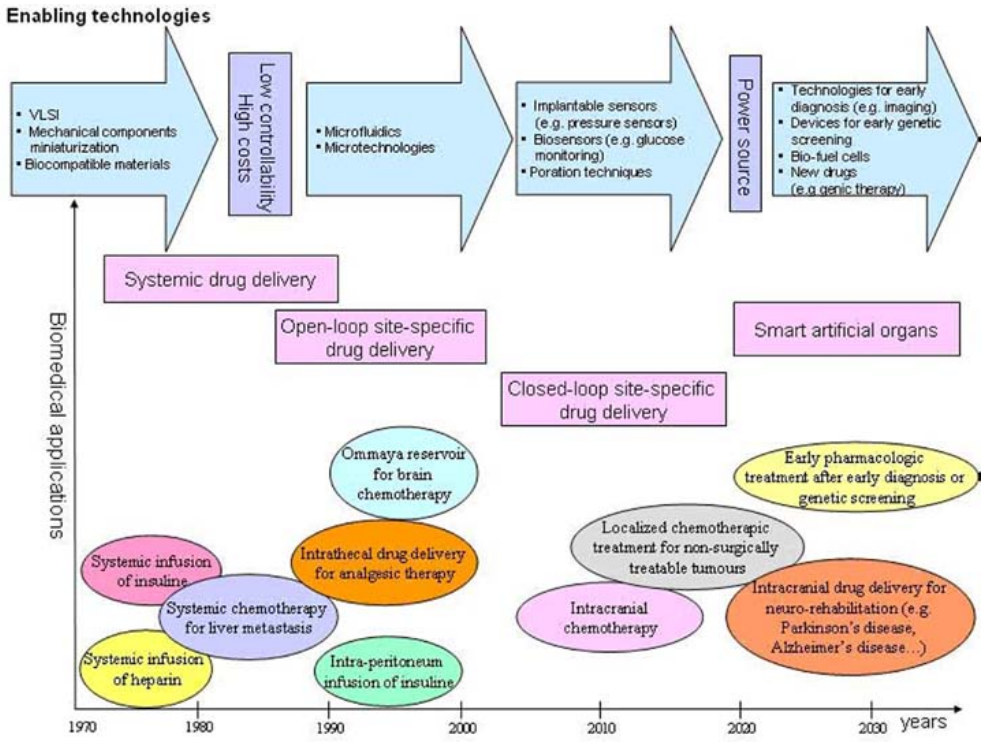

Figure 4.10: A possible future roadmap for implantable drug delivery systems.

ministering themselves the pharmacological therapy.
Moreover, further developments in miniaturization technologies and in new drug discovery, might encourage the development of closed-loop implantable drug delivery systems that can be applied to the early treatment of other classes of non-surgically treatable tumours, or even to the treatment of other pathologies, such as ageing-related diseases (e.g. Parkinson's or Alzheimer's disease).
On the whole, the technology trend is mainly aimed, on one hand, at giving autonomy to the patient during her/his pharmacologic therapy. On the other hand, such therapy is becoming more and more targeted and early, in order to reduce side-effects of systemic toxicity, since an early or preventive treatment might allow for successful results with reduced drug doses and treatment duration.

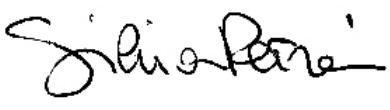

4.4 Case study III: Early assessment of neuro-rehabilitation technology

The third HTA case study that is here presented, relates to the early assessment of a novel mechatronic system that has been developed to be used in neuro-rehabilitation for performing quantitative assessment of patient's recovery after stroke through whole-body isometric force measurements [126]. The ALLADIN (naturAL language bAsed Decision support In Neuro-rehabilitation) system has been developed within a European project of the 6^{th} Framework Programme by a consortium of ten European partners, both with technological and clinical background.
The rationale for the development of this novel instrument for supporting clinical decision making in neuro-rehabilitation comes from several neurophysiological assumptions, together with some clinical evidence on cerebrovascular pathologies.

4.4.1 Rationale for robotic neurorehabilitation

The World Health Organization (WHO) estimates that every year about 15 million people suffer a stroke, that is a pathologic event of vascular origin, involving several types of cerebral dysfunctions, that in most cases leaves people permanently disabled or, in the worse cases, brings them to death. While about 5.5 million of them die, 5 million are left severely impaired [127, 128]. Starting from these few data, the importance of contributing to the effectiveness of a post-stroke neuro-rehabilitation clearly emerges.
After a stroke event, in fact, a functional recovery is usually shown, depending on several factors, such as: patient age, anatomical and functional peculiarities; zone and dimensions of the damage; period of time spent from the onset of the stroke event and the beginning of the rehabilitation therapy, and so on.
In the medical literature several studies can be found, that show how the duration and the strength of the rehabilitation training are of fundamental importance for stimulating motor skills recovery after the occurrence of a stroke event. For this reason, at present, the rehabilitation process involves highly repetitive exercises, often guided from the therapists, that usually are in a one-to-one relationship with the patients. Such a method is both highly resource- and time-consuming.
With the aim of improving and increasing the effectiveness of the post-stroke rehabilitation, several studies in the field of bioengineering have been performed, that have shown the possible advantages in the use of a robot-mediated rehabilitation therapy [129, 130, 131, 132, 133]. Particular attention has been paid to the possibility of more effectively identifying the mechanisms underlying the functional recovery and the motor control.

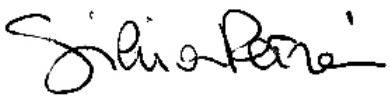

Since there is a large variety of such mechanisms, clinicians often encounter considerable difficulties also in performing a quantitative evaluation of the patient conditions soon after the stroke and in measuring the recovery during the rehabilitation process. Several assessment scales exist, that measure patients' different skills, functionalities or level of impairment. But such scales are often qualitative and lead to subjective evaluations of the therapists, that may not reflect the actual patients' conditions.
The ALLADIN platform has been developed to overcome such drawbacks and to contribute to the development of quantitative assessment tools in neuro-rehabilitation.
We performed an early assessment of the system, after the fabrication of three prototypes and after the first clinical trials. As it will be described in the next paragraphs, we based our assessment procedure on the point of view of all the (technological and clinical) partners involved in the development of the platform.

4.4.2 The ALLADIN structure and technology

The ALLADIN diagnostic device (ADD) consists of several components: a modular platform, where the patient is entered for the assessment, equipped with 8 force/torque (F/T) sensors, that acquire data during the performing of simulated activities of daily living (ADLs); a dedicated database, used for storing all the obtained measures; and a PDA-based natural language system interface to be used by the therapist. The F/T sensors are installed: behind the trunk, below the posterior, at the affected lower arm, at the affected thumb, index and middle finger, at the affected foot and toe. The 6 chosen ADLs are: drinking a glass of water, picking up a spoon, turning a key, lifting a bag, reaching for a bottle and bringing a bottle to the opposite side [134]. A picture of the ALLADIN platform now installed at the CESA Institute of the University Campus Bio-Medico is shown in figure 4.11.

Actually, the 6 ADLs are only initiated, not really performed by the patient. The 8 F/T sensors isometrically measure the initiation of the task. This is motivated by the basic hypothesis underlying the whole project: that is, imagination and initiation of the task have the same functional properties as performing the task itself [134, 135, 136, 137, 138, 139, 140, 141, 142].
The early clinical trials were performed in three rehabilitation institutes participating in the project.
The clinical protocol is as follows: the patient is inserted and secured in the platform seat; each task is first shown on a screen in front of the patient; the patient is then asked to "imagine" the task; eventually, the patient is asked to "execute" the task three times in succession. For every task initiation, six variables from each F/T sensor are recorded, that is the force and the related torque along the x-, y- and z-axis. At the same time, a clinical

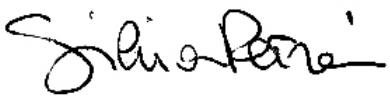

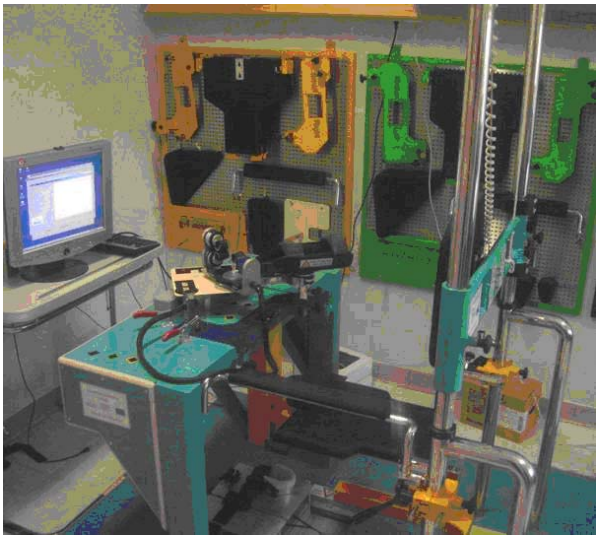

Figure 4.11: An overall view of the ALLADIN platform installed at the CESA Institute of the University Campus Bio-Medico, Rome.

evaluation is performed by using standard clinical assessment scales such as: Fugl-Meyer scale, Motor Assessment Scale, and Stroke Impact Scale. The scores are recorded inside the PDA, together with natural language based evaluation of the patient level of recovery, given by the therapist.
The main aim of such clinical experimentation was to find possible connections among assessment scales, natural language based descriptions and the F/T measures obtained with the ALLADIN platform. The final aim of the ALLADIN project was to contribute to the development of a standard procedure for assessing post-stroke functional recovery, by giving quantitative measures in order to support the clinical decision making in neuro-rehabilitation.

4.4.3 System assessment through a SWOT analysis

The chosen tool for a preliminary technology assessment of the ADD is a SWOT (Strengths, Weaknesses, Opportunities and Threats) survey. Two main reasons led to this choice. The first one is due to the fact that, when dealing with innovation, especially in the biomedical field, an assessment of the technology at its experimental/investigational stage of development is essential in order to help the product development process and to avoid waste of resources for applications that, once on the market, may result as ineffective or even harmful. Secondly, the reason for choosing a SWOT survey as an assessment tool is that a biomedical technology is the result of

the cooperation among different and multidisciplinary backgrounds. Thus, the feedback on the assessment of the technology must be obtained from all these different points of view, and the standard structure of the SWOT analysis is suitable for such task.
At this stage of development of the device, the SWOT analysis has been used mainly for obtaining feedback on the actual usability and acceptability of the product and for driving actions that aim at an integrated device development, for a more rapid introduction on the market.
A SWOT survey is a quite standard strategic planning tool, employed in many organizations for developing strategies, aimed, as an example, at improving a product, or at reinforcing a corporate division, through an environmental scanning of both the internal and the external elements that may affect or make change a business strategy. The internal elements that are examined are the strengths and weaknesses that a system, in our case an innovative biomedical technology, has, that may be, for example, some technical aspects, or other factors that come from the system itself. The external elements to be analyzed, instead, are the opportunities and threats that may come from the market, and that can help or limit the development of the system (see figure 4.12). An example of external threats, in our case,

	Strengths	Weaknesses
Opportunities	S-O strategies	W-O strategies
Threats	S-T strategies	W-T strategies

Figure 4.12: A schematic diagram illustrating the SWOT analysis procedure: through an environmental scan the internal (S,W) and external (O,T) factors are identified, and subsequently combined and used for generating strategies.

may be other biomedical robotic devices that can perform the same tasks of the ADD, but at lower costs, or with a portable device.
The results of a SWOT survey, i.e. the list of the strengths, weaknesses, opportunities and threats of a system, are often added with another part, that consists in asking some questions, for stimulating the strategy generation ("creative" use of SWOT). The questions concern the possible uses of the identified SWOT points. These are usually quite general questions, such as:

- How can we use each strength?
- How can we stop each weakness?
- How can we exploit each opportunity?
- How can we defend against each threat?

For this reason, such kind of analysis is quite suitable for being used by multidisciplinary teams, in such a way that everyone can contribute to the development of a strategy by giving answers and suggestions based on his own point of view.
In the ALLADIN project the SWOT analysis has been chosen as a simple methodological approach for an "in progress" multidisciplinary evaluation of the system, with the aim of encouraging an integrated device development, by examining its acceptability and usability under different points of view. Indeed, in a future perspective, the technical partners may be identified as the producers and the clinical partners as the end users of the device.
A SWOT questionnaire was administered to the ten partners of the ALLADIN project. An overview of the questionnaire is shown in figure 4.13.
On the total amount of 10 sent surveys, 9 filled questionnaires were received back for results analysis, that is, the 90% of responding ratio. Answers concerning similar aspects were grouped together, in order to draft a sort of classification of the most cited answers. A schematic sorting of the points listed in the first part of the questionnaire is given in figure 4.14. Indeed, as it can be seen, lots of internal strengths have been identified, while a smaller number of weaknesses has been found. The same can be said as regards the opportunities and the threats.
The main strengths and weaknesses are shown in figure 4.15- 4.16.
As it can be seen, the technical robustness and the easiness of use are the most cited strengths, both by the technical and clinical partners. This means that, although as an early prototype, the device has already been designed using a correct clinical approach.
However, the major identified weakness is a still to be increased reliability of the system. This means that, in spite of the technical robustness of the prototypes, work has to be done in order to improve the quality of measurements, signals acquisition and sensors correct functioning. Another important point that has been remarked is the lack of a biofeedback, to

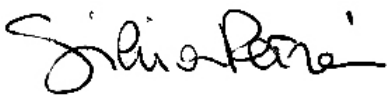

ALLADIN SWOT ANALYSIS

Each Alladin partner should fill in this table by listing and shortly justifying what he considers *strengths*, *weaknesses*, *opportunities* and *threats* of Alladin, according to his own perspective. That is, clinical partner will think over SWOT from a clinical point of view and the technicians from a technical point of view

The required information is grouped into two main categories:
Internal factors: the *strengths* and *weakness* of the technology itself, if compared with the state of the art or other clinical/technical choices.
External factors: the *opportunities* and *threats* presented by the external environment.

A further required effort is to try to find an answer to the following questions:

1. How can we use each Strength?
2. How can we stop each Weakness?
3. How can we exploit each Opportunity?
4. How can we defend/destroy against each Threat?

After receiving the required information by each partner, the teams of SSSA and UCBM will aggregate the data so that possible scenarios for Alladin will be analyzed taking into consideration:

- the technical perspective
- the clinical perspective
- the economic perspective

INTERNAL	Strengths	
	Weaknesses	
EXTERNAL	Opportunities	
	Threats	

Figure 4.13: The SWOT questionnaire submitted to the partners of the ALLADIN project.

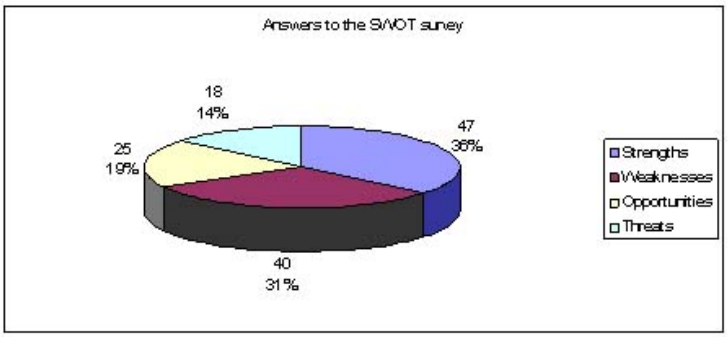

Figure 4.14: A preliminary sorting of the total answers to the SWOT survey.

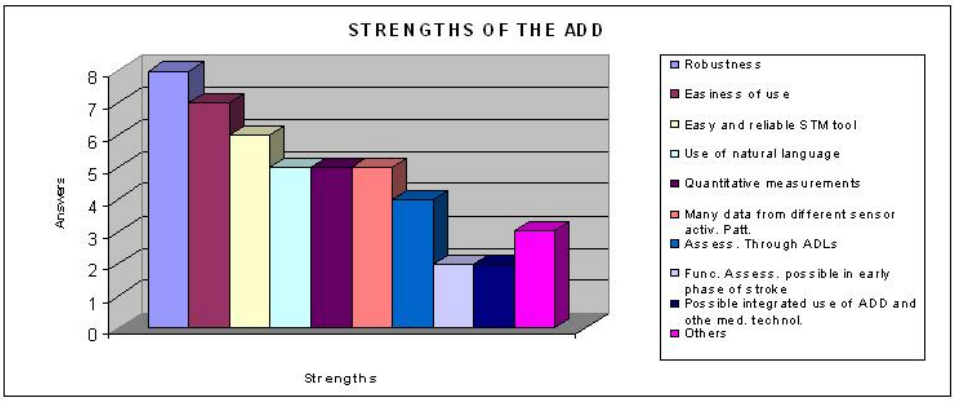

Figure 4.15: The strengths listed by the project partners in the SWOT questionnaire.

inform the patient on the "quality" of his/her performance. This technical weakness will be discussed later also as a possible threat, that may limit both the acceptability of the device and its spread on the market. Another point to be highlighted is the opinion expressed about the use of natural language for entering information about the patients' conditions and recovery level. This point is, as the one concerning robustness and reliability, slightly controversial. Five partners indicated as a strength the possibility of using natural language for entering information on patients, but five considered it as a weakness, in that the total amount of expressions that can be used for describing patients' conditions is still limited. This means that, as it has been done for robustness and reliability, the approach of using natural language has been accepted as a good point, but, at the same time, partners are aware that they still have to work to optimize this technical aspect. The same can be said as regards the strengths of having many and quantitative

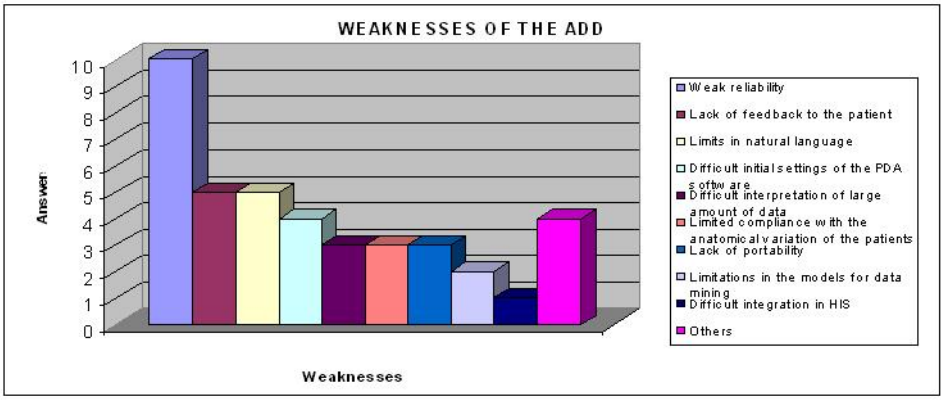

Figure 4.16: The weaknesses listed by the project partners in the SWOT questionnaire.

measurements coming from different sensor activation patterns. Partners highlighted several corresponding weaknesses, that are the difficulty in the interpretation of a large amount of data and the limitations in the models they have, at present, for data mining.
The listed opportunities and threats are shown in figures 4.17-4.18.
As previously stated, a common positive opinion has been expressed about

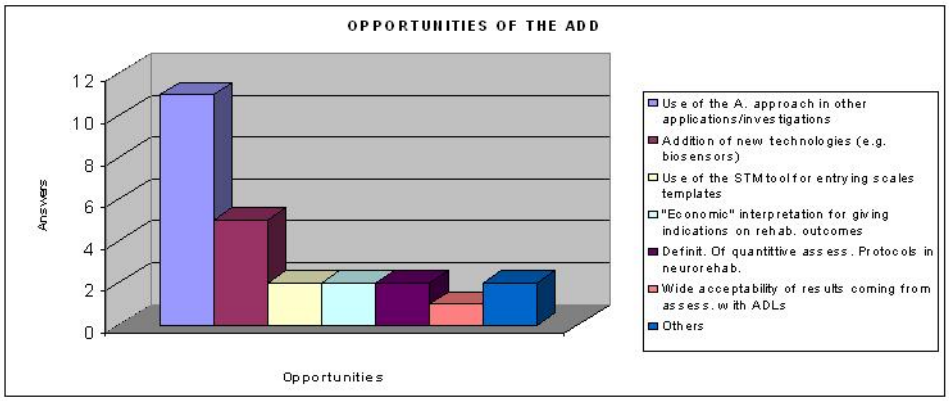

Figure 4.17: The opportunities listed by the project partners in the SWOT questionnaire.

the ALLADIN approach, that involves the use of isometric measurements, the assessment through ADLs, measurements acquired in different body parts at the same time, the data stored in a dedicated database. The main opportunity that has been expressed to be exploited is the possibility of applying the ALLADIN approach to other clinical investigations and bio-

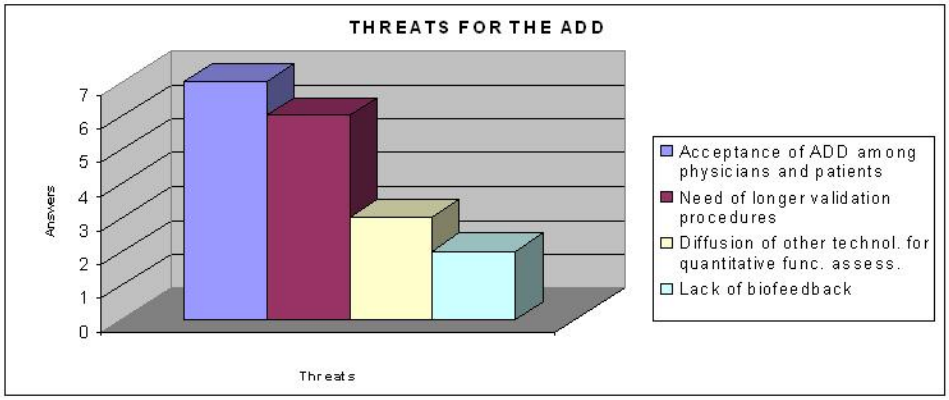

Figure 4.18: The threats listed by the project partners in the SWOT questionnaire.

medical applications. On the other hand, the major threat that has been identified examining the external environment, is the acceptance of the ADD among both physicians and patients. This is a problem that every novel technology encounters, especially in the earlier stages of development. Another threat is, as previously stated, the lack of a biofeedback in the system. Such a threat comes from the possible diffusion on the market of devices for functional assessment that already have this feature embedded in the system.
In the second part of the questionnaire it has been asked to the partners to list some ideas on how to use, reduce, exploit and destroy each strength, weakness, opportunity and threat they had previously identified in the first part. Lots of constructive ideas have been suggested, and it was not easy to group all the ideas as it had been done for the first part of the questionnaire. However, the most recurring suggestions expressed an overall acceptance of the ALLADIN approach, together with a common idea that it is worth going on with the validation procedures of the ALLADIN technology and with clinical trials, in order to disseminate findings and results to strengthen the acceptability of this technology among users (both clinicians and patients).
On the other hand, several technical limitations of the ALLADIN platform still appear according to almost all the partners. Several suggestions have been given on how to reduce such weaknesses, that mainly consist in working on the hardware of the system, improving its flexibility both in terms of fitting of patients and reduction of the overall bulk of the device, always trying to keep the costs as low as possible. Moreover, the need for the development of an effective tool for data mining, to be combined with traditional clinical data analysis, has been expressed.
Eventually, as it has been cited before, one important point has emerged,

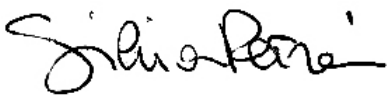

that is the need for the implementation of a biofeedback for the patient. This is to overcome a threat coming from other existing robotic and mechatronic technologies that already implement such feature and give such information. On the whole, the results of the SWOT survey showed that the common efforts should be devoted to the definition of a standard procedure for the assessment of functional recovery after stroke, that can provide quantitative data for interpretation of patients' conditions, useful for decision making in terms of the right choice of the rehabilitative process of each patient.

4.5 Conclusions

In this chapter several examples of application of "non-standard" HTA procedures to the assessment of novel technologies were presented. The main aim of these examples was to give a "reading key" on the use of these new technologies, since they are not yet supported by literature results, clinical data and cost analyses, that usually drive the assessment of a certain technological solution. Anyhow, the application of procedures of "early HTA" may help in deciding wether or not to go on in the development of a certain technology, and may give an outline of possible technology future trends, in order to drive design solutions.
Moreover, HTA may also be used for testing the acceptability of a novel technology among users, before its introduction on the market, in order not to waste time and resources for developing applications that, once on the market, may result ineffective, underused, or even harmful.

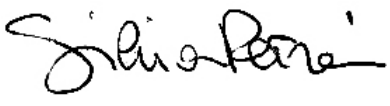

Chapter 5

Conclusions

In this dissertation the main achievements of my research activity, performed during these three years, were presented, together with a general description of the activity carried on in order to come to the results. Chapter 2 and 3 were related to the part of my PhD work where biomechatronic devices for diagnosis (especially microfluidic technologies for molecular diagnostics) and therapy (especially drug infusion devices for tricky anatomic compartments) were critically investigated and designed, following biomechatronic design criteria, that should always be kept in mind when dealing with biomedical technologies.
Then the second part of my dissertation was devoted to the description and application of health technology assessment procedures to the aforementioned biomedical technologies, that are at their early stages of development. Due to their novelty, in fact, it is not possible to apply standard HTA methods for evaluation, and a joint approach, that involves both the biomechatronic design and an early HTA procedure, was proposed, in order to avoid errors or wrong design choices during the development of a new biomedical technology, and to give a possible reading key for the trend of the most promising technologies; for this reason in chapter 4 several examples were provided, by using different HTA approaches.
Concerning the development of novel systems for molecular diagnostics, it has been shown how low-cost technologies, such as the piezoelectric dispensing (inkjet-alike), may be adopted for biomolecular dispensing for bioassays applications, just making several hardware modifications to commercially available technologies (e.g. inkjet printers), thus improving an existing technology.
Moreover, a feasibility study has been presented, concerning a completely original approach, that is, the use of electrokinetic principles for developing miniaturized systems for performing analysis on chip. In particular, a novel solution for realizing PCR thermal cycling in a microfabricated chamber has been investigated. Preliminary results showed that, once chosen the

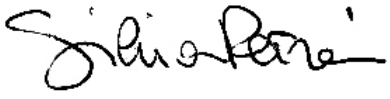

correct chamber geometry and the proper temperature values, it is possible to perform the desired thermal cycling inside a microfabricated chamber equipped with electrodes that, once an ac electric field is applied, drive an electro-convective whirling motion of the solution containing the molecules, thus making it pass through the desired temperature zones that are formed inside such chamber.

As concerns the development of a novel drug delivery device, results confirmed, first of all, that a biomechatronic design approach is the right way for correctly and safely designing novel devices that have to come in contact with tricky anatomic compartments. This means that, this same approach, can also be used in other applications, that is, whenever a detailed analysis of the interaction of a certain anatomic compartment and an external system is required. Eventually, following the biomechatronic approach, a hardware model that simulates the cerebral dynamics has been built, to perform *in vitro* tests of the infusion device prototype onto a system that effectively replicates the behaviour of the compartment of interest. The results of the tests were also encouraging, meaning that the desired infusion rate was provided to the "mock-up" cerebral compartment, keeping the intracranial pressure far below the maximum allowed safety value. In case of unbearable rise in the ICP the control system also correctly worked, by turning the pump off.

The second part of the dissertation concerned the HTA procedures applied to the previously developed technologies. Different assessment procedures were applied to the different technologies, and this was due to two main reasons: first of all, all the investigated technologies were at different stages of development. Then, all the presented case studies, were chosen in such a way that each one of them represents a particular aspect of HTA, that is: as concerns microfluidic technologies for molecular analysis, the technology trend and the main open ethical/legal issues raised were presented, in order to help decision makers in performing early evaluations on the adoption of these novel technologies; the technology trend was investigated for implantable drug delivery systems, and a future technology roadmap was provided, together with a cost-analysis that may help in quantifying the economic advantages of the newly developed technology for treating severe pathologies such as brain cancer; eventually, a survey on acceptability and usability of a novel device such as the ALLADIN platform was carried out, in order to better drive future choices concerning device refinements for its rapid introduction on the market.

All these case studies were chosen because they are complementary to each other, meaning that all of them highlight a different aspect on how early HTA can be performed on novel technologies.

On the whole, the results obtained at the end of my PhD course, strengthened the correctness of the proposed research approach, that may be employed also in other research projects concerning bioengineering, and, more-

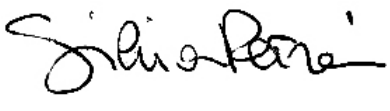

over, it is also in line with future perspectives concerning possible occupational outlets, where a higher education in bioengineering, with added experience both in design and assessment of biomedical technologies, is essential in order to drive, or at least to support, the choice of the proper technologies for diagnosis, therapy and rehabilitation.
Such an activity should be carried on in order to adopt adequate solutions in terms of healthcare policy and to provide patients and end-users with acceptable, usable and safe/reliable technological solutions, aimed at improving pathologies outcome. To this aim, both engineering and technological assessment skills are required.

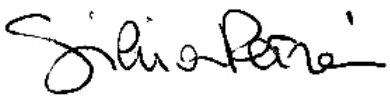

Bibliography

[1] J.W.Hong and S.R. Quake. Integrated nanoliter systems. *Nature Biotechnology*, 21(10):1179–1183, 2003.

[2] P.F. Macgregor and J.A. Squire. Application of microarrays to the analysis of gene expression in cancer. *Clinical Chemistry*, 48(8):1170–1177, 2002.

[3] T. Martinsky. Protein microarray manufacturing. *PharmaGenomics*, March/April:42–47, 2004.

[4] B. Haab. *Protein arrays, biochips and proteomics*. Marcel Dekker Inc., New York, 2003.

[5] J.G.F. Tsai et al. A silicon-micromachined pin for contact droplet printing. In *18th International Conference on Micro Electro Mechanical Systems*, pages 295–298, Kyoto, Japan, 2003. IEEE.

[6] R.J. Hunter. *Foundations of colloid science*. Oxford University Press, New York, 2001.

[7] T.M. Squires and S.R. Quake. Microfluidics: fluid physics at the nanoliter scale. *Reviews of Modern Physics*, 77:977–1026, 2005.

[8] S. Yao and J.G. Santiago. Porous glass electroosmotic pumps: theory. *Journal of Colloid and Interface Science*, 268:133–142, 2003.

[9] S. Yao et al. Porous glass electroosmotic pumps: design and experiments. *Journal of Colloid and Interface Science*, 268:143–153, 2003.

[10] D.J. Laser and J.G. Santiago. A review of micropumps. *Journal of Micromechanics and Microengineering*, 14:R35–R64, 2004.

[11] A. Manz et al. Electroosmotic pumping and electrophoretic separations for miniaturized chemical analysis systems. *Journal of Micromechanics and Microengineering*, 4:257–265, 1994.

[12] C.T. Culbertson et al. Electroosmotically induced hydraulic pumpong on microchips: differential ion transport. *Analytical Chemistry*, 72:2285–2291, 2000.

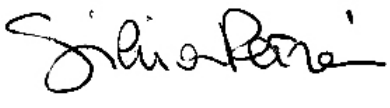

[13] T.E. McKnight et al. Electroosmotically induced hydraulic pumping with integrated electrodes on microfluidic devices. *Analytical Chemistry*, 73:4045–4049, 2001.

[14] W.E. Morf et al. Partial electroosmotic pumping in complex capillary systems. part 1: principles and general theoretical approach. *Sensors and Actuators B*, 72:266–272, 2001.

[15] C.Y. Lee et al. Electrokinetically driven active micro-mixers utilizing zeta potential variation induced by field effect. *Journal of Micromechanics and Microengineering*, 14:1390–1398, 2004.

[16] B. He et al. A picoliter-volume mixer for microfluidic analytical systems. *Analytical Chemistry*, 73:1942–1947, 2001.

[17] P.C.H. Li and D.J. Harrison. Transport, manipulation and reaction of biological cells on-chip using electrokinetic effects. *Analytical Chemistry*, 69:1564–1568, 1997.

[18] C.-J. Kim. Micropumping by electrowetting. In *International Mechanical Engineering Congress and Exposition*, New York, 2001. ASME.

[19] K.-S. Yun et al. A micropump driven by continuous electrowetting actuation for low voltage and low power operations. In *International Conference on Micro Electro Mechanical Systems*, pages 487–490, Interlaken, Switzerland, 2001. IEEE.

[20] U.-C. Yi and C.-J. Kim. Soft printing of droplets digitized by electrowetting. In *12th International Conference on Solid State Sensors, Actuators and Microsystems*, pages 1804–1807, Boston, MA, 2003.

[21] P.K. Wong et al. Electrokinetics in micro devices for biotechnology applications. *IEEE/ASME Transactions on Mechatronics*, 9(2):366–376, 2004.

[22] F. Mugele and J.-C. Baret. Electrowetting: from basics to applications. *Journal of Physics: Condensed Matter*, 17:R705–R774, 2005.

[23] C.H. Kua et al. Review of bio-particle manipulation using dielectrophoresis. Innovation in Manufacturing Systems and Technology (IMST). 2005.

[24] H.A. Pohl. *Dielectrophoresis*. Cambridge University Press, Cambridge, UK, 1978.

[25] M.P. Hughes. Ac electrokinetics: applications for nanotechnology. *Nanotechnology*, 11:124–132, 2000.

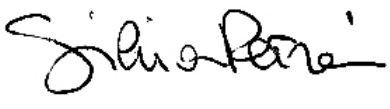

[26] S.J. Lee and S.Y. Lee. Micro total analysis system (μtas) in biotechnology. *Applied Microbiology and Biotechnology*, 64:289–299, 2004.

[27] P. Belaubre et al. Fabrication of biological microarrays using microcantilevers. *Applied Physics Letters*, 82:3122–3124, 2003.

[28] L.J. Kricka and P. Fortina. Microarray technology and applications: an all-language literature survey including books and patents. *Clinical Chemistry*, 47(8):1479–1482, 2001.

[29] S. Moore et al. *Molecular plant biology vol.2*. Oxford University Press, London, 2002.

[30] V.G. Cheung et al. Making and reading microarrays. *Nature Genetics Supplement*, 21:15–19, 1999.

[31] L.J. Kricka. Miniaturization of analytical systems. *Clinical Chemistry*, 44:2008–2014, 1998.

[32] L. Liu et al. Entropic trapping of macromolecules by mesoscopic periodic voids in a polymer hydrogel. *Nature*, 397(6715):141–144, 1999.

[33] S.P. Fodor et al. Light-directed, spatially addressable parallel chemical synthesis. *Science*, 251:767–773, 1991.

[34] T. Okamoto et al. Microarray fabrication with covalent attachment of dna using bubble jet technology. *Nature Biotechnology*, 18:438–441, 2000.

[35] D.J. Duggan et al. Expression profiling using cdna microarrays. *Nature Genetics Supplement*, 21:10–14, 1999.

[36] D.D.L. Bowtell. Options available -from start to finish- for obtining expression data by microarray. *Nature Genetics Supplement*, 21:25–32, 1999.

[37] J.L. DeRisi et al. Exploring the metabolic and genetic control of gene expression on a genomic scale. *Science*, 278:680–686, 1997.

[38] D.A. Lashkari et al. Yeast microarrays for genome wide parallel genetic and gene expression analysis. *Proceedings of the National Academy of Sciences*, 94:13057–13062, 1997.

[39] S. Chu et al. The transcriptional program of sporulation in budding yeast. *Science*, 282:699–705, 1998.

[40] A. Roda et al. Protein microdeposition using a conventional ink-jet printer. *Biotechniques*, 28(3):492–496, 2000.

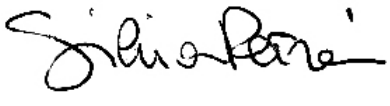

[41] T. Goldmann and J.S. Gonzalez. Dna-printing: utilization of a standard inkjet printer for the tranfer of nucleic acids to solid supports. *Journal of Biochemical and Biophysical Methods*, 42:105–110, 2000.

[42] T. Xu et al. Inkjet printing of viable mammalian cells. *Biomaterials*, 26:93–99, 2005.

[43] T. Hara and I. Endo. *Journal of the Institute of Image Electronics Engineers of Japan*, 11:66–71, 1982.

[44] R. Bashir. Biomems: state-of-the-art in detection, opportunities and prospects. *Advanced Drug Delivery Reviews*, 56:1565–1586, 2004.

[45] E. Verpoorte and N.F. De Rooij. Microfluidics meets mems. *Proceedings of the IEEE*, 91(6):930–953, 2003.

[46] D.C. Duffy et al. Rapid prototyping of microfluidic systems in poly(dimethylsiloxane). *Analytical Chemistry*, 70:4974–4984, 1998.

[47] L. Ceriotti et al. An integrated fritless column for on-chip capillary electrochromatography with conventional stationary phases. *Analytical Chemistry*, 74:639–647, 2002.

[48] F. Cipollone et al. A polymorphism in the cyclooxygenase 2 gene as an inherited protective factor against myocardial infarction and stroke. *Journal of the American Medical Association*, 291(18):2221–2228, 2004.

[49] P. Abgrall and A.-M. Gue. Lab-on-chip technologies: making a microfluidic network and coupling it into a complete microsystem - a review. *Journal of Micromechanics and Microengineering*, 17:R15–R49, 2007.

[50] J.W: Hong et al. Integration of gene amplification and capillary gel elctrophoresis on a polydimethylsiloxane-glass hybrid microchip. *Electrophoresis*, 22(2):328–333, 2001.

[51] P.K. Yuen et al. Microchip module for blood sample preparation and nucleic acid amplification reactions. *Genome Research*, 11:405–412, 2001.

[52] A. Manz et al. Planar chips technology for miniaturization and integration of separation techniques into monitoring systems: capillary electrophoresis on a chip. *Journal of Chromatography*, 593:253–258, 1992.

[53] J.W. Hong et al. A nanoliter-scale nucleic acid processor with parallel architecture. *Nature Biotechnology*, 22(4):435–439, 2004.

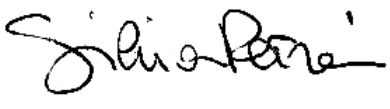

[54] M.U. Kopp et al. Chemical amplification: continuous-flow pcr on a chip. *Science*, 280:1046–1048, 1998.

[55] M. Piedade et al. Architecture of a portable system based on a biochip for dna recognition. In *XX Conference on Design of Circuits and Integrated Systems*, 2005.

[56] J. Burmeister et al. Single nucleotide polymorphism analysis by chip-based hybridization and direct current electrical detection of gold-labeled dna. *Analytical and Bioanalytical Chemistry*, 379:391–398, 2004.

[57] J.M. Gonzales-Buitrago and C. Gonzales. Present and future of the autoimmunity laboratory. *Clinica Chmica Acta*, 365:50–57, 2006.

[58] www.hp.com.

[59] www.epson.com.

[60] L. Lonini et al. Experimental comparison of thermal and piezoelectric inkjet technologies for dispensing an enzyme-conjugated solution into an elisa plate. *Journal of Biochemical and Biophysical Methods*, 2007.

[61] A. Voller et al. Enzyme immunoassays with special reference to elisa techniques. *Journal of Clinical Pathology*, 31:507–520, 1978.

[62] H.P. Le. Progress and trends in ink-jet printing technology. *Journal of Imaging Science and Technology*, 42(1):49–62, 1998.

[63] S. Sakai. Dynamics of piezoelectric inkjet printing systems. Technical report, SEIKO EPSON Co., 2002. Shiojiri, Nagano, Japan.

[64] Ena screen org 506 manual. ORGENTEC Diagnostika GmbH, 2004.

[65] P.R. Selvaganapathy. Recent progress in microfluidic devices for nucleic acid and antibody assays. *Proceedings of the IEEE*, 91(6):954–975, 2003.

[66] A. Gonzalez et al. Fluid flow induced by nonuniform ac electric fileds in electrolytes on microelecrodes. ii. a linear double-layer analysis. *Physical Review E*, 61(4):4019–4028, 2000.

[67] N.G. Green et al. Fluid flow induced by nonuniform ac electric fields in electrolytes on microelectrodes. i. experimental measurements. *Physical Review E*, 61(4):4011–4018, 2000.

[68] N.G. Green et al. Fluid flow induced by nonuniform ac electric fields in electrolytes on microelectrodes. iii. observation of streamlines and numerical simulation. *Physical ReviewE*, 66, 2002.

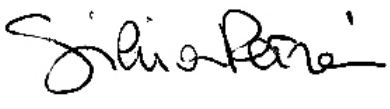

[69] D. Accoto et al. Dispositivo microfluidico per generare elettrocineticamente moti convettivi. domanda di brevetto italiano num. FI006A000185, depositata il 25 luglio 2006.

[70] D.M. Parkin et al. Global cancer statistics, 2002. *CA, a Cancer Journal for Clinicians*, 55:74–108, 2005.

[71] J. Rautio and P.J. Chikhale. Drug delivery systems for brain tumor therapy. *Current Pharmaceutical Design*, 10:1341–1353, 2004.

[72] R.M. Berne and M.N. Levy. *Fisiologia*. CEA, 1995.

[73] D.R. Groothuis. The blood-brain and blood-tumor barriers: a review of strategies for increasing drug delivery. *Neuro-Oncology*, 1999. serial online.

[74] M. Burke et al. Central nervous system, drug delivery to treat. *Encyclopedia of Controlled Drug Delivery*, 1:185–210, 1999.

[75] G. Ambrosi et al. *Anatomia dell'uomo*. Edi.Ermes s.r.l., Milano, 2001.

[76] P.F. Morrison et al. High-flow microinfusion: tissue penetration and pharmacodynamics. *American Journal of Physiology*, 266:292–305, 1994.

[77] J. Johnston et al. Shiley infusaid pump technology. *Annals of the New York Academy of Sciences*, 531:57–65, 1988.

[78] K.T. Heruth. Medtronic synchromed drug administration system. *Annals of the New York Academy of Sciences*, 531:72–75, 1988.

[79] S. Petroni et al. A general model for guiding the design of biomechatronic systems implantable into the brain. In *The First International Conference on Biomedical Robotics and Biomechatronics*, Pisa, Italy, 2006. IEEE/RAS-EMBS.

[80] P. Reilly and R. Bullock, editors. *Head Injury*, chapter Intracranial pressure and elastance, pages 101–120. Chapman and Hall, London, 1997.

[81] J.N. Bruce. Intracerebral clysis in rat glioma model. *Neurosurgery*, 46(3):683–691, 2000. serial online.

[82] N.J. Alperin et al. Mr-intracranial pressure (icp): a method to measure intracranial elastance and pressure noninvasively by means of mr imaging: baboon and human study. *Radiology*, 217:877–885, 2000.

[83] G. Bouvier et al. Direct delivery of medication into a brain tumor through multiple chronically implanted catheters. *Neurosurgery*, 20(2):286–291, 1987.

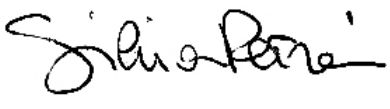

[84] T. Bourouina and J.-P. Grandchamp. Modeling micropumps with electrical equivalent networks. *Journal of Micromechanics and Microengineering*, 6:398–404, 1996.

[85] C. Nicholson and J.M. Phillips. Ion diffusion modified by tortuosity and volume fraction in the extracellular microenvironment in the rat cerebellum. *Journal of Physiology*, 70:1214–1218, 1981.

[86] A. Marmarou. *A theoretical and experimental evaluation of the cerebrospinal fluid system*. PhD thesis, Drexel University, 1973.

[87] M. Ursino and C. Lodi. A simple mathematical model of the interaction between intracranial pressure and cerebral hemodynamics. *Journal of Applied Physiology*, 82(4):1256–1269, 1997.

[88] C. Ying et al. The simulation of intracranial pressure dynamics. In *27th Annual Conference in Engineering in Medicine and Biology*, Shangai, China, 2005. IEEE.

[89] A. Marmarou et al. Compartmental analysis of compliance and outflow resistance of the cerebrospinal fluid system. *Journal of Neurosurgery*, 43:523–534, 1975.

[90] A. Marmarou et al. A nonlinear analysis of the cerebrospinal fluid system and intracranial pressure dynamics. *Journal of Neurosurgery*, 48:332–344, 1978.

[91] C.S. Goodman. Introduction to health technology assessment, 2004. US National Library of Medicine, NIH, available at http://www.nlm.nih.gov/nichsr/hta101/ta101_c1.html.

[92] K. Lumsdon. Beyond technology assessment: balancing strategy needs, strategy. *Hospitals*, 15:25–, 1992.

[93] G. France. Health technology assessment in italy. *International Journal of Technology Assessment in Health Care*, 16(2):459–474, 2000.

[94] D. Banta and W. Woortwjin. Introduction: health technology assessment and the european union. *International Journal of Technology Assessment in Health Care*, 16(2):299–302, 2000.

[95] B. Labella. *Valutazione economica e tecnologie in sanità*. PhD thesis, Scuola Superiore Sant'Anna di Pisa, 2007.

[96] F.H. Knight. *Risk, Uncertainty and Profit*. (Boston and New York: Houghton Mifflin Company, 1921.

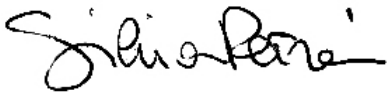

[97] S. Petroni et al. Impact of microfluidic systems for molecular and genomic analysis: technological and socio-economic perspectives. In *Proceedings of the 6th Annual Conference of the Association for Healthcare Technology and Management (HCTM)*, Scuola Superiore Sant'Anna, Pisa, Italy, 2007.

[98] V. Amirkhanian et al. Cost benefit analysis of a multicapillary electrophoresis system. *American Laboratory*, June/July:26–28, 2006.

[99] E. Mounier. Biochips and microfluidics: technologies and market trends. *DrugPlus International*, July/August, 2003.

[100] A.H. Sims et al. Exploiting the potential of gene expression profiling : is it ready for the clinic? *Breast Cancer Research*, 8(5):214–220, 2006.

[101] A.A. Yarpuzlu and N. Atak. Future of health technology assessment studies in gene and cell therapies. *African Journal of Biotechnology*, 6(14):1603–1607, 2007.

[102] S. Petroni et al. Implantable drug infusion systems for cancer therapy in tricky anatomic compartments: the case of brain tumours. technological and socio-economic implications. In *Proceedings of the 6th Annual Conference of the Association for Healthcare Technology and Management (HCTM)*, Scuola Superiore Sant'Anna, Pisa, Italy, 2007.

[103] M. Wrensch et al. Epidemiology of primary brain tumors: current concepts and review of the literature. *Neuro-Oncology*, 4(4):278–299, 2002.

[104] M. Ekman. Economic evidence in brain tumour: a review. *European Journal of Health Economics*, 5, Suppl. 1:s25–s30, 2004.

[105] Cancer facts and figures. available at http://www.cancer.org, 2007.

[106] F. Bray et al. Estimates of cancer incidence and mortality in europe in 1995. *European Journal of Cancer*, 38:99–166, 2002.

[107] F.G. Davis et al. Survival rates in patients with primary malignant brain tumors stratified by patient age and tumor histological type: an analysis based on surveillance, epidemiology and end results (seer) data, 1973-1991. *Journal of Neurosurgery*, 88:1–10, 1998.

[108] A. Grovas et al. The national cancer data base report on patterns of childhood cancers in the united states. *Cancer*, 80:2321–2332, 1997.

[109] M. Sant et al. Survival rates for primary malignant brain tumors in europe. eurocare working group. *European Journal of Cancer*, 8:2241–2247, 1998.

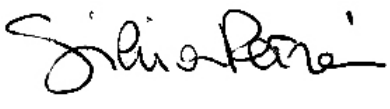

[110] F.G. Davis et al. The conditional probability of survival of patients with primary malignant brain tumors: Surveillance, epidemiology and end results (seer) data. *Cancer*, 85:485–491, 1999.

[111] M.A. Lopez-Gonzalez and J. Sotelo. Brain tumors in mexico: characteristics and prognosis of glioblastoma. *Surgical Neurology*, 53:157–162, 2000.

[112] J.M. Legler et al. Cancer surveillance series [corrected]: brain and other central nervous system cancers: recent trends in incidence and mortality. *Journal of the National Cancer Institute*, 81:1382–1390, 1999.

[113] G.E. Sheline. radiation therapy for brain tumors. *Cancer*, 39:873–881, 1977.

[114] T.A. Hodgson and M.R. Meiners. Cost-of-illness methodology: a guide to current practices and procedures. *Milbank Memorial Fund quarterly: Health and Society*, 60:429–462, 1982.

[115] B.R. Luce and A. Elixhauser. Estimating costs in the economic evaluation of medical technologies. *International Journal of Technology Assessment in Health Care*, 6:57–75, 1990.

[116] S. Bradley et al. I could lose everything: understanding the cost of a brain tumor. *Journal of Neuro-Oncology*, 2007. available online.

[117] L. Kutikova et al. Utilization and cost of health care services associated with primary malignant brain tumors in the united states. *Journal of Neuro-Oncology*, 81(1):61–65, 2007.

[118] P. Blomqvist et al. Brain tumours in sweden 1996: care and costs. *Journal of Neurology, Neurosurgery and Psychiatry*, 69:792–798, 2000.

[119] M. Ekman and M. Westphal. Cost of brain tumour in europe. *European Journal of Neurology*, 12:45–49, 2005.

[120] M. Turini and A. Redaelli. Primary brain tumours: a review of research and management. *International Journal of Clinical Practice*, 55:471–475, 2001.

[121] A.Z. Latif et al. The costs of managing patients with malignant glioma at a neuro-oncology clinic. *British Journal of Neurosurgery*, 12:118–122, 1998.

[122] G. Wellis et al. Direct costs of microsurgical management of radiosurgically amenable intracranial pathology in germany: an analysis of

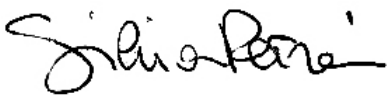

meningiomas, acoustic neuromas, metastases and arteriovenous malformations of less than 3 cm in diameter. *Acta Neurochirurgica (Wien)*, 145:249–255, 2003.

[123] A.A. Brandes et al. Future trends in the treatmant of brain tumours. *European Journal of Cancer*, 37(18):2297–2301, 2001.

[124] D. Osoba et al. Effect of disease burden on health-related quality of life in patients with malignant gliomas. *Neuro-oncology*, 4:221–228, 2000.

[125] Micro and nanotechnology in healthcare and life sciences market sector report. available at www.tfi-ltd.co.uk, 2005.

[126] S. Petroni et al. Early assessment of neuro-rehabilitation technology: a case study. In *Proceedings of the 6th Annual Conference of the Association for Healthcare Technology and Management (HCTM)*, Scuola Superiore Sant'Anna, Pisa, Italy, 2007.

[127] World health organization, the atlas of heart disease and stroke. available at http://www.who.int/cardiovascular_diseases/resources/atlas/en/.

[128] G. Turchetti et al. Innovation in rehabilitation technology: technological opportunities and socio-economic implications. In *Proceedings of the 6th Annual Conference of the Association for Healthcare Technology and Management (HCTM)*, Scuola Superiore Sant'Anna, Pisa, Italy, 2007.

[129] M.L. Aisen et al. The effect of robot-assisted therapy and rehabilitative training on motor recovery following stroke. *Archives of Neurology*, 54(4):443–446, 1997.

[130] H.I. Krebs et al. Robot-aided neurorehabilitation. *IEEE Transaction on Rehabilitation Engineering*, 6(1):75–87, 1998.

[131] J. Winters and P. Crago, editors. *Biomechanics and Neural Control of Posture and Movement*, chapter Rehabilitators, robots and guides: New tools for neurological rehabilitation. Springer-Verlag, 2000.

[132] G.B. Prange et al. Systematic review of the effect of robot-aided therapy on recovery of the hemiparetic arm after stroke. *Journal of Rehabilitation Research and Development*, 43(2):171–184, 2006.

[133] H.I. Krebs and N. Hogan. Therapeutic robotics: a technology push. *Proceedings of the IEEE*, 94(9):1727–1738, 2006.

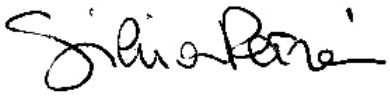

[134] S. Mazzoleni et al. Alladin: a novel mechatronic platform for assessing post-stroke functional recovery. In *Proceedings of the International Conference on Rehabilitation Robotics*, pages 156–159, Chicago, IL, 2005.

[135] S. Clark et al. Differential modulation of corticospinal excitability during observation, mental imagery and imitation of hand actions. *Neuropsychology*, 42(1):105–112, 2004.

[136] P. Dechent et al. Is the human primary motor cortex involved in motor imagery? *Cognitive Brain Research*, 19(2):138–144, 2004.

[137] H.H. Ehrsson et al. Imagery of voluntary movement of fingers, toes, and tongue activates corresponding body-part-specific motor representations. *Journal of Neurophysiology*, 90(5):3304–3316, 2003.

[138] P.L. Jackson et al. Functional cerebral reorganization following motor sequence learning through mental practice with motor imagery. *Neuroimaging*, 20(2):1171–1180, 2003.

[139] S.H. Johnson-Frey. Stimulation through simulation? motor imagery and functional reorganization in hemiplegic and stroke patients. *Brain and Cognition*, 55(2):328–331, 2004.

[140] J.M. Kilner et al. Functional connectivity during real vs imagined visuomotor tasks : an eeg study. *Neuroreport*, 15(4):637–642, 2004.

[141] S. Lehericy et al. Motor execution and imagination networks in post-stroke dystonia. *Neuroreport*, 15(12):1887–1890, 2004.

[142] D.M. Wolpert et al. Perspectives and problems in motor learning. *Trends in Cognitive Sciences*, 5:487–494, 2001.

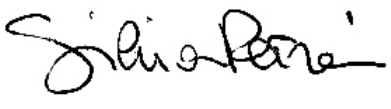

List of publications

S. Petroni, D. Accoto, D. Campolo, M.C. Annesini, and E. Guglielmelli, *A general model for guiding the design of biomechatronic systems implantable into the brain*, The First IEEE/RAS-EMBS International Conference on Biomedical Robotics and Biomechatronics, February 20-22, Pisa, Italy, 2006.

L. Lonini, D. Accoto, **S. Petroni** and E. Guglielmelli, *Experimental comparison of thermal and piezoelectric ink-jet technologies for dispensing an enzyme-conjugated solution into an ELISA plate*, Biochemical and Biophysical Methods, article in press, available online, 2007.

S. Petroni, S. Bellelli, S. Cannizzo, I. Palla, S. Mazzoleni, B. Labella, S. Sterzi, E. Guglielmelli and G. Turchetti, *Early assessment of neurorehabilitation technology: a case study*, The 6th International Conference on the Management of Healthcare and Medical Technology (HCTM '07), Scuola Superiore Sant'Anna, Pisa, 3-5 October 2007.

S. Petroni, D. Accoto, B. Labella, G. Turchetti and E. Guglielmelli, *Implantable drug infusion systems for cancer therapy in tricky anatomic compartments: the case of brain tumours. Technological and socio-economic implications*, The 6th International Conference on the Management of Healthcare and Medical Technology (HCTM '07), Scuola Superiore Sant'Anna, Pisa, 3-5 October 2007.

S. Petroni, D. Accoto, B. Labella, G. Turchetti and E. Guglielmelli, *Impact of microfluidic systems for molecular and genomic analysis: technological and socio-economic perspectives*, The 6th International Conference on the Management of Healthcare and Medical Technology (HCTM '07), Scuola Superiore Sant'Anna, Pisa, 3-5 October 2007.

G. Turchetti, B. Labella, S. Bellelli, S. Cannizzo, I. Palla, S. Mazzoleni, **S. Petroni**, S. Sterzi and E. Guglielmelli, *Innovation in rehabilitation technology: technological opportunities and socio-economical implications*, The 6th International Conference on the Management of Healthcare and Medical Technology (HCTM '07), Scuola Superiore Sant'Anna, Pisa, 3-5 October 2007.

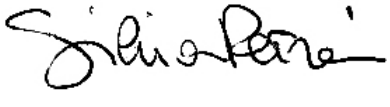

S. Petroni, D. Accoto and E. Guglielmelli, *Recent progress on microfluidic techniques for focusing, sorting and dispensing in life-sciences*, article conditionally accepted, submitted after second revision at Biomedical Microdevices, 2007.

S. Petroni, D. Accoto, B. Labella, G. Turchetti and E. Guglielmelli, *Technological and socio-economic implications in the development of implantable drug infusion systems for cancer therapy in tricky anatomic compartments: the case of brain tumours*, submitted on invitation at International Journal of Biomedical Engineering and Technology, 2008.

S. Petroni, D. Accoto, B. Labella, G. Turchetti and E. Guglielmelli, *Impact of microfluidic systems for molecular and genomic analysis: technological and socio-economic perspectives*, submitted on invitation at International Journal of Biomedical Engineering and Technology, 2008.

S. Petroni, S. Bellelli, S. Cannizzo, I. Palla, S. Mazzoleni, B. Labella, S. Sterzi, E. Guglielmelli and G. Turchetti, *Early assessment of neurorehabilitation technology: a case study*, submitted on invitation at International Journal of Biomedical Engineering and Technology, 2008.